UNIVERSITY OF OKLAHOMA

GRADUATE COLLEGE

FORMULATION DEVELOPMENT TO OBTAIN THIN FILM COATINGS ON SOLID SURFACES USING ADMICELLAR POLYMERIZATION

A DISSERTATION

SUBMITTED TO THE GRADUATE FACULTY

in partial fulfillment of the requirements for the

Degree of

DOCTOR OF PHILOSOPHY

By

SRINIVAS HANUMANSETTY
Norman, Oklahoma
2015

Downloaded from SHAREOK. Persistent Handle URL: https://hdl.handle.net/11244/14610

FORMULATION DEVELOPMENT TO OBTAIN THIN FILM COATINGS ON SOLID SURFACES USING ADMICELLAR POLYMERIZATION

A DISSERTATION APPROVED FOR THE
SCHOOL OF CHEMICAL, BIOLOGICAL AND MATERIALS ENGINEERING

BY

_____
Dr. Edgar A. O'Rear, Chair

_____
Dr. David A. Sabatini

_____
Dr. Robert L. Shambaugh

_____
Dr. Jeffrey H. Harwell

_____
Dr. Lance L.Lobban

© Copyright by SRINIVAS HANUMANSETTY 2015
All Rights Reserved.

To my parents, Hanumansetty Ramanaji and Hanumansetty Bharati, who have been understanding and supportive.

To my best friend and brother Hanumansetty Santosh, who has been a great source of motivation and inspiration.

Acknowledgements

The completion of my Ph.D. would not have been possible without the help and support of many people.

I would like to thank first my advisor Dr. Edgar O'Rear who has not only taught me and guided me but also helped me to develop as an individual thinker. I am thankful for providing me an opportunity to pursue my doctorate at University of Oklahoma. I am grateful for your encouragement and reassurance during hard times. I am also thankful for your encouragement and appreciation for the work I have done. You have been a role model and great mentor I have met and it's been a blessing to work under your guidance. Thank you for this opportunity.

I also want to express my gratitude to Dr. Mathis U. Nollert, Dr. lance L. Lobban, Dr. Robert L. Shambaugh, Dr. Jeffrey H. Harwell and Dr. David A. Sabatini for serving in my committee. I appreciate the time they dedicated to me, comments and incites in improving my dissertation.

I would also like to thank all the reviewers of my publications for providing useful and insightful reviews, enabling me to improve the quality of work I published. I would like to thank Rod Foster for his critical economic perspective on the research projects we worked.

I would like to thank my colleagues Pratik Kothary, Dr. Jayanta Maity, Dr. Saroj Nehra, Jannefer Ma, Rachel Weber for their support and assistance provided in various parts of the project and laboratory work. I would like to acknowledge Dr. Preston Larson for his help in Samuel Roberts Noble Microscopy Laboratory of OU on electron microscopy characterizations. I also would like to acknowledge Dr. Rolf Jentoft for his support with

thermo gravimetric analysis (TGA) and BET equipment. I would like to thank Dr. Daniel E. Resasco for providing Multi-Walled Carbon Nanotubes (MWCNTs) for the project and co-authoring my publications I worked on MWCNTs.

This research would not have been feasible without financial support by Oklahoma Center for the Advancement of Science and Technology (OCAST) and by grant obtained from United States Department of Energy for Center for Application of Single-Walled Carbon Nanotubes. Last but not least, I thank the CBME department at University of Oklahoma for their help and support at various times during my academic life at OU.

Table of Contents

Acknowledgements iv

Table of Contents vi

List of Tables xi

List of Figures xiii

Abstract xvii

Chapter 1 1

1.1 Introduction 1

1.2 Organisation of Dissertation 4

PART I 8

Chapter 2 9

2.1 Abstract 9

2.2 Introduction 10

2.2.1 Theory 14

2.3 Materials and Methods 16

2.3.1 Materials 16

2.3.2. *Experimental Analysis* 17

2.4 Results and Discussion 18

2.4.1 Adsorption Isotherms of Fluorosurfactants 18

2.4.2 Adsolubilization of Fluoromonomers 21

2.4.3 Surfactant Aggregation Numbers on Cotton 26

2.5 Conclusion 29

Chapter 3 31

3.1 Abstract 31
3.2 Introduction 32
3.3 Materials 34
3.4 Preparation of Samples, Admicellar Polymerization 34
3.5 Characterization of Treated Fabric 35
3.5.1 Water Repellency Tests 35
3.5.2 Contact Angle Analysis 35
3.5.3 SEM Study 36
3.5.4 Stain Recovery and Stain Resistance Tests 36
3.5.5 Tensile Strength Measurements 37
3.6 Results and Discussion 37
3.6.1 Appearance of Thin Film 37
3.6.2 Mechanical Characterization 41
3.6.3 Water-Repellency Tests 42
3.6.4 Oil Repellency 45
3.6.5 Stain Recovery and Stain Resistance 46
3.7 Conclusion 49
Chapter 4 50
4.1 Abstract 50
4.2 Introduction 51
4.3 Literature Survey 53
4.4 Theory 55
4.4.1 Calculation of the Specific Mixing Power and Mass Transfer Coefficient 57

4.5 Materials 60
4.6 Experimental 61
4.6.1 Mass Transfer Determination in a Model System of Benzoic Acid Dissolution 61
4.6.2 Application of a Hydrophobic Coating on Cotton Fabric 62
4.7 Results and Discussion 63
4.8 Conclusion 71
4.9 Nomenclature 72
PART II 74
Chapter 5 75
5.1 Abstract 75
5.2 Introduction 77
5.3 Experiments 82
5.3.1 Materials 82
5.3.2 Adsorption and Adsolubilization Analysis 82
5.3.3 Polymer Encapsulation 83
5.3.4 Hydrolysis 83
5.4 Characterization 84
5.4.1 Scanning Electron Microscopy (SEM) 84
5.4.2 Energy Dispersive Spectroscopy 84
5.4.3 Thermo Gravimetric Analysis (TGA) 84
5.4.4 Fourier Transform Infra-Red Spectroscopy 84
5.5. Results and Discussion 85

5.5.1 Adsorption Isotherms 85
5.5.2 Adsolubilization of Monomers 86
5.5.3 Modified Two-Site Adsolubilization Model 88
5.5.4 Binary Adsolubilization Model 89
5.5.4 Polymer Encapsulation 92
5.6 Conclusions 98
Chapter 6 99
6.1 Abstract 99
6.2 Introduction 100
6.3 Experimental 102
6.3.1 Materials 102
6.3.2 Polymer Encapsulation 103
6.4 Characterization 103
6.4.1 Fourier Transform Infrared Spectroscopy (FTIR) 103
6.4.2 Scanning Electron Microscopy (SEM) 104
6.4.3 Thermo Gravimetric Analysis (TGA) 104
6.4.4 Energy Dispersive Spectroscopy (EDS) 104
6.4.5 UV-Vis Spectrophotometry 104
6.4.6 Determination of % Monomer Conversion and Copolymer Composition 105
6.5 Results and Discussion 106
6.5.1 Analysis of Encapsulated MWCNTs 107
6.5.2 Determination of Monomer Conversion and Copolymer Composition 112

6.5.3 Dispersion Stability of Encapsulated MWCNTs:..... 117
6.6 Conclusion..... 118
Chapter 7 119
7.1 Summmary from Part I..... 119
7.2 Summary from Part II..... 120
Bibilography..... 121
Appendix -A: Extended work for adsorption and adsolubilization of C6 fluoromonomer 137
Appendix –B: Analytical tests and equipments used to develop formulations..... 142
Appendix –C Modified two-site Adsolubilzation for calculation of adsolubilization of MWCNTs 154
Appendix –D Theory of Surfactant Science..... 159

List of Tables

Table 1. Comparison of adsolubilization partition coefficient with fluorocarbon and hydrocarbon systems 26

Table 2. Numerical values used for calculating aggregation number in two-site adsolubilization model..... 27

Table 3. Stain release grades according to AATCC test method 130 46

Table 4. Specific Mixing Power per Unit Mass ε (W/kg) and Predicted Mass Transfer Coefficient (x 10^{-5} m/s)..... 65

Table 5. Mass Flux (x10^{-4} mol/m^2 s) and Observed Mass Transfer Coefficient 67

Table 6. Wetting time and spray test data with different reactor volumes..... 69

Table 7. Wetting time and spray test data with different rotational rates..... 69

Table 8. Wetting times spray test and contact angle data for different fabric ratios..... 71

Table 9. Comparison of predicted versus observed for total number of moles in reverse hemimicelle and moles of BA and MMA monomers (ratio 75:25) 90

Table 10. Comparison of predicted versus observed for total number of moles in reverse hemimicelle and moles of BA and MMA monomers (ratio 50:50) 90

Table 11. Comparison of predicted versus observed for total number of moles in reverse hemimicelle and moles of BA and MMA monomers (ratio 25: 75) 91

Table 12. Average diameter of pristine MWCNTs and encapsulated MWCNTs. 93

Table 13. EDS analysis of encapsulated MWCNTs before and after hydrolysis..... 94

Table 14. Average diameter from SEM micrographs 110

Table 15. EDS analysis for elemental composition of encapsulated MWCNTs..... 111

Table 16. Fineman-Ross and Kelen-Tüdos parameters for copolymerization of AA and MMA 114

List of Figures

Figure 1. The process of admicellar polymerization [57] 3

Figure 2. Representation of adsorption isotherm of surfactants [57] 4

Figure 3. Two-site adsolubilization model on cotton surface 10

Figure 4. Two-site adsolubilization model 13

Figure 5. Structure of commercial fluorosurfactants and fluoromonomers 16

Figure 6. Adsorption isotherm of surfactants alone and in the presence of monomers . 18

Figure 7. Ratio of adsolubilized fluoromonomer to adsorbed fluorosurfactant 22

Figure 8. Adsolubilization partition coefficients for (a) FS 230 (b) FS 1620 24

Figure 9. Aggregation number for fluorosurfactants in presence of fluoromonomers... 29

Figure 10. Untreated fibers of interlock knit cotton 38

Figure 11. Interlock knit cotton fibers with PA1 (a,b) and PA2 (c,d) 38

Figure 12. Energy dispersive spectroscopy (EDS) spectrum of: (a) Untreated fiber 40

Figure 13. Stress-strain plot of untreated fabric and treated fabric with formulations PA1 and PA2 41

Figure 14. Comparison of contact angles for treated and commercial reference samples 42

Figure 15. Comparison of durability of treated fabrics with commercial reference samples by the drop test 43

Figure 16. Comparison of spray test of treated fabric and commercial samples 44

Figure 17. Comparison of oil test for treated fabric with commercial reference samples 45

Figure 18. Stain resistance for untreated and treated fabric with PA2 with different staining agents 47

Figure 19. Stain resistance comparison for PA2 and commercial fabrics with different stains 47

Figure 20. Stain recovery of treated fabric with PA2 compared to commercial reference fabrics 48

Figure 21. A typical infrared laboratory dyeing unit 51

Figure 22. Arrangement of canisters in a laboratory dyeing unit. A tilt relative to the horizontal axis of rotation causes end-to-end fluid motion 52

Figure 23. The conceptual simplification of the fluid at the apex and nadir facilitated an estimate if the potential energy change giving rise to mixing in the reactor 57

Figure 24. Pictorial representation of volume of canister 58

Figure 25. Relationship of $h(z)$ and $\theta_1(h)$ in end view of canister 59

Figure 26. Similarity of Sherwood number ($Sh=\beta d/D$) correlations with Reynolds numbers based on Murzin's experiments ($Sh=.107Re^{1.222}$) and on the potential energy theory of this paper ($Sh=.104Re^{1.195}$). Sherwood numbers were calculated for reported values of the mass transfer coefficient for dissolution of benzoic acid in water with a rocking reactor and plotted against the Reynolds number obtained from Murzin's experimental work($Re=\rho\varepsilon^{1/3}d^{4/3}/\mu$) in 26a and from the potential energy theory($Re=\rho vd/\mu$) applied for Murzin's experimental conditions in 26b. 64

Figure 27. Wetting time for different reactor volumes keeping the fabric to liquid ratio constant 68

Figure 28. SEM micrographs: (a,b) untreated cotton fiber and (c,d) treated cotton fiber 70

Figure 29 Schematic representation of admicellar polymerization for MWCNTs 76

Figure 30. Schematic view of modified two-site adsolubilization model (a) Sleeve model (b) Cross-sectional view 80

Figure 31. Adsorption isotherm of SDS without and with presence of monomers. 85

Figure 32. Ratio of monomer (BA and MMA) to surfactant (SDS) 87

Figure 33. Aggregation number calculated using modified two-site adsolubilization model. 88

Figure 34. SEM analysis of 1. Pristine MWCNTs, 2. PBA-MWCNTs, 3. PMMA-MWCNTs, 4. PBA/PMMA-MWCNTs. 92

Figure 35. FTIR analysis of encapsulated MWCNTs before and after hydrolysis 95

Figure 36. TG analysis of MWCNTs and encapsulated MWCNTs 96

Figure 37. Encapsulated MWCNTs dispersed in water. Picture was taken after 3 days dispersion in water. 97

Figure 38. FTIR analysis of pristine MWCNTs and encapsulated MWCNTs 107

Figure 39. TGA of pristine MWCNTs and encapsulated MWCNTs 108

Figure 40. SEM micrographs (1) pristine MWCNTs (2) PAA – MWCNTs (3) PMMA – MWCNTs (4) PAA/PMMA – MWCNTs 110

Figure 41. UV-Vis spectra of pristine MWCNTs and encapsulated MWCNTs 112

Figure 42. Conversion of monomers vs. time 113

Figure 43. Fineman-Ross (a) and Kelen-Tüdos (b) plots for copolymer of AA and MMA with a total concentration of 4mM and mole fraction of AA in co-monomer feed varied from 0.15 to 0.75 116

Figure 44. Comparison mole fraction of AA in co-monomer feed and the mole fraction in copolymer feed. 117

Figure 45. Solubility of encapsulated MWCNTs in aqueous media at different time frames (1) 3 days (2) 40 days 117

Abstract

Hydrophobic and hydrophilic properties are imparted on solid surfaces to enhance the properties of surfaces. From over a decade several methods have been employed to impart thin film coatings onto surfaces. Apart from different polymerization methods, admicellar polymerization process was implemented to impart enhanced properties to selected solid surfaces.

Admicellar polymerization (AP), a surface analogue of emulsion polymerization was used to develop film coatings on surfaces. AP follows three basic steps. First step is adsorption of surfactant molecules on to surface. The second step is adsolubilization of monomer into adsorbed surfactant molecules on surface. The next step is to initiate reaction and once the polymer is formed, modified surfaces are rinsed for removal of excess surfactant. Development of a system for AP involves measurement of surfactant adsorption and adsolubilization or partitioning of monomer into adsorbed structures. Two-site adsolubilization model and binary adsolubilization models were used to calculate the size of surfactant aggregates over the surface of solids. High performance liquid chromatography (HPLC) analytical technique was used to obtain the adsorption and adsolubilization measurements. We have to modify the two-site adsolubilization model to fit for the surfaces we have used. Adsolublized monomers were polymerized to form thin film coatings on surfaces. The modified solid surfaces were analyzed using different analytical techniques SEM, EDS, TGA, BET, FTIR to confirm the polymer formation. Hydrophilic and hydrophobic properties are tested with respective test methods depending on what type of surface used.

Chapter 1

1.1 Introduction

Surface modification of a substrate is a significant and multipurpose method for creating materials with enhanced performance in some specific areas. Materials modified so possess surface properties that are different from their bulk properties. For example, application of a low surface energy fluorochemical film can reduce friction, inhibit adhesion, and impart water repellency. Over past few decades, superhydrophobic and superhydrophilic films were constructed by different components on substrate surfaces to increase their commercial potential. The components are structured with different materials including monomers, polymers and surfactants. Individual components do not possess the properties of superhydrophilic and superhydrophobic, but combination of components enhances the surfaces. Coatings on solid surfaces benefit from both film constructions and nanounit functionalities. Fabrication of thin films on substrate surface is an excellent scheme to fulfill the requirement of connecting units with distinctive properties to the outside world. Thin film coatings in particular represent the interface between the product and the environment and therefore determine aesthetic aspect of goods but also important specific properties such as anti-corrosion, self-cleaning, chemical and scratch resistance. Individual molecules can be arranged such that the thin film coatings will have ability to increase hydrophobicity or hydrophilicity, corrosion resistance, flexibility of materials. Thin film development on surfaces of solids improves the properties and application of solids to multiple fields.

Thin films on solids can be developed using methods like vacuum deposition, spray coatings, electrochemical deposition, layer-by-layer deposition, ion-assisted

technologies, plasma etching, and surface initiated polymerization mechanisms. Thin films prepared from the above-mentioned techniques might deteriorate the surface, requires equipment modifications, increase in cost of treatment and other disadvantages apply. Substrate surfaces should be modified with thin films at reduced cost and minimal amounts of chemicals to achieve enhanced properties. Emulsion polymerization, one of the most common industrial processes is being used to produce thin films on surfaces on any scale. Emulsion polymerization belongs to the class of heterophase polymerization mechanism can be defined in a general way as polymerization or copolymerization in aqueous systems of any combination of monomers. The polymerization leads to formation of water-insoluble polymers or copolymers in the form of individual polymer particles with a size distribution of diameters less than 10μm. Any kind of polymerization mechanism can be employed provided the initiation mechanism is stable in water. The principal advantages of emulsion polymerization include rapid polymerization, low viscosities and presence of dispersion medium. These qualities can be found in admicellar polymerization. In admicellar polymerization, surfactants adsorbed on a surface have been utilized as a guide for polymerization to alter the surface properties.

Admicellar polymerization, a surface analogue of emulsion polymerization has been used to develop polymer films on different substrate surfaces such as polystyrene on silica[1], alumina[2, 3], cotton[4, 5], styrene-isoprene copolymer on glass fiber[6], poly(methylmethacrylate) on alumina metal[7], polypyrrole on mica[8], polyacrylonitrile on carbon nanotubes[9]. Le applied a fluoropolymer to aluminum plates by admicellar polymerization to block corrosion in crevices[8]. The

polymerization method is simple with low energy consumption and when used on to fabrics it will retain its feel and softness, as the polymer films formed were order of 10-100 nanometer thickness.

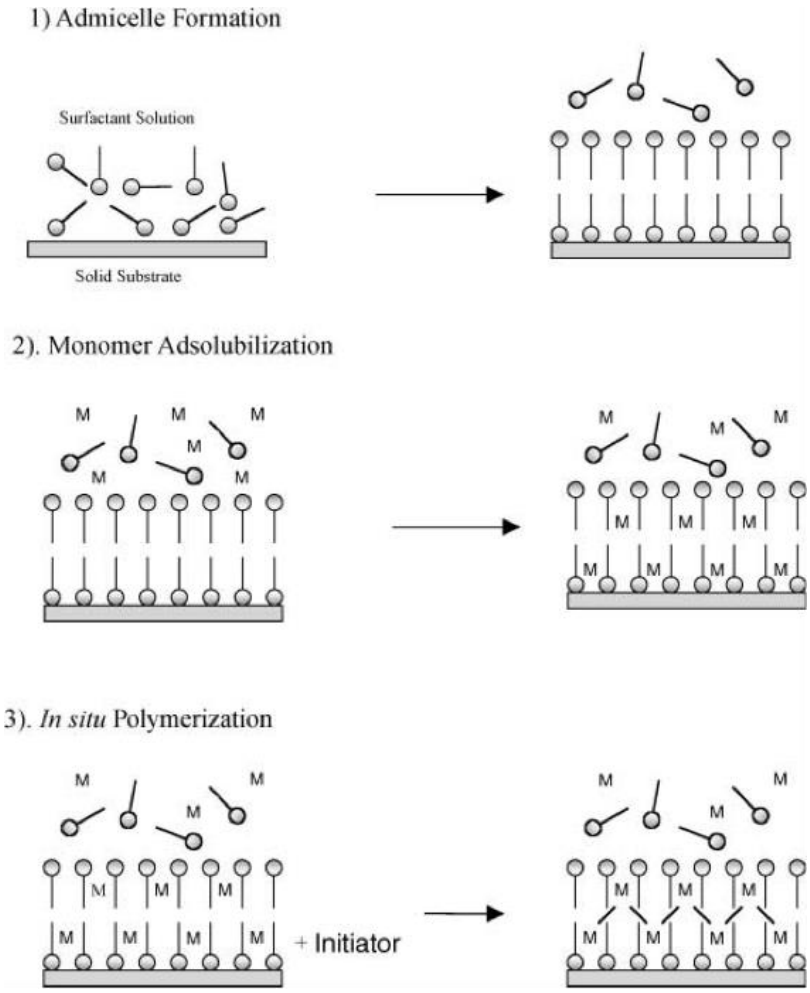


Figure 1. The process of admicellar polymerization [57]

Admicellar polymerization is a three-step process; in the first step surfactants are adsorbed on the fabric and monomers are adsolubilized are incorporated into the surfactant layer; in the second step the monomers are polymerized to give the polymer film with the desired properties and the third step consisted of rinsing of the fabric samples to remove the excess surfactant adhering to the surface. As shown in Figure 1,

adsorption of surfactants and adsolubilization of monomer are the crucial steps in the process. Figure 2 shows the adsorption isotherm of surfactant. Equilibrium supernatant concentration of surfactants were plotted against surfactant adsorbed to obtain the amount of surfactant adsorbed on the substrate surface. Adsolubilization can be defined as the excess concentration of a species at an interface in the presence of an admicelle that would not exist in absence of admicelle. Some earlier work had reported the behavior of surfactant adsorption and adsolubilization on surfaces like precipitated silica[10-12], alumina[3, 13-17], cellulosic surfaces[18]. The study of adsorption and adsolubilization of surfactants is used to identify optimum concentration and can be used in estimating the amount of polymer layer formed on substrate surface.

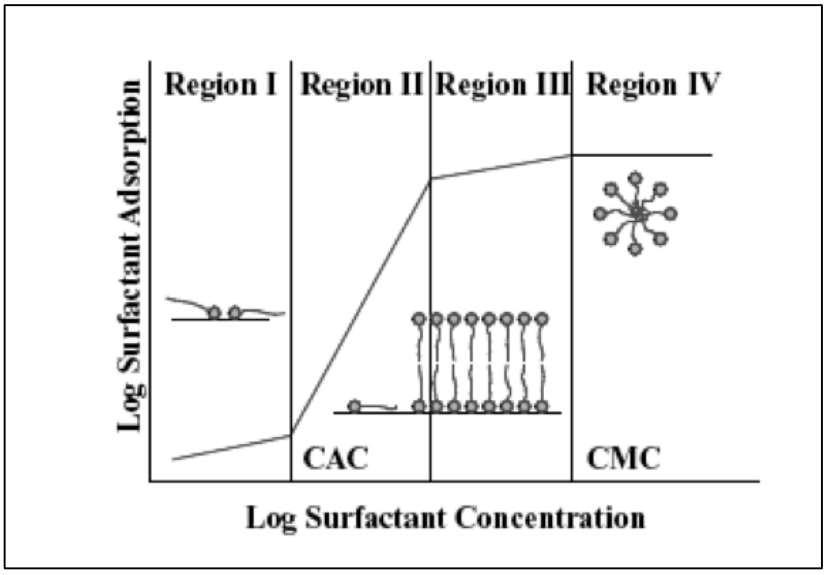


Figure 2. Representation of adsorption isotherm of surfactants [57]

1.2 Organisation of Dissertation

The objective of the research is to utilize admicellar polymerization (AP) to develop formulations to obtain thin film coatings on the substrate surfaces. The solid surfaces used here are cotton and multi-walled carbon nanotubes. Both the surfaces of solids are

of different structure. The limitations to develop formulations were utilize commercially available chemicals, utilize minimal amount of chemicals, highly efficient properties without disturbing the structure of the substrate surface.

The dissertation is divided into two parts. In part I, is about developing thin film coatings to cotton fabric to obtain stain resistant/stain release properties. Cotton has been widely used material to make garments and fabrics for many years. Cotton is more comfortable to wear compared to synthetic fibers and materials and widely used in manufacturing a variety of fabrics and garments such as clothing, draping, upholstery accessories and so on. Due to its chemical structure, which consists mainly of cellulose, it is very absorbent. Enhancing the properties of cotton by imparting stain resistant/stain release properties can extend its usage. Part I contains three chapters. Chapter 2 describes the study of adsorption and adsolubilization measurements on cotton fabric. Adsorption isotherms for the fluorosurfactants and adsolubilization data for the monomers were developed to obtain the amount of chemicals adsorbed on the cotton surface. Aggregation numbers of fluorosurfactants were calculated using the two-site adsolubilization model. Chapter 3 describes formulations developed to obtain thin film coatings on the cotton surface. Admicellar polymerization method was used to develop the thin film coatings on cotton fabric and characterized using different analytical techniques like SEM, EDS, tensile test measurements, stain recovery and stain release tests. The samples prepared with our formulations were tested with commercially available samples to analyze the performance. Chapter 4 describes the scale up of process from laboratory scale to pilot scale unit. Laboratory pilot scale unit Werner Mathis Labomat, was used to scale up the process. The interesting problem here is the

mixing of the system. The mixing in the system resembles a rocking reactor. Equations were developed based on the inclination and position of the reactor to obtain the optimal mixing characteristics. Experiments were conducted with the optimal mixing parameters to analyze the performance of the cotton fabric.

Part II is about the development of thin film coatings to multi-walled carbon nanotubes to develop a nanocomposite, which has hydrophilic properties. Carbon nanotubes (CNTs) are ideal reinforcing fibers for composites because of their high aspect ratio, high mechanical strength, and high electrical and thermal conductivity. Unfortunately, bundling due to intertube van der Waals and solvophobic interactions impairs many applications. As one approach, development of polymer coatings with hydrophilic properties on the surface of nanotubes might facilitate redispersion/solubilization of MWCNTs in aqueous media without any external means. Such modification of MWCNTs could more easily extend the application to multiple fields. Chapter 5 describes the development of formulation to obtain thin film coatings on the MWCNTs surface. In the development of formulation, we used modified admicellar polymerization technique to obtain the coatings on the surface. Adsorption isotherms and adsolubilization data were obtained for the surfactants and monomers used. We modified the two-site adsolubilzation model to obtain the aggregation number of surfactants and we addressed a binary adsolubilization model to predict the co-monomer composition in the formulation. The polymer formed on the surface was analyzed using different analytical techniques like SEM, EDS, TGA and FTIR. Chapter 6 describes about the similar formulation developed to obtain the hydrophilic properties with MWCNTs. We used a different set of monomers to develop the formulations. The

change of monomer is to minimize the time of formulation development. The performance of the polymer formed on the nanotube surface was analyzed using SEM, EDS, FTIR and TGA analytical techniques. Copolymer of a hydrophilic monomer and hydrophobic monomer were formed on the surface on nanotubes. To determine the percentage monomer composition and copolymer composition, Fineman-Ross and Kelen-Tüdos methods were employed. Finally, chapter 7 concludes with summarization of the results and findings obtained from all the chapters.

PART I

Chapter 2

Two-site Adsolubilization Model of Incorporation of Fluoromonomers into Fluorosurfactants Formed on Cotton Fabric

2.1 Abstract

The adsorption of surfactants and adsolubilization of organic compounds on knit cotton fabric are fundamentally important in admicellar polymerization to impart characteristics like water repellency, stain resistance and flame retardancy. The main objective of this research is to study adsorption and adsolubilization of fluororsurfactants and fluoromonomers used to obtain water repellency characteristics. Adsorption of non-ionic (fluoroaliphatic amine oxide) and cationic (fluoroaliphatic quaternary ammonium surfactant) flurorsurfactants at the interface of cotton is investigated with and without fluoroacrylate monomers. Two-site adsolubilization model was used to predict the aggregation number of fluorosurfactant.

Adapted with permission from *Langmuir*. 2014, 30(13), 3665-3672. Copyright 2014 American Chemical Society.

2.2 Introduction

A great deal of work has been done on surfactant adsorption and adsolubilization at solid/liquid interfaces over the past few decades. Adsorbed aggregates (admicelles and hemimicelles) are formed on solid surfaces above the critical admicelle concentration (CAC) and lower than the critical micelle concentration (CMC). Factors like electrostatic attraction, hydrogen bonding, and lateral interactions between adsorbed species help to determine conditions leading to admicelles in a particular combination of surfactant, solvent and substrate[19].

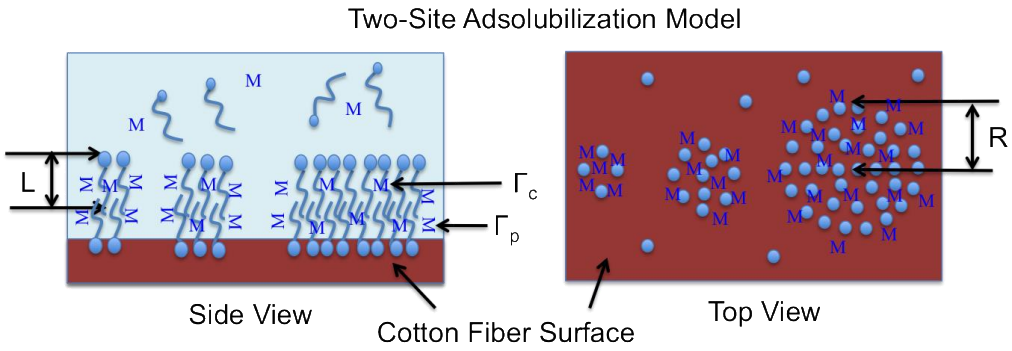


Figure 3. Two-site adsolubilization model on cotton surface

Whether continuous or discrete, admicelles act to concentrate species at the interface as they incorporate sparingly soluble organic compounds that are poorly adsorbed or not adsorbed at all in the absence of surfactant. While surfactant adsorption potentiates adsolubilization, the presence of adsolubilizate can reciprocally influence adsorption of surfactant due to the nature of the interactions of the organic species with the solvent and amphiphile. Fundamental knowledge on adsorption and adsolubilization has aided the development of applications. These include surfactant based separation processes[14, 20], isolation of pharmaceuticals[21, 22], formation of polymeric thin films[1, 5, 23-27], material synthesis for cosmetics and health care[28], waste water

treatment[29-32] and reactions by admicellar catalysis[33]. In particular, adsolubilization of monomer enabled admicellar polymerization over solid substrates like titanium dioxide[34], polyester[35], collagen fibers[36], cotton[5, 24], alumina and silica[37, 38].

The range of utility reflects how adsolubilization can occur over many substrates with suitable choice of surfactant and conditions. Research has been carried out on adsolubilization and the effect of solution pH, surfactant concentration and type of hydrocarbon surfactant for solid surfaces like alumina, precipitated silica, and cellulose fiber by utilizing different hydrocarbon compounds[39-42]. The concept of adsolubilization phenomena of organic compounds on different solid surfaces with single and mixed surfactant systems has been reviewed by Esumi[43].

In general adsolubilization increases with the extent of the admicellar phase. Li and Wang for example, found that adsolubilization of dihydroxybenzene into cetyltrimethylammonium bromide (CTAB) over silica increases with surfactant concentration and saturates at CMC of CTAB[44]. The sites available for incorporation of molecular species are greater as surfactant coverage approaches plateau adsorption while the nature of these sites can change according to the two-site adsolubilization model. The two-site adsolubilization model derives from the concept of patchwise adsorption which incorporates counterion concentrations, surfactant surface aggregation, surface heterogeneities and hydrophobic effect to estimate surface adsorption values[45]. With patchwise adsorption, species can partition within adsorbed surfactant aggregates and at the outer perimeter of aggregates as illustrated in Figure 4. Comparison of findings for alcohols and alkanes provided insight for the two-site

adsolubilization model. At low coverages, the ratio of aliphatic alcohols to surfactant is high and decreases to a constant value for plateau adsorption. Alkanes however partition only into the interior with similar ratio over the full isotherm[46]. Interestingly, See has reported observation of a two-dimensional level transition with adsolubilization of styrene in cetyltrimethylammonium bromide (CTAB) aggregates[47]. These observations were important to the confirmation of the two-site model[45]. Other work by Behrends suggests location within the admicelle is different still for aromatic compounds, the study of which led to a three-site adsolubilization model[48].

Lee et al., applied the two-site adsolubilization model to the adsorption of sodium dodecyl sulfate and adsolubilization of different alcohols and alkanes on alumina [46]. His results yielded estimates of the admicellar aggregation numbers for that system. Aggregation numbers for sodium dodecyl sulfate (SDS) ranged from 60 molecules/aggregate at one hundredth of bilayer coverage (0.06 molecules/nm^2) to 25000 molecules/aggregate at one-half bilayer coverage (3.3 molecules/nm^2). In the region of the isotherm near the onset of cooperative adsorption, aggregation numbers on the order of 60 were found, in good agreement with estimates obtained by fluorescence quenching[49].

Little work has been done on adsolubilization with fluorocarbon systems. Lai et al., studied the adsolubilization of fluorocarbon alcohols in perfluoroheptanoate surfactant admicelles on alumina[50]. He determined adsolubilization constants on the order of 10 to 20 to 150 for 2,2,2-trifluoroethanol (FEtOH), 2,2,3,3,3-pentafluoropropanol (FPrOH) and 2,2,3,3,4,4,4-heptafluorobutanol (FBtOH), a trend opposite to that for similar for hydrocarbon systems. Compared to adsorption of hydrocarbon surfactant and

adsolubilization of hydrogen compound interactions, adsorption of fluorosurfactants and fluorocompounds has stronger hydrogen bonding and can have large partition coefficients. As such, these systems merit further research.

The objective of this paper is to study adsorption of zwitterionic and cationic fluorosurfactants and the adsolubilization of fluoromethacrylates on a cotton surface. The two-site model was used to estimate the aggregation numbers and partition coefficients. This study will advance understanding amount of fluoromonomers and fluorosurfactants adsolubilized to form fluoropolymer on surface of cotton to impart oil/water repellent characteristics[51].

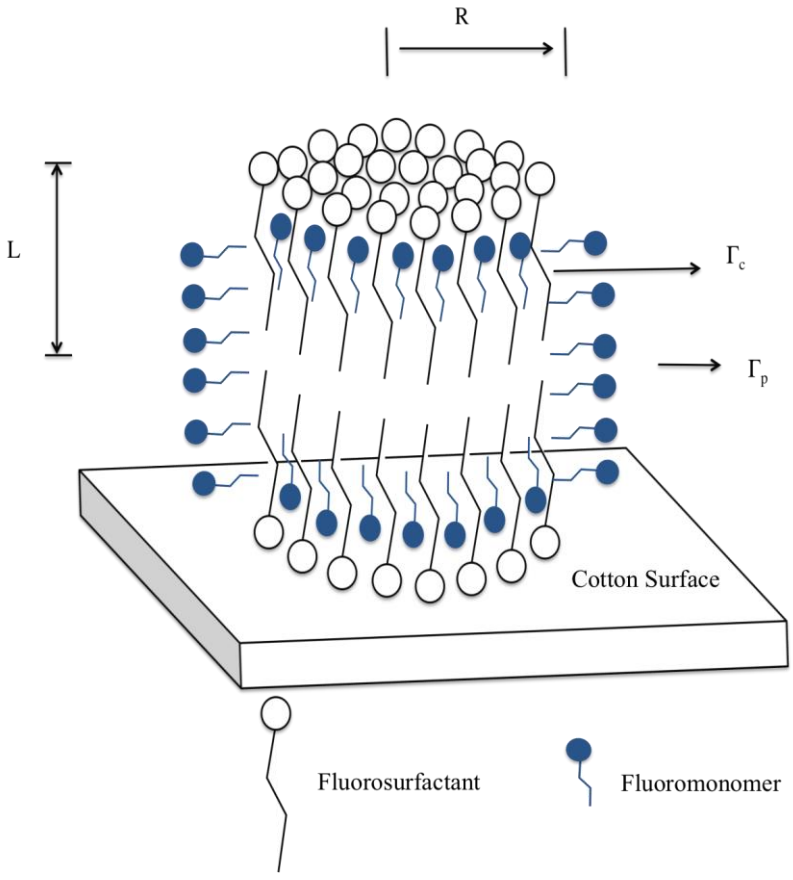


Figure 4. Two-site adsolubilization model

2.2.1 Theory

Figure 4 shows an illustration of the two-site adsolubilization model for fluoromonomer adsolublized into fluorosurfactant admicelles. One site for adsolubilization is in the palisade layer of the admicelle core between headgroups of fluorosurfactant molecules represented as Γ_c. The other site for adsolubilizates with a hydrophobic moiety is on hydrophobic perimeter of cylinder-shaped admicelles represented as Γ_p. The total adsolubilized amount of alcohol (Γ_a) can be expressed as

$$\Gamma_a = \Gamma_c + \Gamma_p \qquad \textbf{Equation 1}$$

The partition coefficient (K) of fluoromonomer between admicellar and bulk phases is defined as follows:

$$\mathbf{K} = \frac{\mathbf{X_a}}{\mathbf{C_a}} \qquad \textbf{Equation 2}$$

$$\mathbf{X_a} = \frac{\mathbf{\Gamma_a}}{\mathbf{\Gamma_s}} \qquad \textbf{Equation 3}$$

where X_a is ratio of adsorbed monomer (Γ_a) per adsorbed amount of fluorosurfactant (Γ_s), C_a is equilibrium concentration of fluoromonomer in supernatant. We assume there are no micelles present in supernatant at equilibrium.

At very high surface coverage, close to bilayer formation, the contribution of Γ_p to two-site adsolubilization becomes much less significant with a decrease in ratio of perimeter area sites to palisade layer sites. In this case when fluorosurfactant adsorption reaches a complete bilayer ($\Gamma_a \cong \Gamma_c$), experimentally measured partition coefficient for fluoromonomer K_b approximates as

$$\mathbf{K_b} = \frac{\mathbf{\Gamma_c}}{\mathbf{\Gamma_s C_a}} \qquad \textbf{Equation 4}$$

In order to express the adsolubilized amount of fluoromonomer on perimeter of fluorosurfactant aggregates, the lateral surface area, A_l, of a right circular cylinder of radius R and height 2L as shown in Figure 4, can be calculated from

$$\mathbf{A_l = 4\pi RL} \qquad \textbf{Equation 5}$$

where L is the chain length of a fluorosurfactant. Since the two bases of right circular cylinder are composed of headgroups of fluorosurfactant aggregates, the mathematical expression can be stated in terms of cross-sectional area per fluorosurfactant molecule (A_s) and the average aggregation number (N_{avg}) are calculated from

$$\mathbf{2\pi R^2 = N_{avg} A_s} \qquad \textbf{Equation 6}$$

From an assumption that the hydrophobic lateral surface area (A_l) resembles an oil/water interface to the fluoromonomer molecules, one can obtain the value of adsorbed molecules for a fluoromonomer monolayer, A_l/A_a in which A_a is cross-sectional area per fluoromonomer molecule. After multiplying this value by the number of cylinder-shaped fluorosurfactant aggregates (Γ_s/N_{avg}), adsolubilized amounts of fluoromonomer on hydrophobic perimeter of cylinder-shaped admicelles can be estimated as

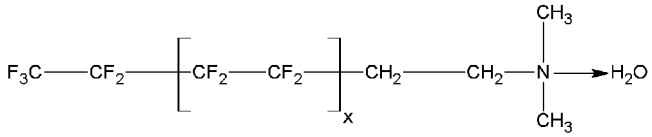
$$\mathbf{\Gamma_P = \frac{A_l \Gamma_s}{A_s N_{avg}}} \qquad \textbf{Equation 7}$$

The combination of equation from 1 and 3-7 yields average aggregation number in terms of known quantities as

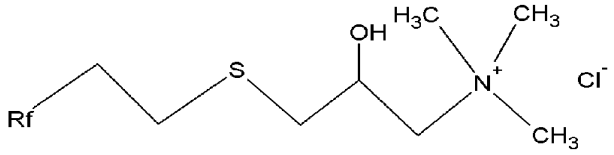
$$\mathbf{N_{avg} = \frac{8\pi A_s L^2}{A_a^2} (X_a - K_b C_a)^{-2}} \qquad \textbf{Equation 8}$$

Numerical values of parameters were listed in Table 1.

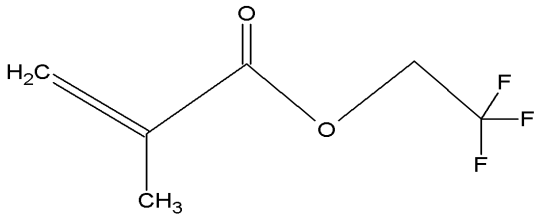
2.3 Materials and Methods



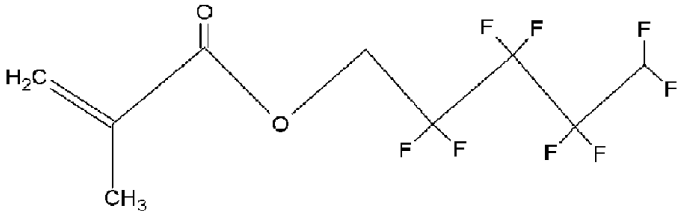
Fluoroaliphatic amine oxide surfactant (FS 230)



Fluoroaliphatic quaternary ammonium surfactant (FS1620)



Tri fluoroethyl methacrylate (TFEM)



Octafluoropentyl methacrylate (OFPM)

Figure 5. Structure of commercial fluorosurfactants and fluoromonomers

2.3.1 Materials

Interlock knit cotton fabric (0.31 m^2/g) was purchased from Alamac American Knits. The fabric obtained was scoured prior to use. Fabric was washed repeatedly until it was free from any remaining surfactant. Zwitterionic fluoroaliphatic amine oxide surfactant (FS230 – 30% active matter) and cationic fluoroaliphatic quaternary ammonium

fluorosurfactant (FS1620 - 20% active matter) were obtained from Mason Chemicals (Figure 5). Fluoromonomers used were octafluoropentyl methacrylate (OFPM) and trifluoroethyl methacrylate (TFEM) purchased from Synquest Laboratories Inc (Figure 5). Chemicals were used as obtained without further purification.

2.3.2. *Experimental Analysis*

Cotton swatches (2.0 g) were placed in 20 ml vials. Fluorosurfactant solutions of various concentrations with a specific concentration of fluoromonomer were added to vials. Solution pH was maintained at 7 without any headspace left in vials. Vials were sealed with aluminum foil and capped with Teflon lined septa held in place with polypropylene caps. Samples were equilibrated at 60 ºC for 2 hrs in shaker bath and kept at room temperature for equilibration for 14 hrs for adsorption and adsolubilization to take place. A small amount of aliquot from vials was filtered with 0.45μm size filters for analysis for HPLC. Adsorption and adsolubilization measurements were determined from concentration changes by using a C18 surfactant column (RESTEK) (dimensions of 250mm x 4.6mm) with an evaporative light scattering detector for surfactants FS230 and FS1620 and a UV-Vis detector for fluoromonomers (245nm).

Mobile phases used for analysis were methanol and water in ratios of 70:30 for FS230 and 80:20 for FS1620 while fluoromonomers OFPM and TFEM were assayed with mobile phase ratio of 70% methanol and 30% water. HPLC analysis was carried out for fluorosurfactants dissolved in HPLC grade water and for fluoromonomers dissolved in HPLC grade isopropanol to obtain retention times and to check for impurities. The peaks obtained by analysis of the fluromonomers and fluorosurfactants were single peaks of high intensity. Calibration curves were obtained for fluorosurfactants and

fluoromonomers followed by measurements to obtain adsorption isotherms and adsolubilization results. Experiments were repeated for different concentrations range from 0.01mM to 100mM for surfactants and 5mM for concentration of monomers.

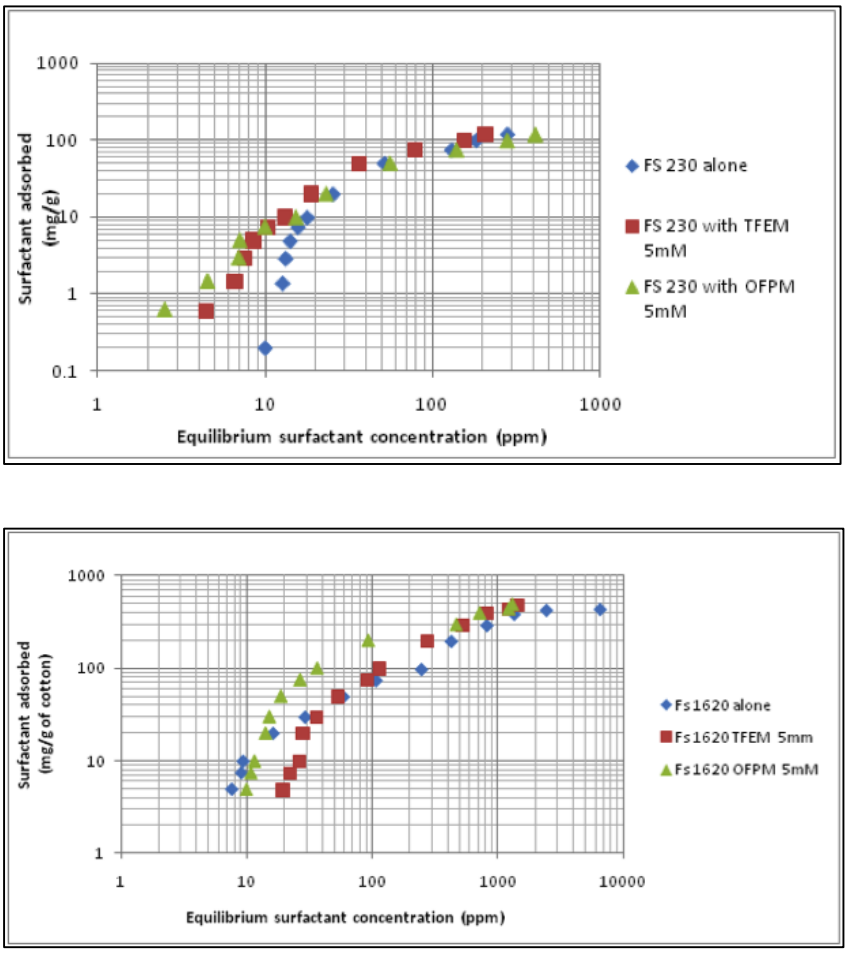


Figure 6. Adsorption isotherm of surfactants alone and in the presence of monomers (a) FS 230 (b) FS 1620

2.4 Results and Discussion

2.4.1 Adsorption Isotherms of Fluorosurfactants

Adsorption isotherms of the fluorosurfactants (FS230 and FS1620) alone and in the presence of fluoromonomers (OFPM and TFEM) are plotted in Figure 6. Adsorption

rises rapidly at lower concentrations with formation of surface aggregates. At the solid-liquid interface, available sites for adsorption on the cotton surface decrease as the supernatant concentration increases. For both surfactants, as surfactant concentration increases the surface becomes saturated leading to onset of micellization. Overall, the adsorption isotherms obtained for FS1620 and FS230 are comparable to isotherms obtained for hydrocarbon surfactants and other fluorocarbon surfactants[14, 50, 52-54]. However, FS230 and FS1620 will have lower CACs and CMCs than corresponding hydrocarbon surfactants because the fluorocarbon chain is more hydrophobic.

In Figure 6b, at around concentration of 200 ppm, a step-wise coverage was observed for FS1620 alone. Inflection points have been widely observed in surfactant isotherms on mineral substrates. These often can be attributed to surface heterogeneities such as the adsorption of cationic surfactants on the edges or basal surfaces of kaolinite[55]. Cotton cellulose does have a high degree of crystallinity with amorphous regions[56] so that surface heterogeneities cannot be ruled out. However, the transition can be explained by another mechanism. Hydroxyl and thioether moieties in FS1620 may hydrogen bond to the cotton substrate at low coverages with a shift in orientation occurring at the inflection point to favor inter-surfactant hydrogen bonding. Reorientation will enable greater lateral interactions of the hydrophobe in addition to intermolecular hydrogen bonding to facilitate the adsorption of additional surfactant. The absence of the inflection point in the presence of the monomer adsolubilizates results from their ability to hydrogen bond in the core.

Presence of monomer affects the adsorption isotherms of the two surfactants differently. Results for FS230 are alike with TFEM and OFPM while the isotherms for FS1620 are

distinct for the two monomers. In Figure 6a, at lower supernatant concentrations, both fluoromonomers significantly increase adsorption of F230. Since the molecular structures of OFPM and TFEM (Figure 5b) differ in the fluoroalcohol component of the methacrylate ester, the similar effect of enhanced adsorption at low surfactant concentration must be due to the carboxylate portion of the adsolubilizate. Given the high ratio of monomer to surfactant under these conditions (Figure 5a), we attribute the shift in the isotherm to a reduction in the rearrangement of water molecules for surfactant in solution versus surfactant in admicelles. For the latter, the hydrophobe is shielded by monomer at the periphery of the admicelles. As coverage increases, the FS230 isotherms merge.

In contrast, the effect of monomer on the adsorption of FS1620 is different for OFPM and TFEM (Figure 5b). Data indicate the presence of OFPM increases surfactant adsorption while TFEM decreases coverage. Structural comparison suggests the fluorocarbon moieties account for the behaviors observed. We suggest greater lateral interaction of the longer fluorocarbon moiety facilitated by the much poorer solubility of OFPM causes enhanced adsorption. It is less clear what causes the reduced adsorption of FS1620 in the presence of TFEM, but it may be due to greater solubility of this surfactant in water with the presence of a rather soluble monomer.

For all cases, the fluoromonomer adsorption has negligible effect on adsorption near the CMC where adsorption of fluorosurfactants levels off. FS230 and FS1620 exhibit a peak adsorption of 100 mg/g of cotton at CMC of 300 ppm and 300 mg/g of cotton at CMC of 3400 ppm, respectively. The CMC's of fluorosurfactants obtained from adsorption analysis were in reasonable agreement with those by surface tension

analysis, as CMC of FS230 is 280 ppm and FS1620 is 3600ppm respectively[57]. CMC of the zwitterionic surfactant is less than that of the cationic surfactant because charge repulsion between head groups is less for the zwitterionic species. The lower adsorption of FS230 compared to cationic FS1620 can be explained by charge attraction since point of zero change (PZC) for cotton is 3[58] and pH in the reactor vial was maintained at 7.

It should be noted that, absent of surfactant, OFPM and TFEM adsorption was negligible. Monomer solubility influenced the behavior in the systems as it does in micellization, playing an important role in either increasing or decreasing the CMC. As chain length of fluorocarbon compounds increase, solubility of monomers in water decrease, thus facilitates partitioning in micelles[50]. At higher concentrations, fluoromonomers can act as co-solvent and reduce hydrophobic attractions and increase the CMC[59].

2.4.2 Adsolubilization of Fluoromonomers

The concentration of fluoromonomers TFEM and OFPM on the surface of cotton required the presence of fluorosurfactant and observations confirm that the level of adsolubilization depends on extent of adsorption of fluorosurfactant. Determination of the relative amounts of surfactant and monomer at the substrate surface for different system compositions help to enhance understanding of the nature of the admicelle with adsolubilization and provides evidence for the two-site conceptualization. The ratio of fluoromonomer adsolubilized to fluorosurfactant adsorbed decreases with increasing supernatant concentration of surfactant before beginning to level off at or near the CMC (Figure 7). This reflects a higher proportion of perimeter sites available for many small

admicelles at low coverage while core sites dominate as coverage approaches saturation.

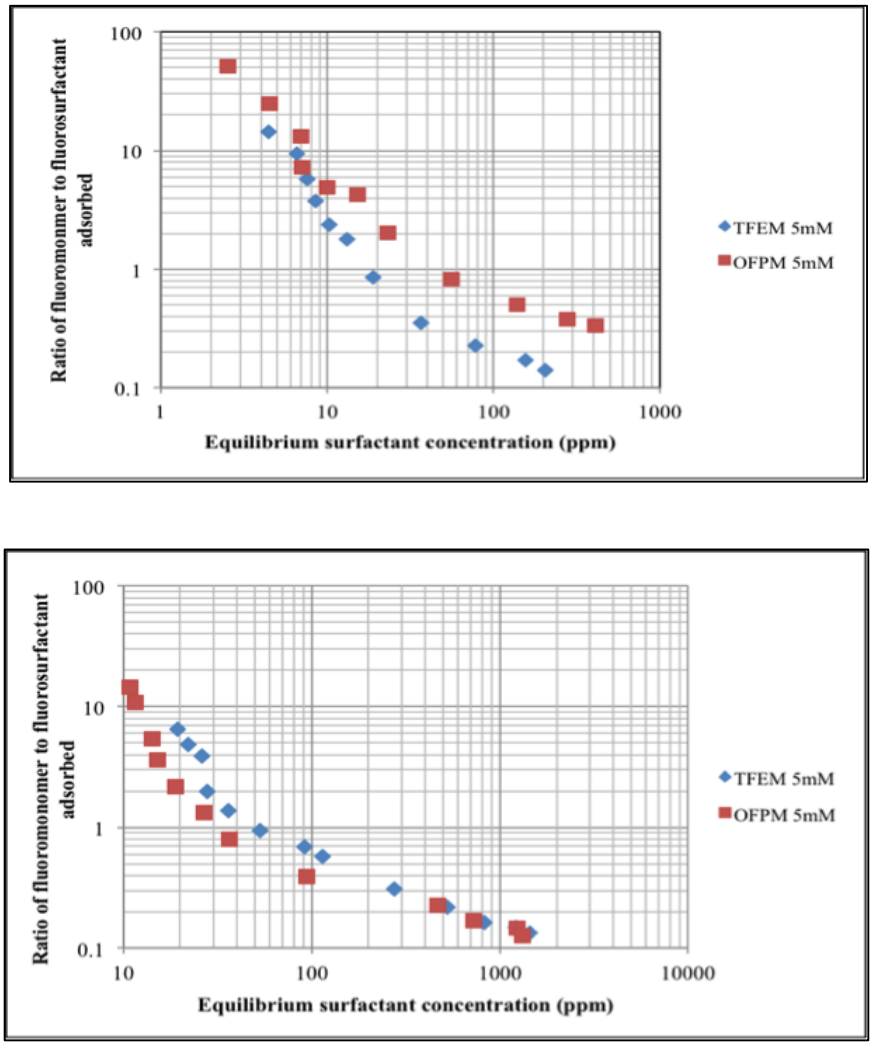


Figure 7. Ratio of adsolubilized fluoromonomer to adsorbed fluorosurfactant

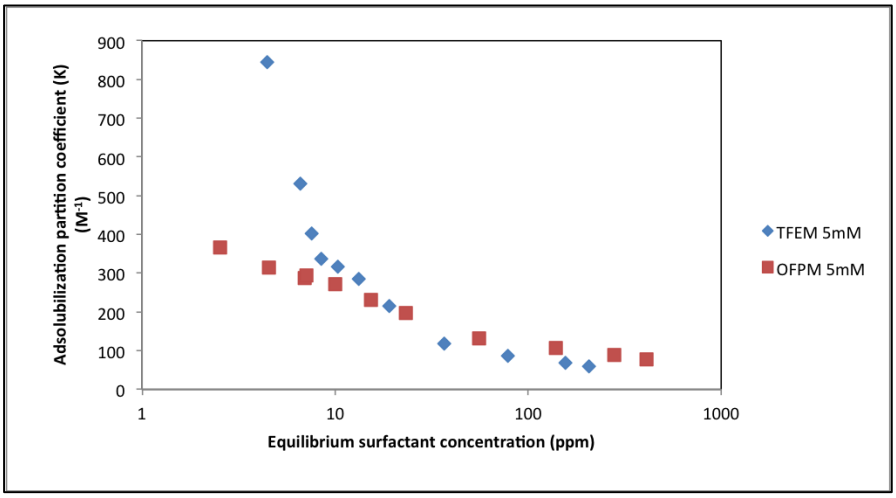
(a) FS 230 (b) FS1620

Similar overall behavior was observed for both zwitterionic and cationic surfactant systems. The effect of monomer chains on the ratio however was different for the two surfactants. In the case of zwitterionic (FS230) surfactant, the chain length dependence of monomer had a distinct effect on the ratio of monomer to surfactant at higher

supernatant concentrations of FS230. Higher ratios were found as the ester alcohol chain length changed from C3 monomer (TFEM) to C8 monomer (OFPM)(Figure 7a).

This finding can be explained by much poorer water solubility of OFPM compared to TFEM. While lateral interactions between fluorocarbon moieties will be superior for OFPM, they cannot explain the results for FS 1620 where similar ratios are seen for the two monomers (Figure 7b). We believe the hydroxyl group in this surfactant causes more water molecules to be present in the admicelles of 1620 and thereby facilitating adsolubilization of TFEM.

The decreasing trend in the ratio of monomer to surfactant generally follows observations by Yeskie[60] for hydrocarbon systems and reflects the transition from perimeter sites to palisade sites. The trend is characteristic of two-site adsolubilization and was observed also for fluorocarbon systems by Lai who studied fluoroalcohol adsolubilization in perfluorheptanoate surfactant on alumina surface[50]. In regions of high surface coverage, the ratio of fluoromonomer to fluorosurfactant decreases due to balance between increase of fluorosurfactant adsorption on the surface and available space for fluoromonomer adsolubilization within the core of admicelles.



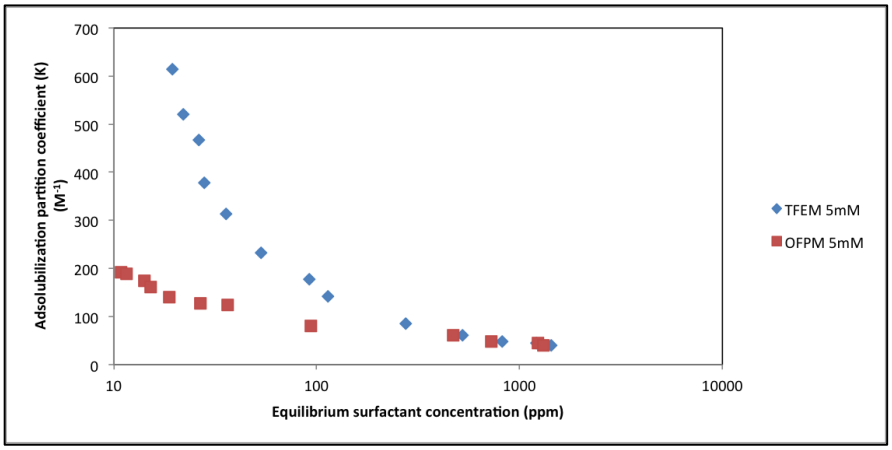


Figure 8. Adsolubilization partition coefficients for (a) FS 230 (b) FS 1620

The partition coefficient for adsolubilization decreases rapidly for TFEM and more gradually for OFPM before becoming constant with increasing equilibrium fluorosurfactant concentration (Figure 8). As surfactant concentration increases, the partition coefficient changes more rapidly for TFEM monomer than for OFPM monomer. This is true for both the zwitterionic and cationic fluorosurfactants. The greater water solubility of TFEM makes it better suited to occupy peripheral sites, which exist in greater proportion at less coverage. In contrast hydrophobic OFPM exhibits little tendency to occupy sites outside of the core. As peripheral sites disappear

with increasing surfactant concentration, the partition coefficient becomes similar for all systems tested with values on the order of 100 M^{-1}.

These results compare favorably with Lai's observations at 0.01M feed concentrations of fluoroalcohol adsolubilized in admicelles of perfluoroheptanoate surfactant[50] in which partition coefficients were reported in the range of 15 M^{-1} to 150 M^{-1} with different fluoroalcohols (Table 1). Lai found that the adsolubilization constant increased with chain length in contrast to the trend for partition coefficients obtained by Yeskie for aliphatic alcohols in sodium dodecyl sulfate[60]. The values for adsolubilization of styrene exhibit a slight dependence on the type of surfactant decreases from anionic to cationic to non-ionic regardless of substrate used (Table 1)[11, 16, 61]. While it is difficult to draw firm conclusions from these data, fluorocarbon surfactant and fluorocarbon adsolubilizates systems generally have lower partitioning coefficient than hydrocarbon surfactant and hydrocarbon species, because fluorocarbon chains are less flexible and the fluorocarbon system is more hydrophobic[41]. This basis can explain Esumi's comparison of the adsolubilization of hexanol and heptafluorobutanol in fluorosurfactants where the hydrophobicities of the alcohols are expected to be similar and yet the adsolubilization constant is greater for hexanol. The admicelle/aqueous partition coefficients for the solutes are governed by molecular packing density in the admicelle, solute-surfactant headgroup interaction and the aqueous solubility of the solutes[62].

Table 1. Comparison of adsolubilization partition coefficient with fluorocarbon and hydrocarbon systems

Surfactant	Monomer	Substrate	Adsolubilization Partition Coefficient (M^{-1})	Reference
Sodium Dodecyl Sulfate (SDS)	Butanol Pentanol Hexanol Heptanol	Alumina	600 150 55 16	[60]
Sodium Dodecyl Sulfate (SDS)	Pyrrole	Alumina	19.9	[63]
Sodium Dodecyl Sulfate (SDS)	Styrene	Alumina	300	[16]
Cetyltrimethylammonium Bromide (CTAB)	Styrene	Precipitated Silica	250	[11]
Triton X-100	Styrene	Silica	220	[61]
Hexadecyltrimethylammonium Bromide (C_{16}TAB)	Naphthalene	Precipitated silica	3000	[64]
Cetylpyridinium Chloride (CPyCl)	2-Naphthol	Silica	870	[65]
Sodium Perfluoroheptanoate	Trifluoroethanol Pentafluoropropanol Heptafluorobutanol	Alumina	15 28 150	[50]
Lithium Perfluorooctanesulfonate (LiFOS)	Hexanol Heptafluorobutanol	Alumina	402 270	[41]
Lithium Dodecyl Sulfate (LiDS)	Hexanol Heptafluorobutanol	Alumina	314 210	[41]
Fluoroaliphatic Amine Oxide Surfactant (FS 230)	OFPM TFEM	Cotton	76 58	
Fluoroaliphatic Quaternary Ammonium Surfactant (FS 1620)	OFPM TFEM	Cotton	66 72	

2.4.3 Surfactant Aggregation Numbers on Cotton

Aggregation numbers of fluorosurfactant were obtained by the two-site adsolubilization model using the parameters given in Table 2. The exact structure of the commercial surfactants weren't known, so molecular weight of both surfactants were inferred based on assumptions for number of carbon atoms and comparing to similar hydrocarbon surfactant CMC[66] with a fluoromethylene equated to 1.5 methylene units. An

increase in the number of carbon atoms increases the length of extended tail of surfactants but has relatively little effect on aggregation number estimation. Cross sectional areas of surfactant head group (A_s) and monomer head group (A_a) were obtained from literature with similar head group[66]. From aggregation number, the number of monomer molecules present in admicelles can be estimated.

Table 2. Numerical values used for calculating aggregation number in two-site adsolubilization model

	FS230		**FS1620**	
Category	TFEM	OFPM	TFEM	OFPM
L[a] (nm)	1.5	1.5	2.5	2.5
A_S[b] (nm^2)	0.47	0.47	0.45	0.45
A_A[c] (nm^2)	0.263	0.263	0.263	0.263
K_{APC}[d] (M^{-1})	58	76	76	66

[a]Theoretical length of fully extended fluorocarbon tail of surfactant. [b]Adsorption density of fluorocarbon surfactant at air/water interface. [c]Adsorption density of fluoromonomer monolayer at oil/water interface. [d]Estimated from an experimentally measured partition coefficient at bilayer coverage.

Analysis with the two-site adsolubilization model yielded aggregation numbers from order 1 to 10^6. As the surfactant molecular density increases at solid/liquid interface, the sites available in the core region increase and Γ_c dominates, so aggregation number rises. Fluorocarbon surfactant can adsorb both from aqueous and hydrocarbon media

because of their thermodynamic stability[67]. Aggregation numbers were slightly higher for OFPM compared to TFEM for the zwitterionic surfactant (FS230) while the opposite was found for the cationic surfactant FS1620. The opposite trend for FS1620 is believed to be due to hydroxyl group of surfactant allowing water in admicelles thereby facilitating adsolubilization of TFEM molecule.

From Figure 9, as density of surfactant increased aggregation number calculated from the model almost followed a linear increasing trend on a log-log plot. Compared to aggregation numbers reported with hydrocarbon alcohols[46] and fluoroalcohols[50], aggregation numbers for both the zwitterionic surfactant and cationic surfactant in this study were similar ranging from 1 to 10 to over 10^6. Affinity between fluorocarbon-fluorocarbon compounds was stronger than hydrocarbon-hydrocarbon compounds because the formation of aggregates depends on degree of interaction between the two compounds and hydrophobicity of fluoromonomers and lower head group charge of flurosurfactants[50, 53]. Aggregates of fluorosurfactants formed on solid/water interface are stronger because of strong C-F bond and of electronegative fluorine that shields carbon[68]. Fluorinated surfactants are more surface active and more hydrophobic than their corresponding hydrogenated surfactant[54].

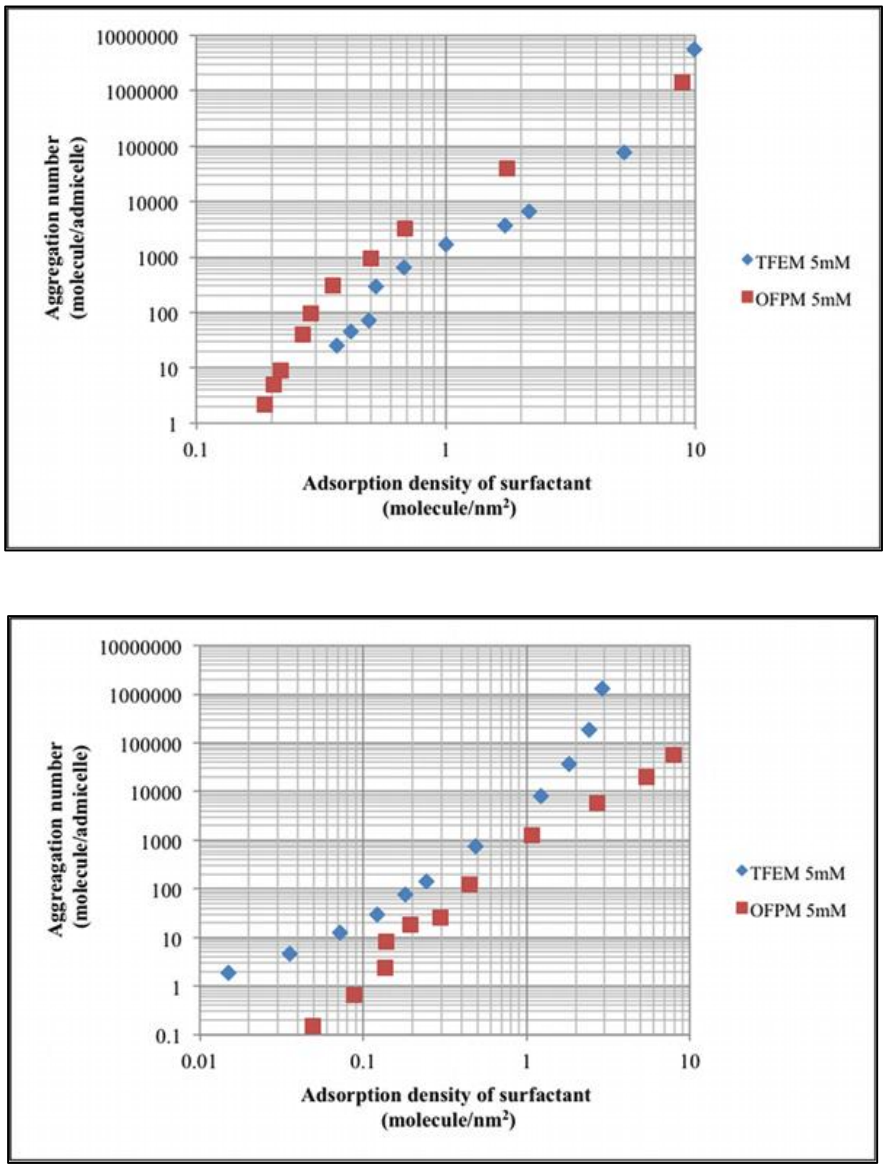


Figure 9. Aggregation number for fluorosurfactants in presence of fluoromonomers (a) FS 230 (b) FS1620

2.5 Conclusion

Experimental measurement of adsorption and adsolubilization for fluorocarbon monomer-surfactant systems yields results consistent with the two-site adsolubilization model. A water-soluble monomer TFEM more effectively occupied peripheral sites.

Partition coefficients and aggregation numbers were comparable to values observed for hydrocarbon and fluorocarbon alcohol-surfactant systems.

Chapter 3

Stain Resistance of Cotton Fabric before and after Finishing with Admicellar Polymerization

3.1 Abstract

Environmental concerns related to perfluoroctanoic acid (PFOA) led to a re-examination of the methods for imparting stain resistance and stain repellency to textiles. Non-PFOA fluoropolymer finishes have been formed on cotton knits by admicellar polymerization, a surface analogue of emulsion polymerization. Fabric samples were characterized by a drop test, contact angle measurements, SEM, elemental analysis and durability studies. Stain resistance and stain release properties were assessed by reflectance and AATCC tests with results comparing favorably with swatches from commercially available garments. Admicellar polymerization enabled the formation of durable finishes that exhibited high performance in stain resistance and stain repellency.

Adapted with permission from *Appl. Sci.* 2012, 2(1), 192-205. Copyright 2012 MDPI.

3.2 Introduction

In recent years, several technologies have been developed for modifying cotton blends and cotton as multi-functional textiles. Surface modification of cotton fabrics can impart wrinkle free finishes, self-cleaning properties, anti-microbial activity, UV protection, and flame retardancy[69, 70]. Self-cleaning features include stain release and stain repellent or resistant finishes[71]. The latter of these, acts to block the uptake of the blemishing agent. Liquids like coffee, soda, oil and water, bead up on fabric when spilled and can be wiped off without staining the fabric. In contrast, a stain release fiber coating may allow oil and aqueous staining materials to penetrate the fabric and then, when the fabric is laundered, ideally enables the stain to be easily removed.

Fluorochemical coatings dominate the stain repellency textile apparel market. Out of all existing textile chemicals, only fluorochemicals have shown the unique property to provide fabrics a sufficiently low surface energy coating able to resist penetration of both oil and water-based stains (polar and non-polar liquids). Unfortunately, fabrics modified with fluorochemicals by conventional textile finishing methods often show poor performance with laundering or wear [72].

Application of perfluorochemicals can be accomplished in a variety of ways, many of which impart hydrophobicity and/or oleophobicity to fabrics in addition to other desirable properties. Scientists at the German Textile Research Centre North West, for example, obtained a hydrophobic coating of perfluoro-4-methylpent-2-ene by photonic surface treatment with a pulsed UV-laser [69]. Similarly, pulsed plasma polymerization of monomers with long perfluoroalkyl chains by Badyal and co-workers yielded a hydrophobic thin film coating [73]. Superhydrophobic mats have been prepared with

initiated chemical vapor deposition involving polymerization of perfluoroalkylethyl methacrylate [74] while Gleason and co-workers used initiated chemical vapor deposition to coat electrospun non-woven fabrics, also with superhydrophobic character [75]. In a very different approach, direct fluorination of twaron fiber with elemental fluorine not only changed the nature of the fiber surface, it also increased mechanical and thermal properties of a fiber composite [76]. Sol-gel methods have been successfully employed to impart oil/water repellency and anti-bacterial capability to cotton using fluorocarbon polymer/SiO_2 and silver nanoparticle-doped silica hybrid materials, respectively [77, 78]. Lastly, nanoparticles of fluorochemical coated silica and of gold have been applied to cotton and other fabrics to create a chemically inert fiber surface with superlyophobic properties [79-84]. This broad range of approaches reflects the interest and challenges in this area.

Admicellar polymerization is an in situ polymerization reaction proceeding within surfactant aggregates formed at the interface between the substrate and a supernatant solution. The technique, a surface analogue of emulsion polymerization, has been used to form a variety of polymeric thin films on different solids such as polystyrene and poly methyl methacrylate over silica and alumina [1-3, 85]. Recently, admicellar polymerization has been expanded into the textile area with application of finishes to impart functionality like flame retardancy, blocking of UV radiation, and water repellency [86-88]. This method is a simple, water-based process using low energy and a small amount of chemicals. Since the thickness of the film formed is typically on the order of nanometers to tens of nanometers, the fabric surfaces retain softness and feel.

In this paper we examine the use of admicellar polymerization to prepare knit type cotton fabric with stain release/stain resistant features. The fluoropolymer finishes are characterized by standard and improvised test methods and compared to commercially available stain release/stain resistant fabrics for performance and durability.

3.3 Materials

Interlock type knit cotton fabric was purchased from Alamac American Knits (Lumberton, North Carolina, USA). The fabric was scoured and then prior to use, rinsed several times in a washing machine until it was free from surfactant. Reference samples from a commercially available, off-the-shelf stain resistant knit shirt (designated Ref. 1) and from commercially available, off-the-shelf stain resistant woven slacks (Ref. 2) were purchased from local stores for comparison purposes. Short and long chain partially fluorinated alkyl acrylates were purchased from Synquest labs Inc. (USA) while fluorosurfactants were obtained from Mason Chemicals (USA). A water-soluble persulfate initiator and an acrylamide-bonding agent were purchased from Sigma Aldrich (USA). All chemicals were used without further purification.

3.4 Preparation of Samples, Admicellar Polymerization

Modification of interlock knit cotton swatches was carried out in 24 mL glass vials. Reaction media consisted of fluorsurfactants at the cmc and either a short chain or long chain fluoroalkyl acrylate ester fluoromonomer (5 mM) with the corresponding respective polyacrylates designated as PA1 and PA2. Concentrations of initiator (5 mM) and bonding agent (1 mmol/g) in DI water at pH 4 were added to vials. Swatches of washed cotton fabric weighing 2.0 g were added to the vials. The reaction was carried out at 80 °C in a shaker bath at 80 rpm with an adsolubilization period of 2 h and a

polymerization time of 2 h before being rinsed and dried in an oven at 80 °C. Samples were repeatedly home laundered using detergent (Tide) in a laboratory washing machine at 30 °C for 20 min and dried in conventional tumble dryer at 60 °C for 45 min to test durability of treated fabric.

3.5 Characterization of Treated Fabric

Modified cotton knits and reference samples were characterized by wetting times, static contact angle determination, SEM, elemental analysis, stain resistance and stain recovery measurements.

3.5.1 Water Repellency Tests

Two test methods were employed for assessing water repellency. The first involved a simple drop test, with 20 µL water being deposited from a pipette at a height of 1 cm. Time for absorption of water (wetting time) on a fabric surface in the drop test was determined up to maximum of 30 min, at which point the sample passed. A second method was performed according to AATCC test method 22 (spray test). This method requires larger samples that were prepared by carrying out admicellar polymerization in a Werner Mathis Labomat Type BFA 16 beaker dyeing unit.

3.5.2 Contact Angle Analysis

Contact angle is a quantitative measure of the wetting of a solid by a liquid, which can evaluate the potential for water and stain repellency. We performed static contact angle measurements using an optical tensiometer (KSV T2000) and software supplied with the instrument. A 20 µL drop of distilled, deionized water of surface tension 72.75 mN/m was deposited on fabric by syringe from a height of 2 cm. Observations occurred over a 10 min period with replicates at five different sites on the fabric.

3.5.3 SEM Study

SEM images of modified and unmodified interlock swatches were taken using a JEOL JSM 880 after the samples were sputter coated with a thin layer of gold. Elemental analyses were carried out using ZEISS 960A SEM equipped with Oxford Link energy dispersive spectroscopy (EDS) with a thin window and using IXRF EDS 2008 software at beam energy of 5 keV. Elemental analyses provided an indication of fluorine content at the surface of the fibers.

3.5.4 Stain Recovery and Stain Resistance Tests

Stain tests were performed on untreated control and treated fabric samples and compared to results for the commercial reference samples. Standardized measurements followed AATCC test method 130, referred to as the oily stain release method, and AATCC test method 118, referred to as the oil repellency test. In AATCC test method 118, 50 µL drops of different grades of hydrocarbon oil specified in the protocol are applied to the fabric material and scored on a scale from 1 to 8. Higher values indicate the point at which ever lighter aliphatic oils penetrate the fabric in a period of 30 s or less and thus greater oil repellency. In AATCC test method 130, the fabric is placed on a blotting paper and 5 drops corn oil of 40 µL each are deposited in the center. A blotting paper is laid on top followed by a 5 lb weight for 60 s. The fabric is washed in the specified manner at 41 °C and evaluated according to the test protocol. To further assess stain resistance and recovery, we examined the effects of common staining materials like oil, mustard and ketchup by reflectance measurements of the fabric samples. Stain resistance measurements were performed after wiping with tissue paper while stain recovery evaluation was done after washing. Reflectance was determined by

using an Ultrascan colorimeter (Hunter Lab) at a wavelength of 440 nm. Percentage of stain resistance and percentage of stain recovery were calculated using the formulas as shown in equation 9 and 10.

$$\%\text{ of Stain Resistance} = \frac{\text{Reflectance of stain on treated fabric after wiping}}{\text{Reflectance of untreated fabric}} \times 100 \quad \textbf{Equation 9}$$

$$\%\text{ of Stain Recovery} = \frac{\text{Reflectance after one wash - Reflectance after staining}}{\text{Reflectance before staining - Reflectance after staining}} \times 100 \quad \textbf{Equation 10}$$

3.5.5 Tensile Strength Measurements

Dumbbell-shaped samples were punched out (using dumbbell shaped die cutter, ASTM D638) from fabric. Tensile strength measurements were performed at room temperature using computerized model testing machine (SSTM tester from United Testing Systems) at a speed of 0.5 in/min according to ASTM D1708. Four measurements for each sample were done.

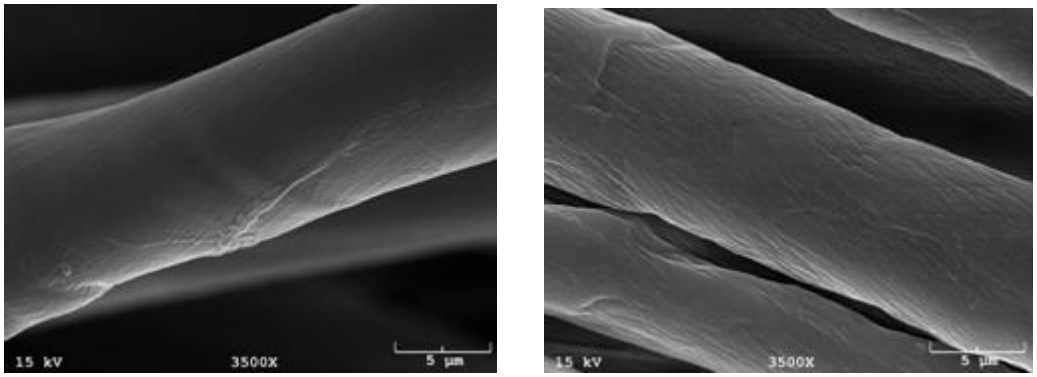
3.6 Results and Discussion

3.6.1 Appearance of Thin Film

SEM images and elemental analysis of the fabric samples before and after admicellar polymerization were obtained. Figure 10(a,b) shows fibers in the untreated cotton fabric samples, the surface of fibers is smooth with striations evident in places. It is devoid of polymer aggregates and any other agglomerations over the surface.

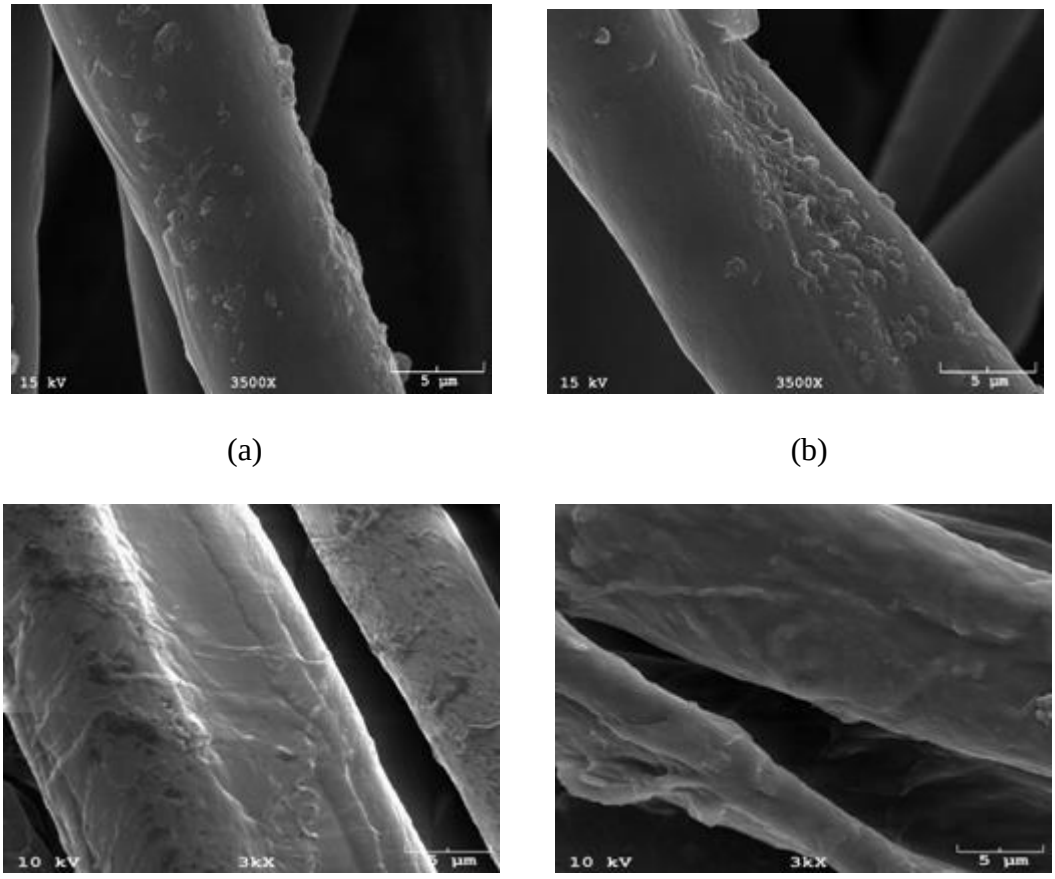
Figure 11 (a,b) shows fibers of treated cotton fabric with PA1 after modification by admicellar polymerization. Compared to untreated samples shown in Figure 10, striations are not visible while a coarse, bumpy appearance indicates formation of fluoropolymer on the fiber surface. Figure 11(c,d) shows fibers in the treated cotton fabric with PA2. In this case, striations are also not visible and fluoropolymer coating can be seen on the surface of fibers. With the longer chain fluorocarbon of PA2, the

coating appears to be more evenly spread as a uniform layer. It is evident in both cases that the coatings are thin.



(a) (b)

Figure 10. Untreated fibers of interlock knit cotton

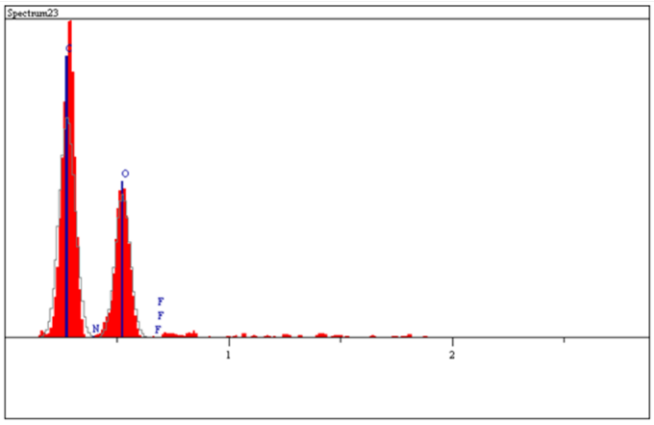


(a) (b)

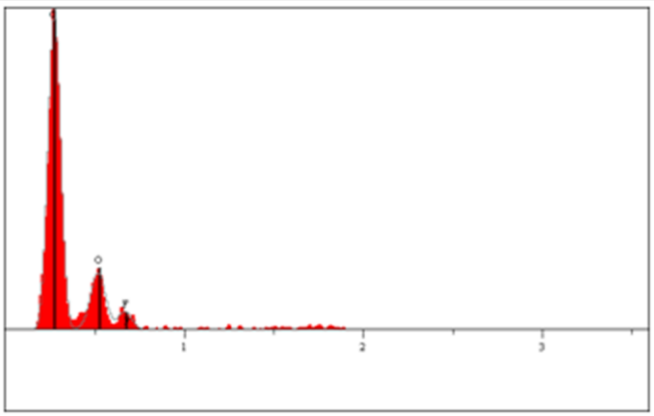
(c) (d)

Figure 11. Interlock knit cotton fibers with PA1 (a,b) and PA2 (c,d)

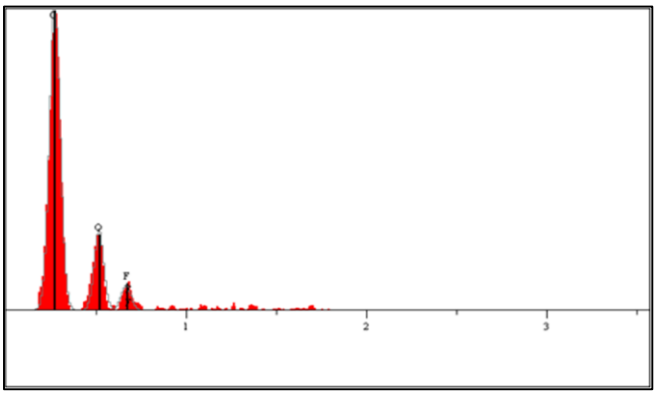
The EDS spectrum of an untreated control sample (Figure 12a) does not exhibit a significant fluorine peak with the resulting elemental analysis for carbon, nitrogen, oxygen and fluorine indicating a fluorine content of only 0.33 atomic%. Carbon and oxygen, the main constituents of the cellulose substrate, give strong peaks. In treated fabrics (Figure 12 (b,c)), distinct peaks are observed for fluorine along with those for carbon and oxygen. Fluorine content in PA1 was 6.89% while in PA2 was 10.53%, consistent with the longer fluorocarbon chains of the latter. The levels of carbon and oxygen observed reflect contributions from penetration of the electron beam through the film and/or regions where the fiber surface was not covered.



(a)



(b)



(c)

Figure 12. Energy dispersive spectroscopy (EDS) spectrum of: (a) Untreated fiber (b) treated fiber with PA1 (c) treated fiber with PA2

3.6.2 Mechanical Characterization

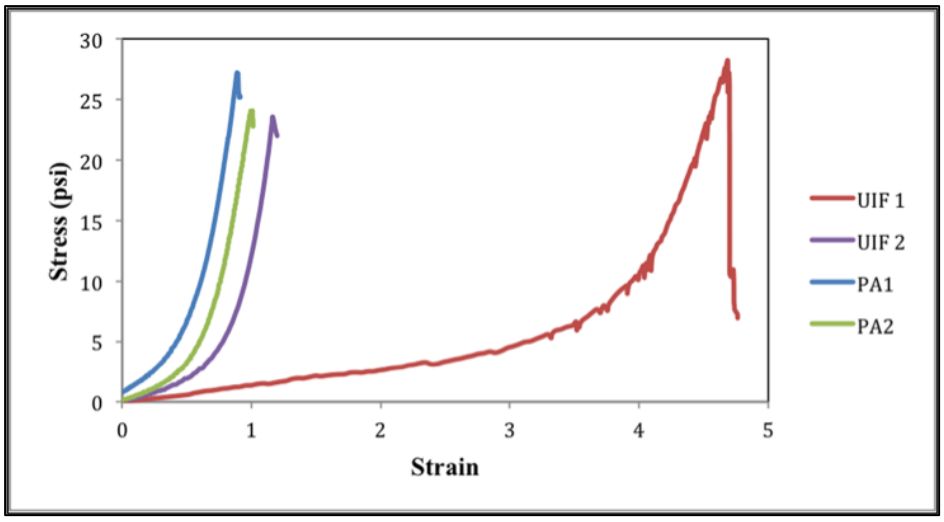


Figure 13. Stress-strain plot of untreated fabric and treated fabric with formulations PA1 and PA2

Figure 13 shows stress-strain relationships of untreated fabric and treated fabric with two formulations PA1 and PA2. UIF1 and UIF2 are results of untreated interlock fabric in two orthogonal directions indicating anisotropic behavior. The Young's moduli of treated fabrics PA1 and PA2 correspond to the higher modulus of the untreated interlock knit, regardless of direction. Greater stiffness of PA1 and PA2 suggest the adhesion between fibers due to formation of polymer bridges between fibers. Between PA1 and PA2, Young's modulus does not differ greatly but PA1 is somewhat stiffer than PA2. These trends mirror observations previously reported for plain and modified pique fabric [86]. Although the Young's modulus increases, these fabrics retain soft feel after modification.

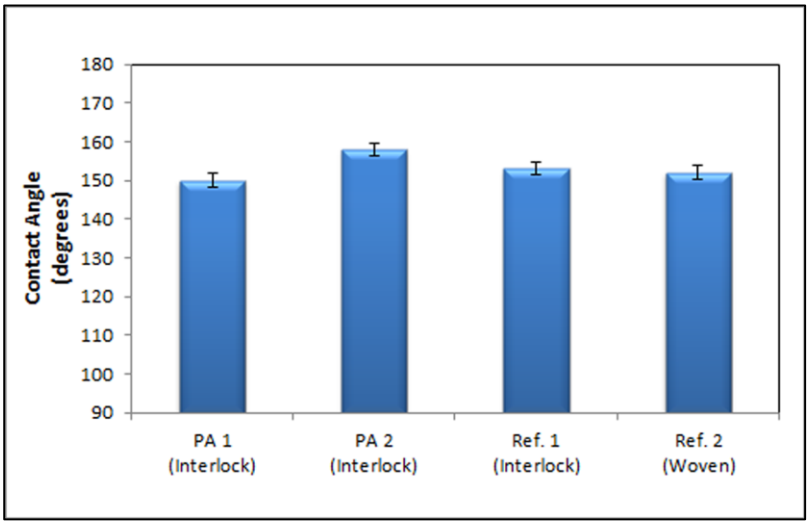


Figure 14. Comparison of contact angles for treated and commercial reference samples

3.6.3 Water-Repellency Tests

Evaluation of fabric hydrophobicity is difficult to assess by any one method. The drop test enables a quick and easy determination, while multiple methods of testing help us to know performance and quality of the material more precisely. To ascertain the water-repellency characteristics of the fabric, the resistance of the fabric to surface penetration by a spray and resistance to surface wetting should be measured. Tests have to be carried out in combination with each other in order to obtain a complete understanding of performance. Samples were assessed for performance using drop test, spray test and contact angle measurement.

Interlock cotton knit modified with polyacrylates PA1 and PA2 displayed drop test results greater than 30 min. In fact, superhydrophobic character was found with contact angles of 150° for PA1 and 160° for PA2. Figure 14 shows static contact angle results for the various fabric samples, all of which displayed strong hydrophobic character. With a contact angle near 160°, PA2 had the highest value observed. The remaining fabric samples have contact angles around 150° or less. Contact angles in this range

result from a combination of chemical composition and surface microstructure. The microstructure includes fibers within the cotton yarns and possibly texture on the surface of the fibers due to the presence of the fluoropolymer. The SEM and EDS data suggest that the higher fluorocarbon content explains why PA2 exhibits a higher contact angle than PA1.

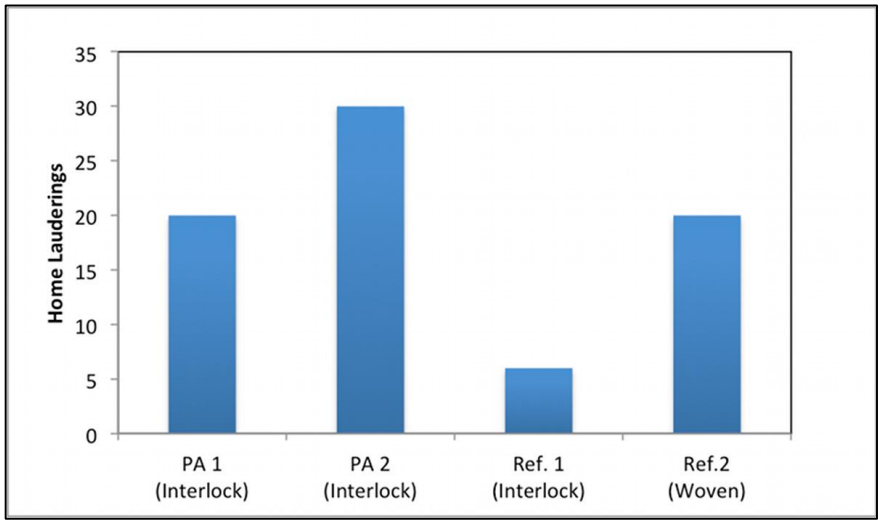


Figure 15. Comparison of durability of treated fabrics with commercial reference samples by the drop test

Samples were repeatedly home laundered with washing and drying steps to gauge durability characteristics. Results for the drop test with number of laundering cycles appear in Figure 15. Treated fabric with PA1 passes with as many as 20 washes while PA2 can hold its treatment up to 30 home launderings. As shown above, PA2 has greater fluorine content and, as such, would be expected to have lower solubility which might explain its ability to endure more home launderings. Findings for fabrics modified by admicellar polymerization were compared to commercial materials. The off-the-shelf knit sample (Ref. 1) fared poorly as it failed the drop test after only 5 washes. The interlock knit material PA1 with the lower fluorochemical content

compared well to the woven commercial sample (Ref. 2) with both passing the drop test for 20 washes. The interlock knit PA2 surpassed them all with 30 washes.

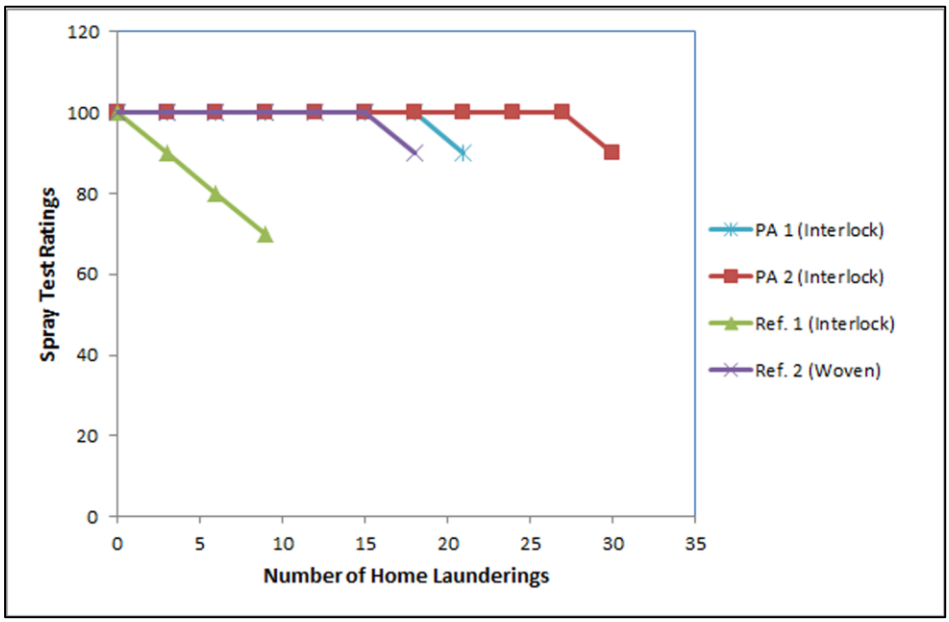


Figure 16. Comparison of spray test of treated fabric and commercial samples

In the spray test (AATCC 22), repellency of fabric is assessed in a dynamic system by comparison to wetting patterns on a standard chart. Measurements of spray test rating were made after a series of home laundering which were discontinued once the fabric failed the drop test. From Figure 16, the interlock commercial sample (Ref. 1) is seen to exhibit a decrease in performance with each home laundering down to a rating of 60 when the drop test result was less than 30 min. The woven material (Ref. 2) performed well with a rating of 100 up to 15 home launderings where it decreased to a rating of 90. Performance of PA1 was comparable to the woven fabric. Notably, PA2 showed substantially greater durability. Trends observed among the different fabric samples by the spray test were consistent with those of the drop test.

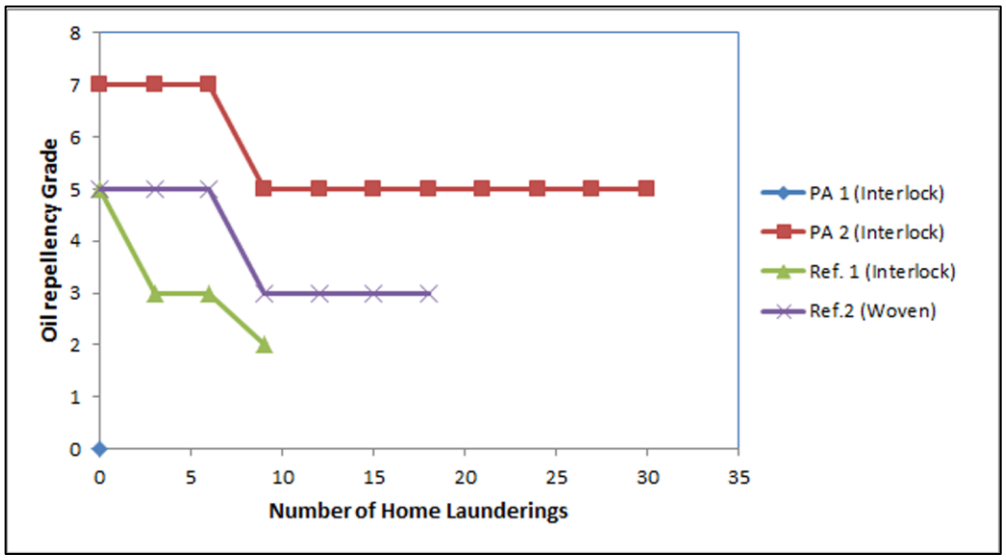


Figure 17. Comparison of oil test for treated fabric with commercial reference samples

3.6.4 Oil Repellency

Oil test results performed according to AATCC test method 118 are reported in Figure 17. Treated fabric with PA1 did not show any oil repellency. In contrast, application of PA2 by admicellar polymerization yielded an initial oil repellency of grade 7. This value dropped to grade 5 after half a dozen home launderings and then remained at grade 5 after many cycles. In fact, it was in these oil repellency tests where the effects of the longer chain fluoroalkyl moiety in polyacrylate PA2 were most evident in its effect on oil repellency. Both off-the-shelf reference samples were rated initially at grade 5. However, interlock sample Ref. 1 degraded rapidly to ratings of 3 and 2. The performance of the woven fabric Ref. 2 paralleled that of PA2, only 2 grades lower throughout. With the exception of PA1, the oil test results for durability corresponded to findings by the water repellency tests.

3.6.5 Stain Recovery and Stain Resistance

Table 3. Stain release grades according to AATCC test method 130

Types of fabric	Stain release grade
Interlock (PA1)	1
Interlock (PA2)	4.5
Interlock (Ref.1)	3
Interlock (Ref.2)	2

The main advantage of a stain resistant and stain recovery finish for fabric is that, when a spill occurs, it can be cleaned easily. Removal of stains during low temperature home launderings is often recommended. Assessment of performance under such conditions can be done according to standard tests, such as AATCC test 130. Results for stain release (Table 3) roughly followed the oil repellency findings except the woven commercial fabric received a lower rating than the commercial interlock fabric. At a grade of 4.5, sample PA2 received the highest rating of the group and PA1 the poorest at 1.

Fabrics were stained with vegetable oil, French's mustard and Heinz tomato ketchup in additional tests. On the basis of the oil repellency and oil release results, sample PA1 was excluded from further testing. After wiping the stain with a tissue paper, stains remained visibly attached to untreated cotton, but, for treated fabric with PA2, all the stains were wiped away. To quantify this, we measured the reflectance of the fabric after wiping the stains for oil, mustard and ketchup. Figure 18 shows the stain resistance performance of treated cotton with PA2 and untreated cotton. PA2 exposed to oil

showed stain resistance of 100% indicating oil can be wiped off immediately. When stains were dropped on untreated cotton, stains penetrated and contributed to lower reflectance. For treated cotton, the various agents did not penetrate and could be wiped off easily so reflectance returned nearly to 100%.

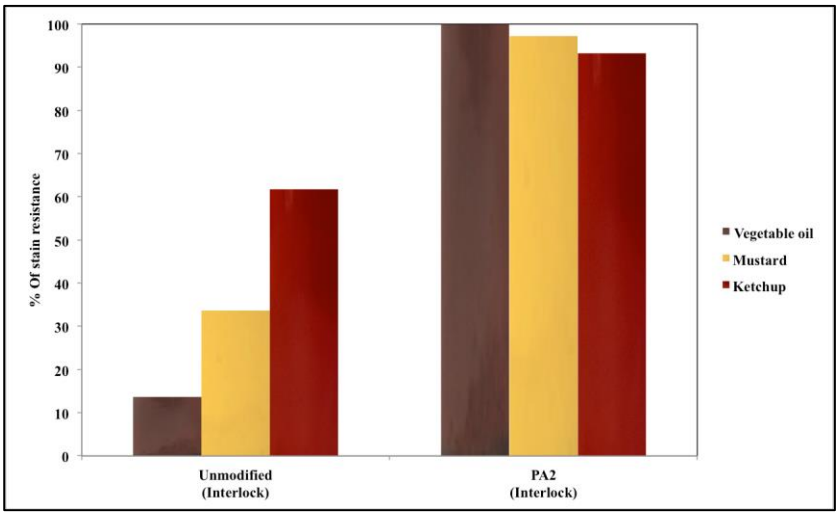


Figure 18. Stain resistance for untreated and treated fabric with PA2 with different staining agents

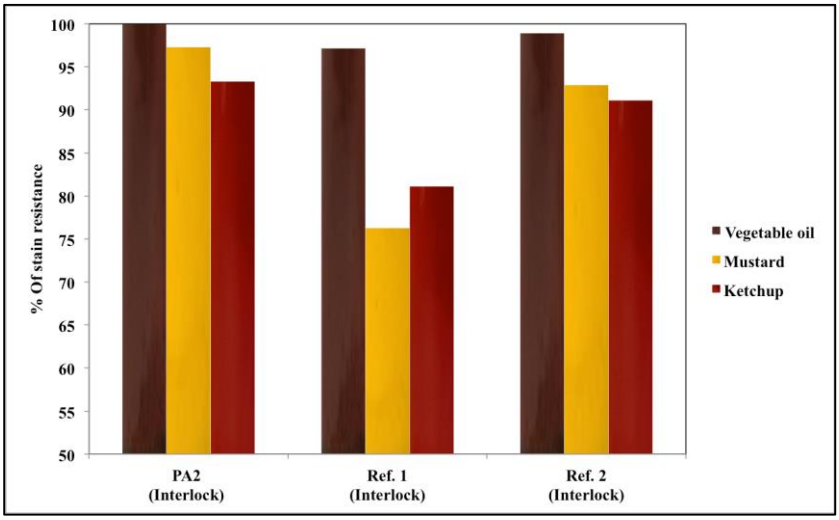


Figure 19. Stain resistance comparison for PA2 and commercial fabrics with different stains

Staining tests were also performed on the commercial reference samples and compared with PA2. Figure 19 presents reflectance measurements of stain resistance for treated and reference samples after exposure to oil, mustard and ketchup. All fabrics performed well in resisting blemishes by oil. Overall, PA2 performed comparably to the woven commercial material and outperformed the commercial knit. The commercial interlock type fabric (Ref. 1) showed poor performance compared to the fabric modified by admicellar polymerization with only about 75% of stain resistance with mustard and about 80% with ketchup. It is a significant finding that the coated cotton knit could function at a level comparable to a fabric with a tighter weave.

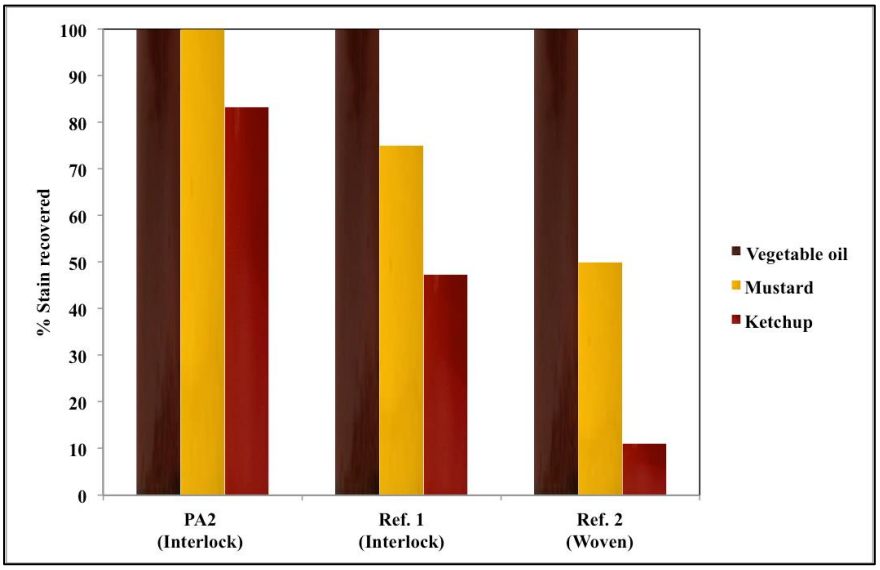


Figure 20. Stain recovery of treated fabric with PA2 compared to commercial reference fabrics

Similar experiments for stain recovery of the fabric were carried out by doing one home laundering and then assessing the level of stain recovery using reflectance measurements. Results for stain recovery are presented in Figure 20. All materials

perform well in removal of oil by washing. Otherwise, stain recovery of PA2 was substantially better than the reference samples.

3.7 Conclusion

Application of fluorocarbon finishes by admicellar polymerization can yield durable cotton fabrics with excellent stain resistance and stain recovery properties. Performance of these fabrics, prepared in a laboratory, compare well to that of commercial production materials examined.

Chapter 4

Admicellar Polymerization and Mixing in a Laboratory Dyeing Unit- A Variant of Rocking Reactors

4.1 Abstract

Mass transfer in a laboratory-dyeing machine, consisting of cylindrical canisters mounted on a carousel with a horizontal axis, has been examined to adapt the unit for modification of cotton by admicellar polymerization. Canisters located at the periphery of the carousel are canted relative to the axis of rotation so that fluid in the canister moves front-to-back and back-to-front over the course of one revolution in a fashion similar to a rocking reactor. Dissolution of benzoic acid in water at 30^{o}C has been used to determine mass transfer coefficients β in the dyeing system as a function of rotational rate and fill volume. Mixing in the dyeing system improved with canister fill fraction to an optimum of 0.9 while rotation rate had little effect over the available range. Findings for β as well as predictions for β obtained from estimates of specific mixing power are compared to values from the literature for a rocking reactor.

The process of admicellar polymerization on cotton was subsequently examined in the laboratory-dyeing machine. Cotton with a water repellent coating prepared in the unit was evaluated using various techniques. Conditions favorable to mass transfer in the model experiments were consistent with those providing optimal performance of the water-repellent coating applied by admicellar polymerization

Adapted with permission from *Ind. Eng. Chem. Res.* 2011, 50(10), 6418-6425.

Copyright 2014 American Chemical Society.

4.2 Introduction

Admicellar polymerization (AP) comprises a general method to modify surfaces with a thin film. Fundamentally similar to emulsion polymerization, adsorbed surfactant structures function as a two dimensional solvent to localize the reaction of monomer at the solid-solution interface. The original embodiment of the technique involved free radical polymerization over porous mineral oxide powders[16]. A robust technique, AP has been used to coat fillers, glass fibers for composites, pigments and magnetic particles for affinity separations[2, 3, 25, 89-93].



Figure 21. A typical infrared laboratory dyeing unit

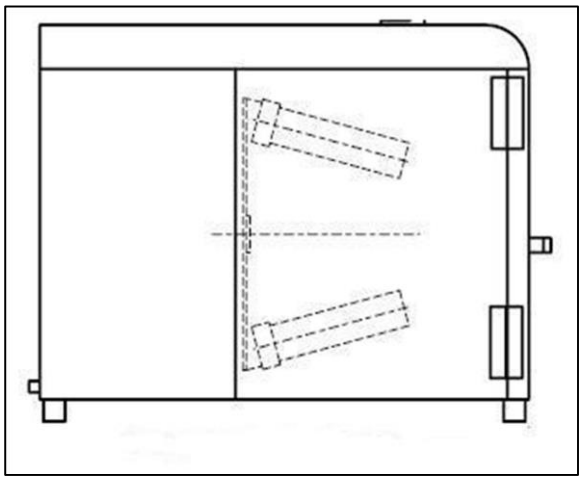


Figure 22. Arrangement of canisters in a laboratory dyeing unit. A tilt relative to the horizontal axis of rotation causes end-to-end fluid motion (*http://www.mathisag.com/user_content/editor/files/Prospekte/bfa12_24-e-web.pdf*)

Recently, the method has been expanded into the textile area with application of finishes to impart functionality such as protection from microbes, flame retardancy, blocking of UV radiation, and water repellency[4, 5, 35, 94, 95]. Scale up in the textile industry often involves the intermediate use of an infrared heated, exhaustive dyeing laboratory unit such as the Werner Mathis Labomat BFA 16 (Figure 21). The heterogeneous nature of dyeing and also admicellar polymerization means that interphase mass transfer can be an important factor in implementing these processes, though little work seems to have been done on the subject of mass transfer in the laboratory dyeing reactors. Mixing in these units, to a first order, is an interesting variant on the motion in a rocking reactor. In this paper, we review literature on the application and operation of rocking reactors and examine mixing with both theory and experiment for different operating conditions. The theory evolves from estimates of mass transfer coefficients based on specific mixing power while experimental

assessment of mass transfer for the laboratory dyeing unit centered on the dissolution of benzoic acid in water in the Werner Mathis Labomat BFA 16 as a model system. The objective of this work is to help adapt the laboratory-dyeing machine for modification of textiles by admicellar polymerization. Lastly, we examine performance of a water repellent coating formed by AP under different operating conditions in the laboratory-dyeing unit.

4.3 Literature Survey

Batch rocking reactors and autoclaves have been utilized in a wide range of applications in chemistry and biotechnology. The rocking motion facilitates mixing for heterogeneous systems that often involve high temperature and pressure. Layer, for example, used a rocking bomb at 220^{o}C to carry out the reaction of ethylene oxide with a phenol in base[96], a process important to the commercial synthesis of many surfactants. At even higher temperatures of 400-450^{o}C and a pressure of 6.8 x 10^{6} Pa(67 atm), a rocking autoclave reactor enabled the study of the properties of coke after thermal and hydrothermal cracking of residual and deasphalted oils[97]. In similar reactor systems, others investigated the catalytic hydrogenation of coal for its conversion to a synthetic liquid fuel[98] and catalytic perhydrogenation of rosin to impart absence of color and oxidation resistance[99]. The use of rocking reactors has not been limited to extreme conditions as lower temperature systems have been applied for fermentation and cell cultures. Ryoo developed a rocking drum reactor for solid substrate fermentation of cooked yellow corn grits with *Rhizopus oligosporus* to address typical problems of uneven distribution of air, moisture and metabolic heat[100]. Popular in the biotechnology community, bioreactors with rocking motion provide a

low shear environment well-suited to culturing bacteria, plant and animal cells in addition to tissue constructs[101-103]. Rocking reactors have been used to produce monoclonal antibodies, recombinant proteins, viruses and secondary metabolites.

Early work on the operating conditions for rocking reactors in mid-20th century focused on heterogeneous reactions involving gases. Hoffman et al. employed the palladium catalyzed hydrogenation of nitrobenzene in 5% acetic acid as a model reaction to investigate the effects of rate and angle of rocking, cylindrical reactor dimensions, and free space on agitation[104]. Slow motion pictures yielded a qualitative description of the motion in the glass reactors while sufficient catalyst ensured that the quantitative measurements of the rate of hydrogenation reflected mass transfer of hydrogen from the gas phase to the surface of the catalyst. At lower frequencies of oscillation, little gas-liquid mixing occurred in the reactors. Formation of waves that crested and broke at the ends appeared as the frequency rose so that the gas-liquid contact improved and the rates of hydrogenation increased. The gas envelope disappeared at still higher oscillation rates yielding a reduction in mass transfer and an optimum that varied linearly with the total angle swept during rocking (35 oscillations/min at 30^{o} to 50 oscillations/min at 120^{o}). The authors concluded that the major design factors influencing agitation for mass transfer of a gas were oscillation rate and the angle of rocking. Snyder et al also studied the catalyzed hydrogenation of nitrobenzene in acetic acid as well as the cupric catalyzed oxidation of sulfite in a single 1 L, 90^{o} sweep rocking reactor[105]. Controlling for temperature, catalyst concentration and reactant concentration, he found that the optimal absorption rate per unit volume of liquid for the hydrogenation reaction to be at a low filling ratio (25% liquid volume to reactor

volume) and a high rocking frequency (55 cycles/min). In contrast, the oxidation reaction was not very sensitive to the rocking rate. The authors attributed the difference to the effect of acetic acid on interfacial surface area.

There is little work on mass transfer in rocking reactors reported in the literature where none of the reactants are in the gas phase. Murzin[106] examined the dissolution of benzoic acid flakes to find the mass transfer coefficients β experimentally for two cylindrical rocking reactors, one with an oscillating rocking motion and the other reciprocating horizontally, and compared these to values calculated using estimates of the specific mixing power obtained from measurement of temperature transients. β was calculated from equation 11:

$$\boldsymbol{\beta = 1.0\left(\frac{\varepsilon D^4}{\upsilon d^2}\right)^{\frac{1}{6}}} \qquad \textbf{Equation 11}$$

Where ε is the specific mixing power, D is the diffusion coefficient, ν is the kinematic viscosity (ratio of dynamic viscosity and density μ/ρ), and d is the particle diameter or equivalent diameter[106]. Differences between the experimental and calculated values ranged from about five percent to several hundred percent. The lack of extensive literature and the limitations of prior research on solid-liquid mass transfer in rocking reactors indicate a need for further work.

4.4 Theory

An interesting variation on rocking reactors is widely utilized in the textile industry as infrared laboratory dyeing machines. Understanding the basic operation of the dyeing unit helps to illustrate the similarity with a rocking reactor and thus establish a basis for the analysis below. A typical system is presented in Figure 4.1a with stainless steel, cylindrical canister vessels mounted on a carousel, which rotates about a horizontal

axis. Canisters are canted (Figure 22) so that, during the course of one revolution of a canister, movement of an air void (or liquid phase) from front to back and then back to front causes mixing.

The theory in this study builds on the prior work by Murzin using specific mixing power to find mass transfer coefficients. We assume that the major driving force for mixing by rocking is flow due to gravity. We obtain a value for the mixing power by approximating the change in potential energy for the end-to-end motion of the fluid in the reference frame of the reactor. An estimate for the potential energy contribution was found by determining the height change of the center of mass for the idealization of undeformed liquid at the apex subsequently flowing and settling at the bottom (Figure 23). Since fluid will flow before reaching the apex and not completely settle under typical operating conditions, these estimates are expected to be upper limits. This approach, admittedly a rough estimate for a very complicated flow in the dyeing machine, has an advantage in not requiring experiments to predict β for various operating conditions. Below, we describe calculations for the mass transfer coefficient in the laboratory dyeing unit version of the rocking reactor.

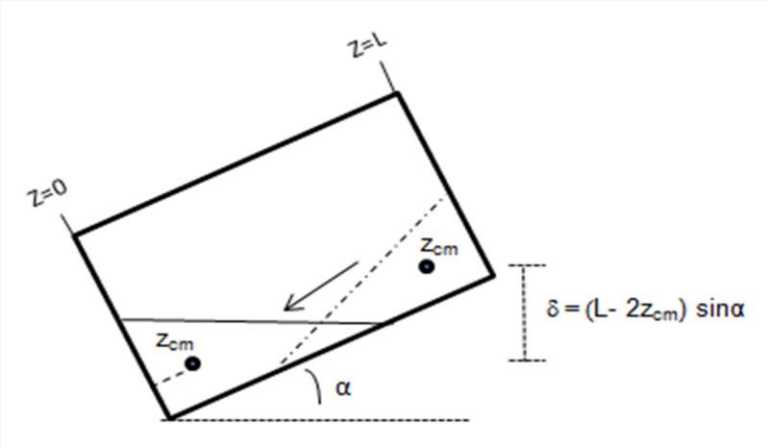


Figure 23. The conceptual simplification of the fluid at the apex and nadir facilitated an estimate if the potential energy change giving rise to mixing in the reactor

4.4.1 Calculation of the Specific Mixing Power and Mass Transfer Coefficient

Liquid volumes in the cylindrical reactor were used to find the center of mass displacement so that the specific mixing power could be estimated from the potential energy change during one revolution and the carousel rotational rate. With an assumption of uniform density, the center of mass in the liquid corresponds to the center of volume. One uses different mathematical expressions to find the volume based on the amount of liquid contained, length-to-radius ratio of the reactor (L/R), and its maximum angle of inclination (α). For a near horizontal orientation, there are three basic cases (Figure 24(a), Figure 24(b) and Figure 24(c)) to consider.

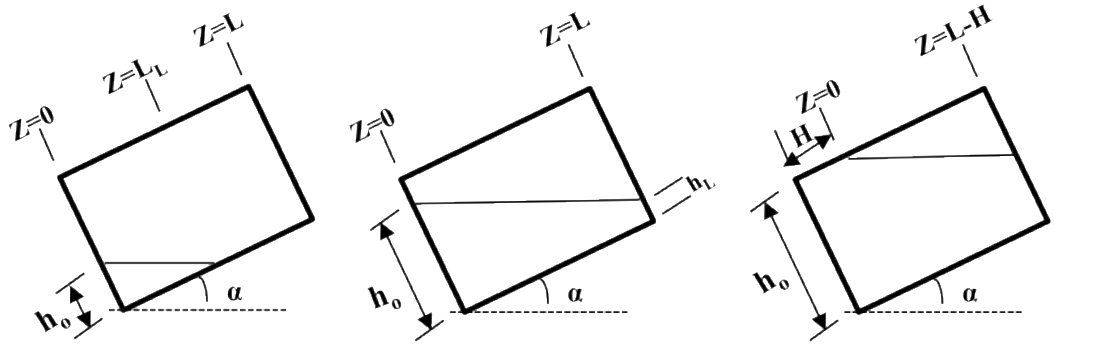


Fig. 24.a Case I: $h_o \leq 2R$, and $L_L \leq L$ and $L_L \geq L$

Fig. 24.b Case II: $h_o < 2R$, and $H > 0$

Fig. 24.c Case III: $h_o = 2R$

Figure 24. Pictorial representation of volume of canister

Fill levels for the first 2 cases are parameterized by h_o, the "height" of the liquid at the lower end of the cylinder (Figure 24a). Case II is distinguished from Case I by the liquid reaching the upper end of the reactor ($L_L > L$, Figure 24b) while Case III reflects the fact that the liquid level now exceeds the height at the lower end ($h_o > 2R$, Figure 24c). For case III, the parameter H is used to capture the volume present in the cylinder. To simply find the volume, one could address Case III by adapting Case I to the volume of the vapor and subtracting from the total reactor volume. However, this simple method cannot be used to find the location of the center of mass and an expression for calculating the volume for Case III is also given below.

The volume for Case I is readily found from integration in cylindrical coordinates:

$$V = \int_{V_{Liquid}} dV = 2\int_0^{L_L}\int_0^{\theta}\int_{\frac{R-h}{\cos\theta}}^{R} r\,dr\,d\theta\,dz \qquad \textbf{Equation 12}$$

which simplifies to:

$$\mathbf{V = \int_0^{L_L}[R^2\theta_1 - (R-h)^2\tan\theta_1]dz} \qquad \textbf{Equation 13a}$$

Where

$$\theta_1 = \arccos\left(\frac{R-h}{R}\right) \quad h = h_0\left(1-\frac{z}{L_L}\right) \quad L_L = \frac{h_0}{\tan\alpha} \qquad \textbf{Equation 13(b-d))}$$

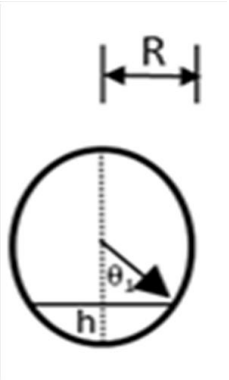


Figure 25. Relationship of h(z) and θ_1(h) in end view of canister

with R being the radius of canister and h being the height of the liquid in the canister at axial location z as illustrated in Figure 25. For Case II, the liquid volumes are defined by truncated cylindric sections and L_L is not actually realized. Volume then can be found with equation 3a with the upper limit changed to L. Case III can be treated as the combination of a disc of radius R and height H with a shortened cylinder of height (L-H) treated mathematically the same as Case II. This yields

$$V = \pi R^2 H + \int_0^{L-H} [R^2\theta_1 - (R-h)^2 \tan\theta_1]dz \qquad \textbf{Equation 14}$$

Equations for the volume were put in dimensionless form by dividing through by R^3 and the expressions entered directly into Mathcad, enabling construction of tables of the dimensionless volume V*(i.e. V/R^3) as a function of the dimensionless fill level parameters h_o* and H*(or h_o/R and H/R). While the integrals in the equations can be readily evaluated, these forms are more easily manipulated with the capabilities of the software to find the axial location of the center of mass which generally involves changing the integration limits until the dimensionless volume V* is halved. For Case I (Figure 24a) with fixed α, we generated tables of V*(h_o*) along with L_L*(h_o*) for $0 < h_o^* \leq 2$ (or $L_L/R(h_o/R)$ for $0 < h_o \leq 2R$) using equations 13a and 13d. The table of L_L* helped in determining the value of h_o* and the volume V* where the onset of Case II

occurred. Transition from Case I to Case II corresponded to $L_L^* = L^*$ or $L_L/R = L/R$. For Case II (Figure 24b), we employed equation 13a with integral upper limit L* to find $V^*(h_o^*)$ until the fill parameter $h_o^* = 2$, the dimensionless diameter, signaled conditions for Case III (Figure 24c). Finally, application of equation 14 yielded V*(H*) for Case III.

From these tables constructed with equations 12-14, the axial location of the center of mass z_{CM}^* (or z_{CM}/R) could be determined for a given fill level. By symmetry, the center of mass at the apex will be the same distance from the upper end in the idealization (Figure 23). The height change from tilting of the reactor according to the model can then be found from $\delta = (L\text{-}2\ z_{CM}) \sin \alpha$ with the power of mixing given by

$$P = \frac{2\rho g \delta V_{liquid} \omega}{2\pi} \qquad \textbf{Equation 15}$$

and thus the specific power of mixing:

$$\boldsymbol{\varepsilon = \frac{g\delta\omega}{\pi}} \qquad \textbf{Equation 16}$$

Where ρ is the solvent density, g is the acceleration due to gravity, and ω is the angular velocity of the carousel. Combining with equation 11, we obtain an expression (equation 17) to predict the mass transfer coefficient based on the operating conditions, specifically the fill volume (reflected in the center of mass) and rotational rate.

$$\beta = 1.0 \left(\frac{g(L - 2Z_{CM} \sin\alpha D^4}{\upsilon d^2} \right)^{\frac{1}{6}} \qquad \textbf{Equation 17}$$

4.5 Materials

Pique type cotton fabric was purchased from Alamac American Knits. The fabric was obtained scoured and prior to use, the fabric was washed several times in a washing machine until it was free from any remaining surfactant. The benzoic acid was obtained

from Sigma Aldrich (USA). The monomers used were 2,2,3,3,4,4,5,5-octafluoropentylmethacrylate (OFPM) and 2,2,2-trifluoro ethyl methacrylate (TFEM) purchased from SynQuest Laboratories Inc (USA). The surfactants the fluoroaliphatic amine oxide nonionic surfactant Masurf FS230 and a fluoroaliphatic quaternary ammonium cationic surfactant Masurf FS1620 were obtained from Mason Chemicals. Potassium persulfate (Fisher) was the initiator for admicellar polymerization. All chemicals were used without further purification.

4.6 Experimental

4.6.1 Mass Transfer Determination in a Model System of Benzoic Acid Dissolution

Experiments to examine mass transfer with benzoic acid were carried out in a Werner Mathis Labomat Type BFA 16 beaker dyeing unit. One-liter canisters were filled to the desired volume and preheated to 30^{o}C prior to addition of 4.0 g benzoic acid. Separate runs for volumes of 250 mL, 500 mL, 750 mL and 900 mL ensured a more precise temperature setting with the single thermocouple provided for monitoring and control. The programmed temperature was maintained by infrared heating elements and a combined air-water cooling system in the unit. Experiments were repeated at each volume for rotational rates of 10 rpm, 25 rpm, 45 rpm and 65 rpm. After 15 min, an aliquot was removed to determine benzoic acid concentration by titration against a 0.1 N sodium hydroxide solution using phenolphthalein as indicator. The experimental mass flux j in the dyeing machine at 30^{o}C was determined from $j = (c(t_2) - c(t_1))V_{liquid}/A_{total}\Delta t$ with t_1=0 min, t_2=15 min and $\Delta t = t_2 - t_1$. Mass transfer coefficients from experiments were calculated from $\beta = j/[c_{sat} - (c(t_2) + c(t_1))/2]$ with a saturation concentration of $c_{sat} = 3.3 \times 10^{-2}$ mol/L used for benzoic acid in water at 30^{o}C[107]. The

benzoic acid flakes were of varying sizes, but mostly on the order of 3 mm x 3 mm x .4 mm. This yielded a typical surface area of 0.23 cm^2 and a volume of 3.6 x 10^{-3} cm^3. The number of particles was estimated from the mass charged to the reactor (4.0 g), density of solid benzoic acid (1.266 g/cm^3) and the volume of a single particle from which the total surface area was then found. This surface area was taken as constant for the very thin benzoic acid flakes.

4.6.2 Application of a Hydrophobic Coating on Cotton Fabric

Operating conditions favorable for mass transfer should improve performance of a fabric at set reaction time and reagent concentrations. Pique knit cotton with BET surface area of 0.32m^2/g was coated with a copolymer of TFEM-OFPM by admicellar polymerization as previously described[86] in a laboratory dyeing unit as a function of fill volume keeping fabric to liquid ratio constant at 1:25. The different fill volumes used were 500 mL, 750 mL, 900 mL and 950 mL. Performance of the polymer coating on pique knit cotton was also studied with change in rotational rate. Rotational rates varied as 10 rpm, 25 rpm, 45 rpm and 65 rpm with a constant fill volume. Next, the performance at a higher fabric to liquid ratio was studied by increasing the ratio to 1:10 from 1:25.

We examined the modified fabric by SEM & elemental analysis and evaluated fabric for hydrophobicity by a simple drop test (20 µl water deposited from a height of 1cm), the spray test (AATCC Method 22) and contact angle measurement. Time for absorption of water in the drop test was determined up to a maximum of 30 min. SEM images were obtained by using JEOL JSM 880 and samples were sputter coated with thin layer of gold. Elemental analyses were carried out using ZEISS 960A SEM

equipped with Oxford Link energy dispersive spectroscopy (EDS) with a thin window and using IXRF EDS 2008 software at a beam energy of 5 kev. Contact angle measurements were obtained using sessile drop analysis using I.T. Concept Tracker contact angle analyzer.

4.7 Results and Discussion

Mass transfer can be an important factor influencing the rate of heterogeneous processes. Finding, for example, conditions suitable for a heterogeneous catalytic reaction system to operate in the rate limited regime means addressing mass transfer issues. Rocking reactors have often been used for heterogeneous processes. In investigating catalytic hydrogenation in a rocking reactor, Hoffmann[104] described qualitatively the nature of the flow and its relation to mass transfer. Three regimes were observed as function of oscillation rate with a significant effect on transport of the gas. The complexity of the liquid motion reported by Hoffmann presumably affects mixing and mass transfer in solid-liquid systems like those present in admicellar polymerization.

Temkin investigated the role of external mass transfer in catalytic reaction systems and obtained equation 11 to estimate mass transfer coefficients based on the specific mixing power ε[108, 109]. Employing a rocking reactor, Murzin et al. determined mass transfer coefficients β with ε from dissolution experiments of benzoic acid in water, similar to model studies of mixing for the liquid phase hydrogenation of cinnamaldehyde with a Ru-Sn catalyst[110] and the solid-liquid mass transfer in a Creusot-Loire Uddeholm vessel for stainless steel refining[107]. Murzin compared his experimental findings for β to values predicted with equation 11 and ε with limited success[106].

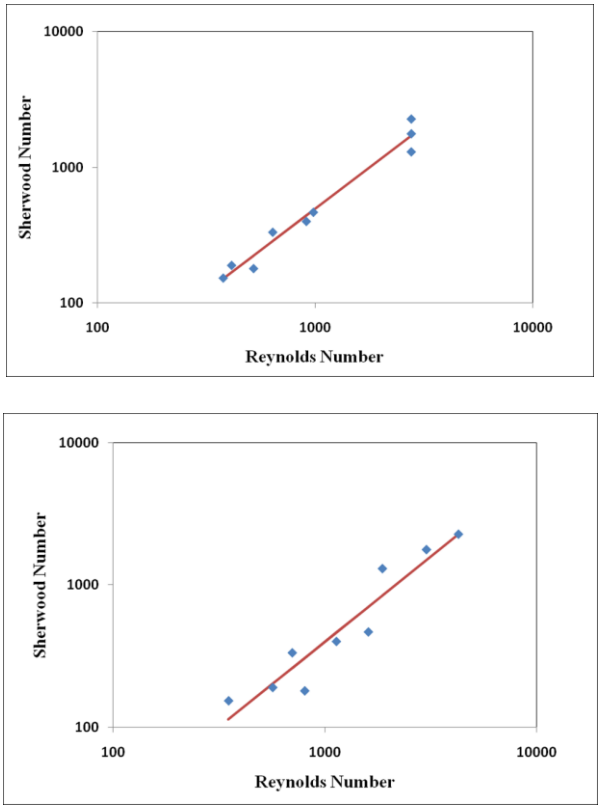


Figure 26. Similarity of Sherwood number (Sh=βd/D) correlations with Reynolds numbers based on Murzin's experiments ($Sh=.107Re^{1.222}$) and on the potential energy theory of this paper ($Sh=.104Re^{1.195}$). Sherwood numbers were calculated for reported values of the mass transfer coefficient for dissolution of benzoic acid in water with a rocking reactor and plotted against the Reynolds number obtained from Murzin's experimental work($Re=\rho\varepsilon^{1/3}d^{4/3}/\mu$) in 26a and from the potential energy theory($Re=\rho vd/\mu$) applied for Murzin's experimental conditions in 26b.

Traditionally mass transfer coefficients for a system appear in the form of a dimensionless correlation such as $Sh = aRe^{b}Sc^{c}$, where Sh, Re and Sc are the Sherwood, Reynolds and Schmidt numbers, respectively. Murzin's equation 11 can be rearranged to $Sh = Re^{1/2}\ Sc^{1/3}$ with $Sh=\beta d/D$, $Re=\rho\varepsilon^{1/3}d^{4/3}/\mu$ and $Sc=\nu/D$. The limited experimental results provided in Murzin's paper for β with only dissolution of benzoic acid in water

preclude a rigorous determination of the dependence of the Sherwood number on the Schmidt number. Figure 26a, however, shows a logarithmic plot of the dimensionless mass transfer coefficient Sh as a function of the Reynolds number. For a Reynolds number as defined above, regression analysis yields the following relationship for the Sherwood number $Sh=.107Re^{1.222}$. If the one-third dependence on the Schmidt number is assumed to be valid, the results for water imply $Sh=0.012Re^{1.222}Sc^{.333}$.

Murzin's experimental results for β were also examined using the theory developed in this paper. We produced a mass transfer correlation for the Sherwood number with Sh defined as above and the Reynolds number defined as $Re=\rho vd/\mu$ with $v=(L-2z_{cm})\omega/\pi$ from the potential energy theory. Figure 26b presents a plot of the Sherwood number versus this Reynolds number with linearized regression yielding $Sh=.104Re^{1.195}$. Thus, the two approaches, one rooted in experimental measurement and the other in theory, appear to be remarkably consistent in the dependence of the Sherwood number on Reynolds number for a rocking reactor.

Table 4. Specific Mixing Power per Unit Mass ε (W/kg) and Predicted Mass Transfer Coefficient (x 10^{-5} m/s)

RPM* / Vol.(mL)	10		25		45		65	
	$\varepsilon(Re_{pot})$	β	$\varepsilon(Re_{pot})$	β	$\varepsilon(Re_{pot})$	β	$\varepsilon(Re_{pot})$	β
250	.11(115)	5.6	.28(287)	6.6	.51(516)	7.2	.74(746)	7.7
500	.079(80)	5.3	.20(201)	6.2	.36(362)	6.9	.52(523)	7.3
750	.049(49)	4.9	.12(123)	5.7	.22(221)	6.4	.32(320)	6.8
900	.025(25)	4.4	.062(63)	5.2	.11(111)	5.7	.16(164)	6.1

*ω=1.047, 2.618, 4.712 and 6.807 s^{-1}

Our interest in rocking reactors lay in gaining insight to mass transfer in the laboratory dyeing unit. Using values of the specific mixing power estimated from potential energy changes (equation 16) and Murzin's theory (equation 11), we predicted the mass transfer coefficients as a function of rotational rate and fill volume. Predictions (

Table 4) indicate mixing power per unit mass is expected to increase in direct proportion to the rotational rate. It should decrease in a slightly weaker dependence with liquid volume. The latter result seems reasonable as the center of mass cannot undergo displacement to the same degree as the container becomes full. Predicted mass transfer coefficients β ranged from 4.4×10^{-5} to 7.7×10^{-5} m/s for water volumes of 250-900 mL and rotational rates of 10-65 rpm. In line with the values for specific mixing power, β is expected to increase with rotational rate and decrease with fill volume. More simply, β increases with the Reynolds number as the correlations above imply. For these calculations, the diffusion coefficient for benzoic acid in water[111] at 298 K was taken as $D = .9 \times 10^{-9}$ m^2/s while those used for the viscosity and density of water at 303 K were $\mu = 6.975 \times 10^{-4}$ Pa-s and $\rho = 995.7$ kg/m^3. Equivalent diameter d was obtained from the fraction of undissolved mass remaining w and the initial equivalent diameter ($d = d_{initial}\ w^{1/3}$ with $d_{initial}=1.9 \times 10^{-4}$ m). These predicted results of benzoic acid dissolution were then compared to the experimental values obtained for the dyeing reactor.

Table 5. Mass Flux ($x10^{-4}$ mol/m^2 s) and Observed Mass Transfer Coefficient ($x10^{-5}$ m/s) t = 0-15 min

RPM / Vol.(mL)	10		25		45		65	
	j	β	j	β	j	β	j	β
250	.93	.32	.98	.33	.99	.34	1.0	.34
500	2.3	.81	2.9	1.0	3.1	1.1	3.2	1.2
750	4.1	1.5	4.5	1.6	5.9	2.3	6.1	2.4
900	5.1	1.8	6.0	2.2	7.2	2.8	7.6	3.0

Our experimental findings for mass flux j and mass transfer coefficient β for dissolution of benzoic acid in water in the laboratory dyeing unit appear in Table 5. The mass transfer coefficient β ranged over .3 – 3.0 x 10^{-5} m/s, similar in magnitude, but smaller than predicted. Moreover, the trends observed were different from a simple rocking reactor. While there was a slight dependence on rotational rate, β varied to a greater extent with fill fraction. In marked contrast to the rocking reactor, the mass transfer coefficient and thus the Sherwood number increased with the liquid level. Correlation of these results yielded $Sh = 24.77Re^{.192}\gamma^{1.762}$, where γ is the fill fraction.

The potential energy-based theory worked well in representing mass transfer coefficients from the literature for a simple rocking reactor, but its transference to the laboratory dyeing unit proved unsatisfactory. The fluid motion is clearly more complex with the rotational motion of the carousel. We attribute the increase of mass transfer with fill volume to swirling due to the Coriolis forces arising from conservation of angular momentum. As the liquid in the canister flows end-to-end, its radial location changes giving rise to the "secondary" flow. This can explain the dependence on fill

level observed. The effect of angular momentum should increase with the greater mass as the fill level rises. Clearly, flow in the infrared laboratory dyeing machine poses an interesting multiphase fluid mechanics problem.

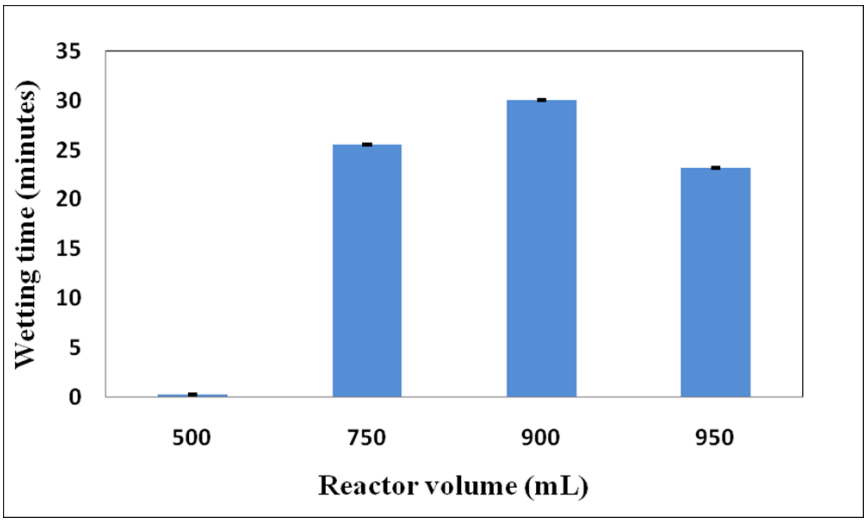


Figure 27. Wetting time for different reactor volumes keeping the fabric to liquid ratio constant

The mass transfer studies provided insights into the adaptation of the dyeing unit for admicellar polymerization. In parallel with the model mass transfer studies, we applied a co-polymer of TFEM and OFPM to cotton fabric samples with polymerization carried out at different fill levels in the Labomat dyeing unit. In these experiments, the volume of the reaction media should be above a minimum necessary to cover the fabric and yet allow sufficient air to promote mixing. For the 75 cm x 18 cm swatch of fabric used, the portion submerged in the liquid during the course of a rocking cycle varies with the fill volume. At 500 mL, the loosely rolled fabric sample is only partially submerged while it is nearly covered at 750 mL. Reaction volumes of 900 mL and 950 mL covered the fabric while reducing the air void to drive mixing.

A simple drop test and the AATCC spray test were used to assess performance. The fabric in the 500 mL canister displayed almost zero wetting time while the remaining swatches exhibited water repellency to differing degrees (Figure 27). Among these, the 900 mL modified cotton yielded a contact angle of 116^{o} and attained the 30-minute upper limit of the drop test. Spray test results were consistent with these findings, and

Table 6. Wetting time and spray test data with different reactor volumes

Reaction volume (mL)	Wetting time (min)	Spray test ratings
500	0.2	0
780	25.5	90
900	30	100
950	23.2	80

the highest rating being obtained for the 900 mL modified cotton (Table 6). For the range of rotational rates, the coating performance was nearly independent of the rotational rate (Table 7). Thus the optimal conditions for admicellar polymerization fit nicely with the results for the greatest mass flux found for benzoic acid. SEM images

Table 7. Wetting time and spray test data with different rotational rates

Rotation rate (rpm)	Wetting time (min)	Spray test ratings
10	30	100
25	30	100
45	30	100
65	30	100

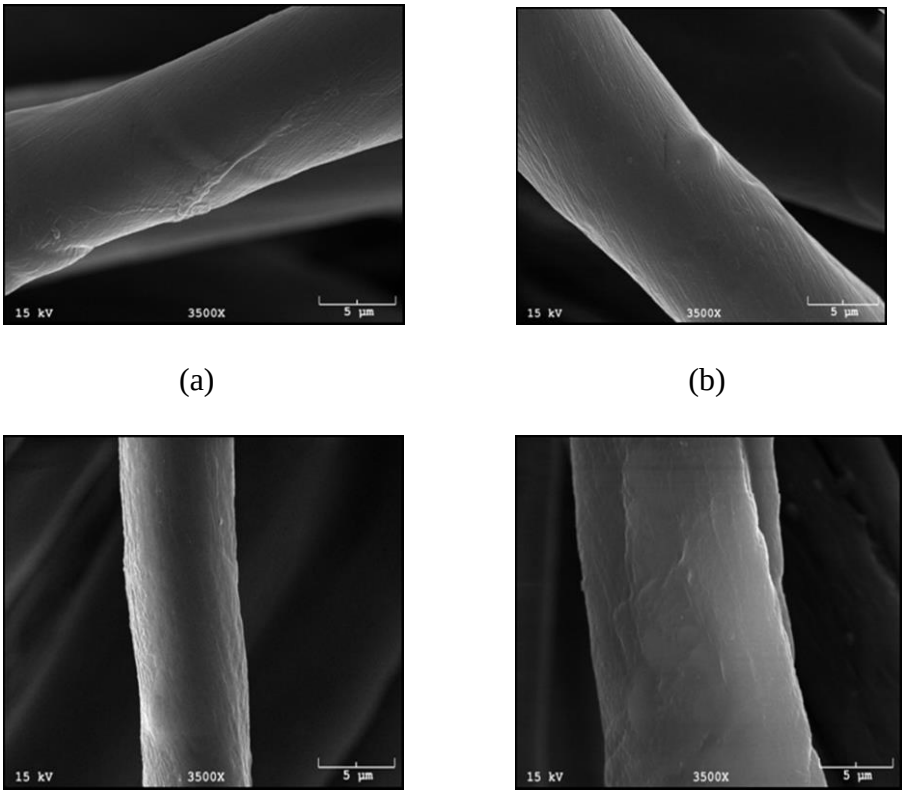


Figure 28. SEM micrographs: (a,b) untreated cotton fiber and (c,d) treated cotton fiber

and elemental analysis of the fabric samples prepared under optimal conditions were obtained. Figure 28(a) and Figure 28(b) shows fibers in the untreated cotton fabric samples, the surface of fibers is smooth and with striations evident in places. It is devoid of polymer aggregates and any other agglomerations. Figure 28(c) and Figure 28(d) shows fibers in the treated cotton fabric. Striations are not visible and a coating can be seen on the surface of fiber. Fiber edges are more ragged and as smooth and straight. The fluropolymer coating on fiber surface of treated fabric gives a bumpy appearance compared to untreated fabric. No large agglomerates appear on the fabric surface, which indicates a uniform coating. Elemental analysis of fabric samples

showed fluorine content of plain cotton fabric to be 0.33% while that of the polymer layer was 9.88%. This confirmed the presence of the polymer film.

Table 8. Wetting times spray test and contact angle data for different fabric ratios

Fabric to Liquid ratio	Wetting time (Min)	Spray test ratings	Contact angle
1:25	30	100	116^{o}
1:10	30	90	108^{o}

Another important parameter in textile processing is the fabric to liquid ratio. Mass flux depends on both the mass transfer coefficient and the concentration difference between the surface and the bulk fluid. A greater fabric-to-liquid ratio will more effectively deplete the solution of chemicals in a batch reactor. As such runs were carried out to examine performance with solid-to-liquid ratio in the dyeing unit (Table 8). As the fabric-to-liquid ratio is increased from 1:25 to 1:10, the quality of the finish is diminished. This is indicated by the spray test rating which goes from 100 to 90; and the contact angle, which decreases from 116^{o} to 108^{o}.

4.8 Conclusion

Performance of fabrics modified by admicellar polymerization in a laboratory dyeing unit matched well with results from model studies for mass transfer. Fill volume had a much greater effect than rotational rate on hydrophobicity of modified cotton and n the observed mass transfer coefficients. Estimates of specific mixing power based on potential energy provided good representation of results for mass transfer from the

literature for a rocking reactor, but proved unsatisfactory for the laboratory dyeing system.

4.9 Nomenclature

β	Mass transfer coefficient
ε	Specific mixing power (W/kg)
ν	Kinematic viscosity (m^2/s)
d	Particle diameter (m)
D	Diffusion Coefficient (m^2/s)
α	Angle of inclination
L	Length of canister (m);
L*	= L/R
L_L	Length of liquid along the z-axis (m)
R	Radius of canister (m)
h	Height of liquid in canister as function of axial position z;
h*	= h/R
h_0	Height of liquid at the lower end of canister (m)
H	Wetted length parallel to the z-axis along the top of canister (m)
θ_1	Maximum angular location of liquid as a function of z
ρ	Solvent density (kg/m^3)
g	Acceleration due to gravity (m^2/s)
ω	Angular velocity (s^{-1})
δ	Height change of center of mass for end to end flow (m)
j	Mass flux (mol/m^2s)
A_{total}	Total surface area of benzoic acid flakes (m^2)
c_{t2},c_{t1}	Concentration of benzoic acid at times t_1 and t_2 (mol/L)
c_{sat}	Saturated concentration of benzoic acid (mol/L)
V	Volume of fluid contained (m^3);
V*	= V/R^3
r, θ, z	Cylindrical coordinates

P	Power of mixing (W)
z_{cm}	Axial location of center of mass
μ	Viscosity of solvent (Pa-s)
γ	Fill Fraction, $V/V_{canister}$

PART II

Chapter 5

Hydrophilic Encapsulation of Multi-Walled Carbon Nanotubes using Admicellar Polymerization

5.1 Abstract

Admicellar polymerization (AP), a surface analogue of emulsion polymerization was used to obtain a thin layer of hydrophilic polymer coating on multi-walled carbon nanotubes (MWCNTs). The hydrophilic nature can facilitate integration of carbon nanotubes into a variety of composite materials. To develop hydrophilic polymer by AP, acrylate monomers were copolymerized using sodium dodecyl sulfate as a surfactant. Development of a system for AP involves measurement of surfactant adsorption and adsolubilization or partitioning of monomer into adsorbed structures (reverse hemimicelles). A modified two-site adsolubilization model was used to calculate the size of surfactant aggregates over the surface of MWCNTs and a binary adsolubilization model was employed to predict number of monomers adsolubilized from single component experiments. Adsolubilized monomers were polymerized to form a polymer nanocomposite, which was then hydrolyzed to obtain a hydrophilic nanocomposite. SEM, Energy Dispersive Spectroscopy (EDS), Thermo Gravimetric Analysis (TGA) and FT-IR confirmed the formation of polymer on multi-walled carbon nanotubes (MWCNTs). Modified MWCNTs readily dispersed in aqueous media and were stable after 3 days.

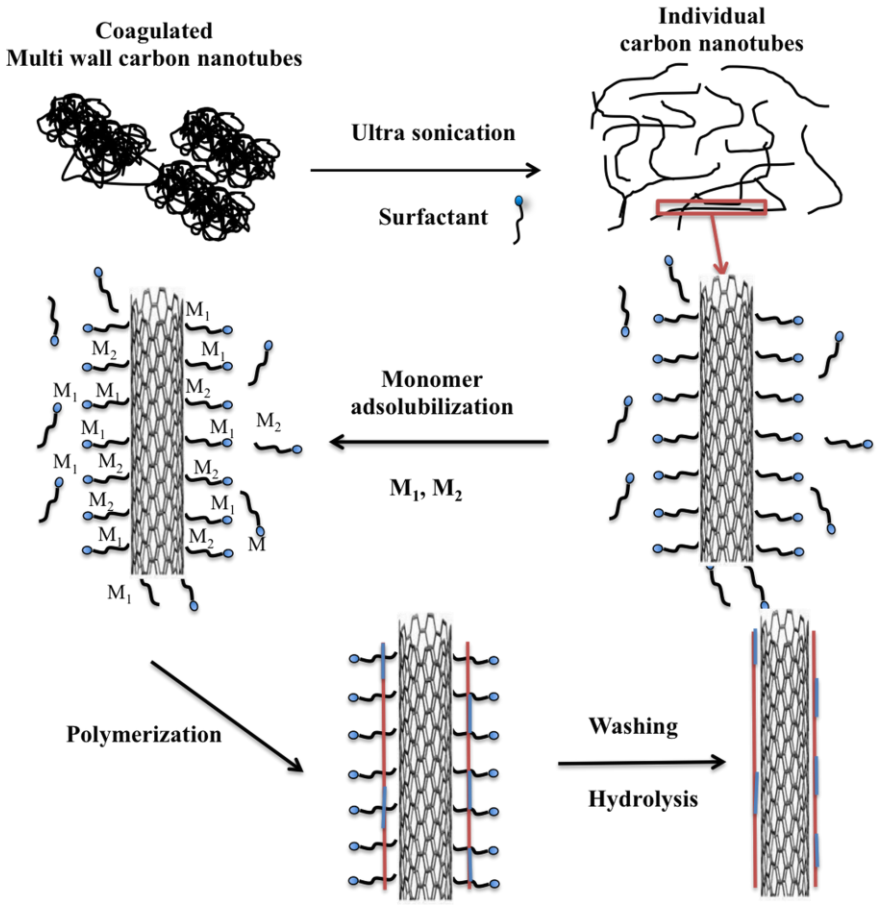


Figure 29 Schematic representation of admicellar polymerization for MWCNTs

Reprinted from Colloids and Surfaces A: Physicochemical and Engineering Aspects, 474, S Hanumansetty, E O'Rear, DE Resasco, Hydrophilic Encapsulation of Multi-Walled Carbon Nanotubes using Admicellar Polymerization, 1-8, Copyright (2015), with permission from Elsevier.

5.2 Introduction

Carbon nanotubes (CNTs) are ideal reinforcing fibers for composites because of their high aspect ratio, high mechanical strength, and high electrical and thermal conductivity. Unfortunately, bundling due to intertube van der Waals and solvophobic interactions impairs many applications. Mixing of nanotubes with most common solvents or polymers results in formation of clumps, bundles and ropes. Dispersion of nanotubes in liquid media for separation of bundles generally requires surfactant or chemical functionalization of nanotubes, expanding applications of nanotubes to numerous fields. A number of groups have shown that imparting enhanced electrical, mechanical and thermal properties [112-119] to polymer composites with carbon nanotubes can be achieved by chemical modification or polymer encapsulation.

Nanocomposites can be expressed in two different forms, nanoparticles incorporated into a continuous bulk polymer matrix and discrete nanoparticles encapsulated in a thin film of polymer. Methods have been developed for each. Polymerization techniques like in situ polymerization[120], miniemulsion polymerization[121] and others [122, 123] are used to prepare nanocomposites that incorporate nanoparticles in polymer matrix. Discrete nanoparticles can be coated with a thin film using polymerization methods such as free radical polymerization[124, 125] and soap free emulsion polymerization[126]. Others have employed various techniques to apply polymer coatings like poly(methyl methacrylate)[127] and polyaniline[128] on CNT surfaces. Redispersion/solubilization of discrete nanocomposites often requires external means like sonication to dissolve them in aqueous media, since the polymers are hydrophobic. To increase the solubility of nanotubes in water, a hydrophilic polymer (e.g. polyacrylic

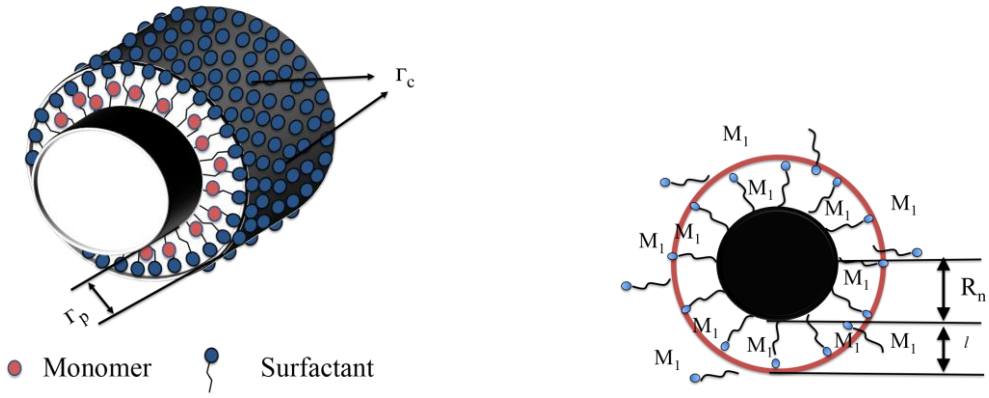
acid[129] and polyacrylonitrile[9]) can be used. However, unfavorable bonding between a hydrophilic polymer and nanotubes might mean a poorly integrated unstable material. In particular, strongly hydrophilic polymer might dissolve away from nanotubes in aqueous media. Having a hydrophobic component can be expected to anchor the polymer or copolymer to MWCNTs. As one approach, copolymerization of a hydrophilic monomer and a hydrophobic monomer on the surface of nanotubes might facilitate redispersion/solubilization of modified MWCNTs in aqueous media without any external means.

In recent years, new routes of encapsulation of carbon nanotubes with a thin film of copolymer coating have appeared to enable new applications. Nanocomposites readily dispersible in water can be employed for bioelectrochemical reactions[130], radiation therapies[131] and drug delivery methods[132]. Mu et al[133] used surface–initiated atom transfer radical polymerization to obtain a double layer hybrid nanocomposite of MWCNTs with polystyrene as inner layer and polyacrylic acid doped polyacrylonitrile as outer layer. The hybrid nanocomposite is used as conductor-insulator-semiconductor sandwich-structured and is partially water-soluble. Wang et al[134] modified multi-walled carbon nanotubes by formation of block copolymer of poly(tert-butyl methacrylate) and polystyrene which was hydrolyzed to polymethacrylic acid (PMAA) and tested for dispersion stability in different solvents like water, ethanol, acetone and chloroform. Zou et al., prepared large compound vesicle functionalized MWCNTs using copolymer of poly(3-(trimethoxysilyl)-propyl methacrylate) and polyethylene glycol[135]. With polyethylene glycol being hydrophilic, biocompatible and nontoxic, the large-compound vesicle functionalized MWCNTs were water-soluble with potential

use in drug delivery methods. A concern is that polymerization methods used to prepare copolymer of nanocomposites can degrade the electronic structure of nanotubes as the treatments often involve acids. Damage to the surface of carbon nanotubes surface can be mitigated by surfactant-assisted polymerization methods[9, 124, 127]. Association of monomer and nanotubes can be achieved on CNT surface without disturbing the π system while dispersion stability is high for nanocomposites prepared using surfactants. For example Xia et al. prepared nanocomposites of poly(methyl methacrylate-co-n-butyl acrylate) to disperse carbon nanotubes in latex using a surfactant assisted polymerization method[136] and Kim et al. developed redispersible SWCNTs in organic solvents using polymerizable surfactant by free radical polymerization[125] where the nanotube surfaces were not harmed.

In this paper we examine the application of an emulsion polymerization analogue, admicellar polymerization, to encapsulate multi walled carbon nanotubes (MWCNTs). The monomers butyl acrylate and methyl methacrylate are employed in combination with the surfactant sodium dodecyl sulfate to form a copolymer on carbon nanotubes. The copolymer formed on MWCNTs was hydrolyzed with sodium hydroxide to form hydrophilic encapsulated MWCNTs. The process of developing a system for admicellar polymerization involves measurement of surfactant adsorption and the adsolubilization or partitioning of monomers into adsorbed structures (reverse hemimicelles for MWCNTs). In addition modified two-site adsolubilization[137, 138] and binary adsolubilization[14] models were used to predict aggregation number and partition coefficients beween surfactants structures and the bulk solution.

Aggregate morphology around nanotubes is still in debate with the most probable configurations proposed in literature being cylindrical micelles, hemispherical micelles, and a random layer[139]. Based on observations and literature, we assumed that, above a low threshold, the aggregate morphology around MWCNTs consists of a sleeve around nanotube surface. This structure allowed adaptation of the two-site adsolubilization model to estimate aggregation numbers. As initially conceived, the two-site adsolubilization model was based on disc shaped admicelles formed on hydrophilic substrates much larger in scale than CNTs. Our modification involves cylindrical shell around the surface of MWCNTs with a reverse hemimicellar configuration (Figure 30). The fundamental hypothesis for the model remains the same, that there are two sites at which monomers can be adsolubilized, one within the palisade layer and the other at the perimeter of aggregates.



(a) (b)

Figure 30. Schematic view of modified two-site adsolubilization model (a) Sleeve model (b) Cross-sectional view

For the model, molecular parameters of surfactant and monomers (e.g., cross sectional areas of monomer headgroup (A_A)), were obtained from literature [66]. From

measurements of adsorption and adsolubilization, the aggregation number can be estimated using equation 18.

$$N_{avg} = \frac{2\pi(l^2+2lR_n)}{A_A}\left(\frac{\Gamma_a}{\Gamma_s} - \left(\frac{K_b C_a}{1-(K_b C_a)}\right)\right)^{-1} \qquad \textbf{Equation 18}$$

where N_{avg} is average aggregation number, R_n is radius of nanotube, *l* is the length of tail of surfactant molecule, A_A is cross-sectional area per monomer molecule, Γ_a is total amount of adsolubilized monomer, Γ_s is amount of surfactant adsorbed on MWCNTs, K_b is partition coefficient of monomer between hemimicellar and bulk phase, C_a is equlibrium concentration of monomer in supernantant.

Barton et al., developed a binary adsolubilization model to predict the amount of adsolubilized species from single component experiments[14]. That work was based on the partitioning of aliphatic alcohols into SDS aggregates over alumina. We extended the application of this model to investigate a reverse hemimicellar system formed on nanotube surface. In this approach one needs to specify the adsorbed amount of surfactant, which corresponds to specifying the extent of second phase or number of reverse hemimicelles. The partition coeficients can be determined from single component experimental data as it becomes constant at higher surfactant concentration. From equation 19, we can predict number of moles of the two monomers adsolubilized in SDS reverse hemimicelles.

$$\mathbf{N_{tot} = \frac{VC_1N_{tot}K_1}{[(K_1N_{tot})+(VM_{sol})]} + \frac{VC_2N_{tot}K_2}{[(K_2N_{tot})+(VM_{sol})]} + \left(\left[SDS_0 - SDS_{eq}\right]V\right)} \qquad \textbf{Equation 19}$$

Where N_{tot} is total number of moles in the reverse hemimicelles, N_1 and N_2 are moles of adsolubilized monomers, C_1 and C_2 are initial concentration of monomers, M_{sol} is

molarity of water, K_1 and K_2 are partition coefficients of adsolubilized monomers and V is volume of aqueous phase.

5.3 Experiments

5.3.1 Materials

All chemicals were used as received. SouthWest Nano Technologies Inc. provided the multi-walled carbon nanotubes (MWCNTs) with a BET surface area of 295 m^2/g. Sodium dodecyl sulfate (SDS) surfactant was purchased from Alfa Aesar USA while the monomers butyl acrylate (BA) and methyl methacrylate (MMA) were acquired from Sigma Aldrich USA. Initiator azobisisobutyronitrile (AIBN) was purchased from Fisher Scientific USA. Sodium hydroxide was obtained from EM Science USA.

5.3.2 Adsorption and Adsolubilization Analysis

MWCNTs (3 mg) were placed in 20 ml vials with SDS solutions at pH 7 of increasing concentrations from 0.01 mM to 100 mM. Samples were sonicated using sonic-dismembrator (Fischer Scientific F550) at 25% power setting for 10 min. Monomers with a total set concentration of 5 mM were added to vials. The samples were sealed with aluminum foil and capped with teflon-lined septa held in place with polypropylene caps without any headspace left in vials. Vials were placed in a shaker bath at room temperature for 14 hrs in order for adsorption and adsolubilization to occur. Amicon Ultra-0.5 centrifugal filter devices were used to separate supernatant surfactant solution from the MWCNTs using centrifuge at 10000 rpm for 30 min. A small aliquot from centrifuged vials was filtered with 0.45μm size filters for analysis by HPLC. Adsorption and adsolubilization measurements were determined from concentration changes by using a C18 surfactant column (RESTEK) (dimensions of 250mm x 4.6mm) with an

evaporative light scattering detector for surfactant SDS and a UV-Vis detector for monomers BA (242nm) and MMA (231mm). Mobile phases used for analysis were methanol and water in ratios of 85:15 for SDS while monomers BA and MMA were assayed with similar mobile phase ratio. Calibration curves were obtained for surfactant and monomers followed by measurements to obtain adsorption isotherms and adsolubilization results.

5.3.3 Polymer Encapsulation

MWCNTs (10 mg) were placed in vials along with sodium dodecyl sulfate (6mM) solution. Samples were sonicated using an ultrasonic sonic dismembrator at room temperature for 10 min. Combination of monomers with a total concentration of 5mM were added to vials and placed in a shaker bath at 30^{o}C for equilibration for 14 hrs for adsorption and adsolubilization to take place. Initiator concentration with a ratio of 1:2 with monomers was added to vials and polymerization reaction was carried out for 14 hrs at 80^{o}C at 80 rpm in shaker bath. Samples were removed from shaker bath and vacuum dried at 80^{o}C overnight. The samples were washed with methanol to remove trace amount of surfactant. To remove unreacted monomer and labile surfactant, samples were Soxhlet extracted with acetone for 48 hrs.

5.3.4 Hydrolysis

The dried samples after Soxhlet extraction were dissolved in 20 ml methanol and 1 ml of sodium hydroxide (5mM) dissolved in methanol was added to vials. Samples were placed in shaker bath at 100^{o}C for 4 hrs for hydrolysis[140, 141]. Samples were washed with methanol and dried in vacuum for 12 hrs.

5.4 Characterization

5.4.1 Scanning Electron Microscopy (SEM)

The encapsulated nanotubes were examined by SEM using a Zeiss NEON high resolution SEM with a beam voltage of 5 keV. Samples for SEM were sputter coated with a thin layer of iridium.

5.4.2 Energy Dispersive Spectroscopy

Energy dispersive spectroscopy (EDS) of encapsulated nanotubes before and after hydrolysis was carried out using INCA Energy 250 Energy Dispersive X-ray SEM microanalysis system with analytical drift detector at beam energy of 5 keV. Elemental analyses provided an indication of carbon, oxygen, sodium and sulfur content on the surface of MWCNTs.

5.4.3 Thermo Gravimetric Analysis (TGA)

Thermo gravimetric analysis was performed using a NETZSCH STA 449F1 TG instrument. TGA studies were carried out as 10 mg samples in alumina crucibles. The flow rate of argon was 30 ml min^{-1} with a protective inert gas argon flow rate of 20 ml min^{-1}. Temperature was increased from ambient temperature to 900 ˚C at a heating rate of 10˚C min^{-1}.

5.4.4 Fourier Transform Infra-Red Spectroscopy

Samples were weighed and mixed with KBr in mortar and pestle. Specac's Atlas series manual hydraulic press was used to prepare KBr pellets for FTIR analysis. FTIR spectra of samples were recorded by the KBr pellet testing techniques using Bruker Tensor 27 FTIR spectrophotometer in the wavenumber range from 4000 to 400 cm^{-1} for 128 scans with a resolution of 4 cm^{-1}.

5.5. Results and Discussion

5.5.1 Adsorption Isotherms

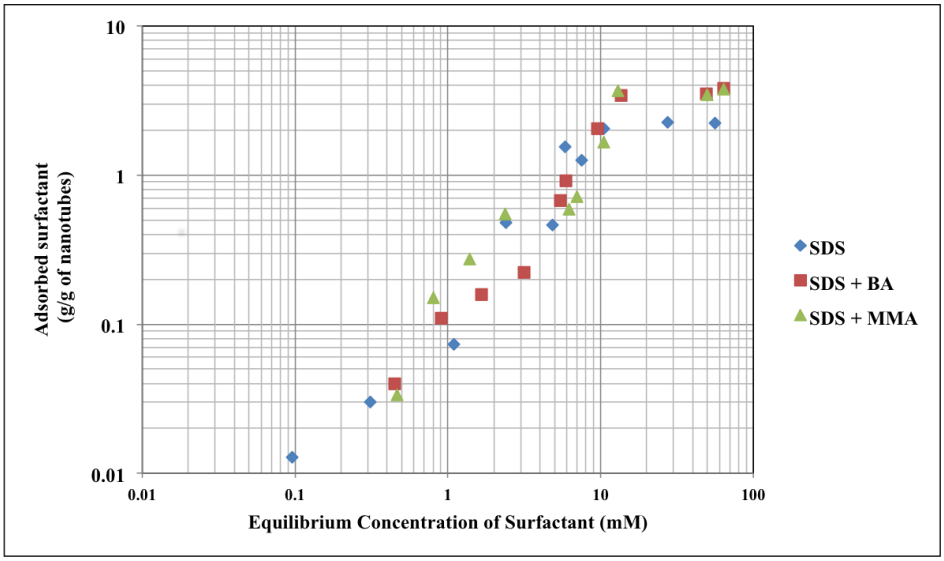


Figure 31. Adsorption isotherm of SDS without and with presence of monomers**.**

Adsorption isotherms of SDS alone and in presence of monomers (BA and MMA) are plotted in Figure 31. The adsorption isotherm obtained for MWCNTs is comparable to adsorption isotherms obtained by Mattaredona et al[142] on single wall carbon nanotubes (SWCNTs). As concentration of surfactant increases, adsorption increases and plateaus at or near CMC because available sites for adsorption on the nanotube surface decrease as the supernatant concentration increases. Adsorption of SDS on MWCNTs enhances the stabilization of nanotubes in water, as it diminishes the hydrophobic interactions between them. SDS produces an efficient surface coating that induces electrostatic or steric repulsions that counterbalances the van der Waals forces between MWCNTs.

As the supernatant concentration of SDS increases, presence of monomer BA has negligible effect on the adsorption isotherm. At intermediate concentrations of

surfactant however MMA does seem to have an effect, as there is an increase in SDS adsorption. MMA, being poorly soluble in aqueous media, might have caused increased adsorption of SDS on MWCNTs surface. Monomer solubility influences the behavior in the system as it does in micellization, playing an important role in either increasing or decreasing the adsorption amounts of surfactants. SDS exhibits an adsorption of 2 g/g of nanotube alone and 3 g/g of nanotube in presence of BA and MMA monomer at around 10 mM supernatant concentration. Compared to adsorption of SDS on other surfaces like hydrotalcite[143], silica[144, 145] and alumina[146, 147], peak adsorption of SDS is higher on MWCNTs with and without presence of monomers. On the other hand peak adsorption on MWCNTs is less compared to single wall carbon nanotubes (SWCNTs) as the available surface for adsorption is higher for SWCNTs. The plateau in adsorption of SDS on the nanotubes occurs around 10 mM, near the critical micelle concentration (CMC). The presence of monomers has negligible effect on the CMC, but amount of SDS adsorbed on MWCNTs at CMC has increased.

5.5.2 Adsolubilization of Monomers

For adsolubilization of monomers (BA, MMA) on MWCNT surface, presence of surfactant is important. In absence of surfactant, monomer BA and MMA adsorption was negligible. Observations confirm that amount of monomer adsolubilized depends on the extent of adsorption of surfactant. The ratio of monomer adsolubilized to surfactant adsorbed decreases with increasing supernatant concentration of surfactant before beginning to level off at or near the CMC (Figure 32). This reflects a higher proportion of perimeter sites available for many small reverse hemimicelles at low coverage while core sites dominate as coverage approaches saturation.

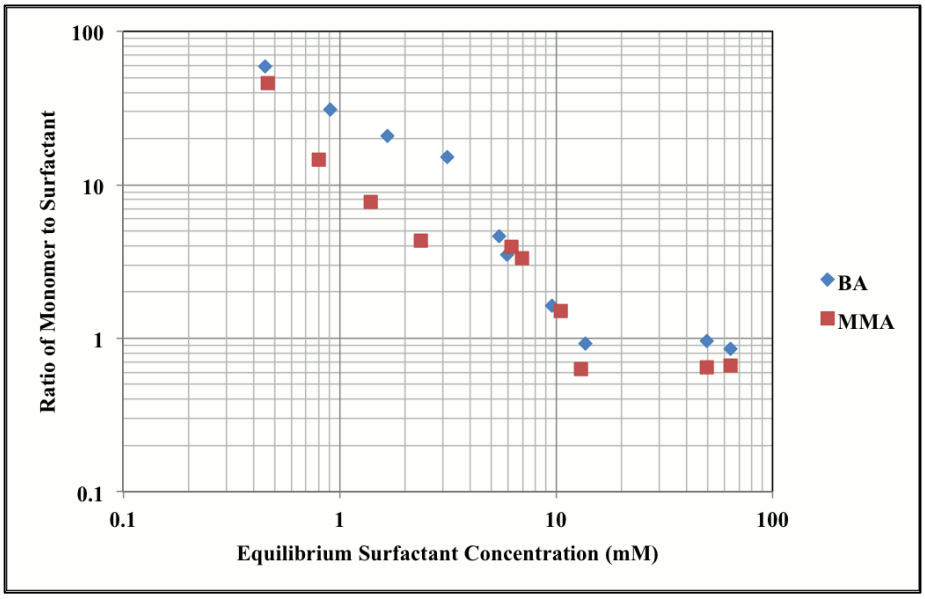


Figure 32. Ratio of monomer (BA and MMA) to surfactant (SDS)

Findings attained by Yeskie et al[148] on alcohols have similar trends, the ratio of monomer decreases with increasing surfactant concentration which reflects the transition from perimeter sites to palisade sites. In regions of high surface coverage, the ratio of monomer to surfactant decreases due to a balance between a loss of peripheral sites at edge of the surfactant aggregate and available space for monomer adsolubilization within the core of reverse hemimicelle. Determination of relative amounts of surfactant and monomer at the substrate surface for different system compositions helps to enhance understanding of the nature of reverse hemimicelle with adsolubilization and provides evidence for the two-site conceptualization.

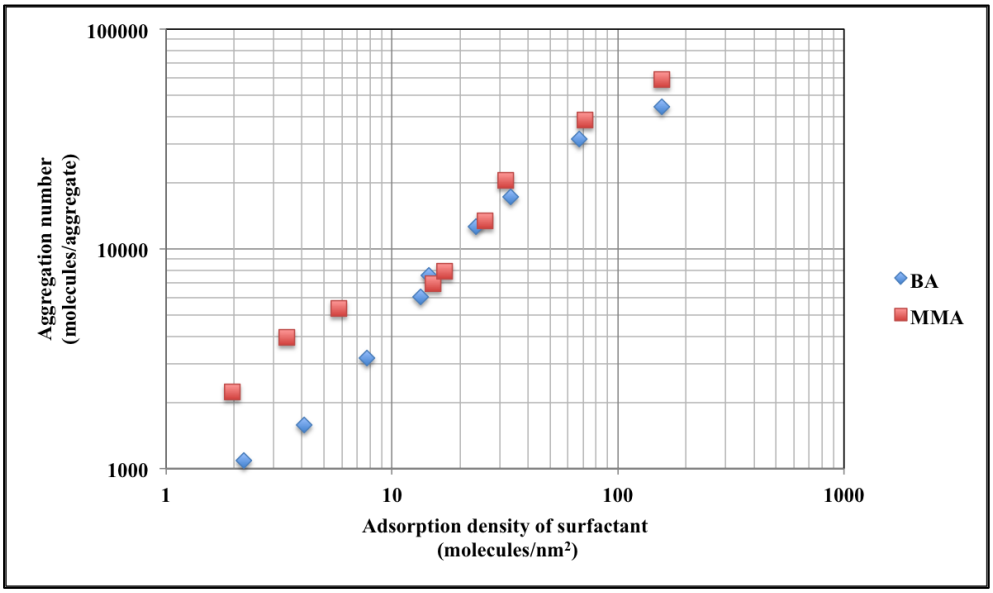


Figure 33. Aggregation number calculated using modified two-site adsolubilization model.

5.5.3 Modified Two-Site Adsolubilization Model

Patchwise adsorption of surfactant aggregates gives rise of the two-site adsolubilization model with species concentrating within the aggregate structure and at the periphery. The change in substrate to nanotubes necessitates a revision to the model. With an assumption that SDS on MWCNTs forms a reverse hemimicelle structure, a sleeve around the surface of nanotubes replaces the bilayer disc over alumina[137]. Two sites are formed on the surface, one in the palisade layer or core layer along the full length of the cylindrical shell (Figure 30) and the other at its two ends. Unlike the disc structure, peripheral sites do not increase with the size of aggregates, only with the number of aggregates. From Figure 33, as the density of surfactant increases, the aggregation number calculated from the model followed a near linear increasing trend on a log-log plot. Analysis with the modified two-site adsolubilization model yielded aggregation numbers ranging from order 10^3 to 10^5. These values were similar to Lee et al[137]. For

the nanotubes, aggregation numbers of adsorbed surfactants depend on substrate morphology as well as nature of the interaction of the adsolubilizate. As the surfactant molecular density increases at solid/liquid interface, the sites available in the core region increase and Γ_c dominates.

5.5.4 Binary Adsolubilization Model

The binary adsolubilization model enables prediction of the number of monomer molecules at the solid/liquid interface in a multi component system from single component data. Barton et al., used the binary adsolubilization model to investigate separation of n-heptanol and 2-methyl-2-hexanol with sodium dodecyl sulfate surfactant admicelles[14]. It is necessary to specify the extent of adsorbed phase or number of hemimicelles, which is similar to predetermining the relative volume in a liqud-liquid extraction. We examined the suitability of the binary adsolubilization model to predict the number of monomer molecules adsolubilized in our reverse hemimicelle system. Table 9, Table 10 and Table 11 shows the results predicted versus observed for number of moles of monomer of BA and MMA with different ratios of monomers from 25:75, 50:50 and 75:25 with increasing surfactant concentration. Similar trends were found with predicted values being higher than observed at low surfactant coverage while being closer at higher levels of coverage. This makes sense since parameters used in the model are derived from the plateau region of the single component isotherms[14]. The deviation in predicted versus observed values at the low end of the isotherm is due to variation of partition coefficient and different reverse hemimicelle structures. At higher surfactant concentrations, predicted versus observed data looks similar because of

Table 9. Comparison of predicted versus observed for total number of moles in reverse hemimicelle and moles of BA and MMA monomers (ratio 75:25)

BA: MMA - 75:25					
SDS+BA+MMA		**BA**		**MMA**	
N_{Total}		N_1		N_2	
Predicted	**Observed**	**Predicted**	**Observed**	**Predicted**	**Observed**
38.54	7.14	25.65	3.37	12.58	2.14
68.79	29.37	35.92	9.94	20.64	6.97
96.05	93.54	47.94	32.36	31.44	24.24
175.91	170.82	84.94	74.58	47.83	50.87
272.92	260.86	113.33	97.14	70.10	49.32
320.60	311.48	150.67	136.33	86.01	73.92

Table 10. Comparison of predicted versus observed for total number of moles in reverse hemimicelle and moles of BA and MMA monomers (ratio 50:50)

BA: MMA - 50:50					
SDS+BA+MMA		**BA**		**MMA**	
N_{Total}		N_1		N_2	
Predicted	**Observed**	**Predicted**	**Observed**	**Predicted**	**Observed**
38.26	9.21	23.53	3.73	11.49	2.77
79.89	26.44	38.42	9.56	25.97	9.14
113.31	129.10	54.09	56.67	42.02	45.69
185.31	175.43	75.02	68.48	70.25	69.14
292.50	287.08	95.90	93.31	86.16	84.44
371.77	351.20	106.40	96.75	96.87	107.90

Table 11. Comparison of predicted versus observed for total number of moles in reverse hemimicelle and moles of BA and MMA monomers (ratio 25: 75)

BA: MMA - 25:75					
SDS+BA+MMA		**BA**		**MMA**	
N_{Total}		N_1		N_2	
Predicted	**Observed**	**Predicted**	**Observed**	**Predicted**	**Observed**
39.02	9.09	8.75	1.86	24.31	3.72
67.42	31.42	19.48	4.97	37.59	8.94
88.23	83.69	27.09	19.29	45.33	37.43
154.05	149.38	45.91	39.43	75.45	71.42
220.86	213.81	66.16	62.19	92.52	87.13
353.34	338.15	88.78	85.22	140.47	136.97

formation of reverse hemimicelles on the surface of nanotube and stable monomer adsolubilization occurs in the core sites of reverse hemimicelles.

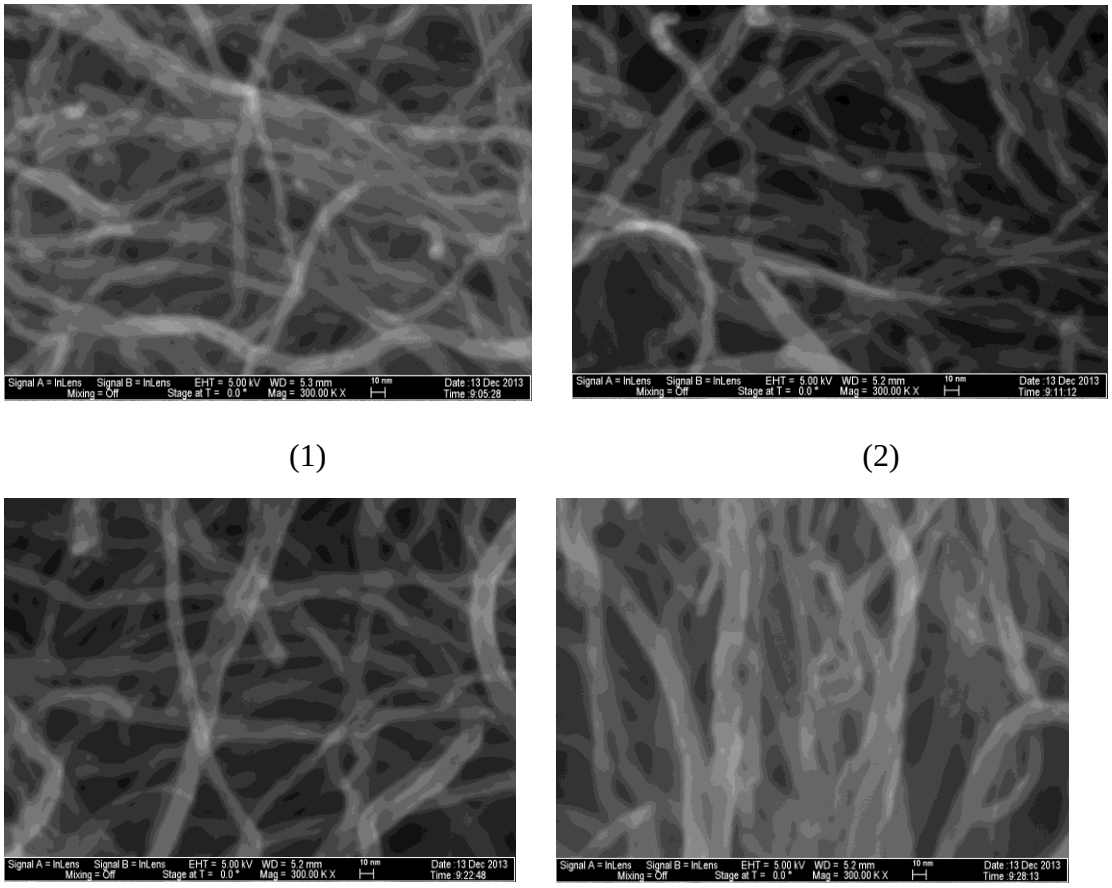


Figure 34. SEM analysis of 1. Pristine MWCNTs, 2. PBA-MWCNTs, 3. PMMA-MWCNTs, 4. PBA/PMMA-MWCNTs.

5.5.4 Polymer Encapsulation

SEM images obtained for pristine MWCNTs and for PBA-MWCNTs, PMMA-MWCNTs and PBA/PMMA-MWCNTs are shown in Figure 34. The average diameters of entangled nanotubes were measured using ImageJ image processing program. Polymer encapsulation by admicellar polymerization increases the diameter of MWCNTs (Table 12) compared to diameter of pristine MWCNTs. The diameters (Table 12) of PBA-MWCNTs, PMMA-MWCNTs and PBA/PMMA-MWCNTs were similar (13–15 nm) which confirms formation of polymer layer around 9 nm carbon

nanotubes in all the samples. Thus the thickness of polymer around MWCNTs formed is about 5nm. Compared to diameters in the range of 30-80 nm reported in previous works on encapsulated MWCNTs, we achieved thin film encapsulation using admicellar polymerization on MWCNTs[127, 136].

Table 12. Average diameter of pristine MWCNTs and encapsulated MWCNTs**.**

Type	Diameter (nm)
MWCNTs	9.1
MWCNTs with PBA	13.3
MWCNTs with PMMA	14.5
MWCNTs with PBA/PMMA	14.6

To analyze the elemental composition, energy dispersive spectroscopy (EDS) was carried out on encapsulated MWCNTs before and after hydrolysis (Table 13). Compared to pristine MWCNTs, carbon content is reduced and oxygen content increased in encapsulated samples. The change confirms formation of polymer as the polymer composition consists of mainly carbon and oxygen. The carbon content observed is higher than expected for polymers. When testing, high-energy x-ray beams can cause surface melting of polymer and expose the nanotubes, thus higher percentages of carbon are observed in all encapsulated samples. After hydrolysis of encapsulated MWCNTs with sodium hydroxide, oxygen and sodium content increased and carbon content decreased in PBA-MWCNTs and PBA/PMMA-MWCNTs as expected. The sulfur content was attributed to residual surfactant SDS, trace amounts present in all coated samples even after washing and using Soxhlet extraction.

Table 13. EDS analysis of encapsulated MWCNTs before and after hydrolysis

Sample	Carbon	Oxygen	Sodium	Sulphur
	Before hydrolysis (wt.%)			
MWCNTs	97	1.5	0	0
MWCNTs with PBA	73.7	15.2	10.2	0.9
MWCNTs with PMMA	82.3	10.7	5.9	1.1
MWCNTS with PBA and PMMA 75:25	78.4	12.3	7.4	0.4
	After hydrolysis (wt.%)			
MWCNTs with PAA	66.6	18.1	17.2	0.9
MWCNTs with PMMA	80.6	11.8	6.5	1.1
MWCNTS with PAA and PMMA 75:25	73.1	16.7	9.5	0.4

FTIR spectra of PBA-MWCNTs, PMMA-MWCNTs and PBA/PMMA-MWCNTs are shown in Figure 35. Characteristic peaks of PBA and PMMA can be found in the respective samples. The C=O characteristic peak in carbonyl group at 1733 cm^{-1} is clear in all the samples as well as peaks at 2923 cm^{-1} and 2854 cm^{-1} corresponding to stretch mode of C-H bond vibration. The bending vibration of $–CH_2$ or $–CH_3$ groups at 1454 cm^{-1} and 1390 cm^{-1} are seen in all samples. Peaks between 1000-1200 cm^{-1} can be attributed to stretching vibration of C-O group of polymer. In samples after hydrolysis, the significant peak for PBA-MWCNTs and PBA/PMMA-MWCNTs between 1350-1500 cm^{-1} which corresponds to bending vibration of $-CH_2$ and C-O bonds for

carboxylic acids and salts of acetate, which are formed during hydrolysis of acrylate polymers[149].

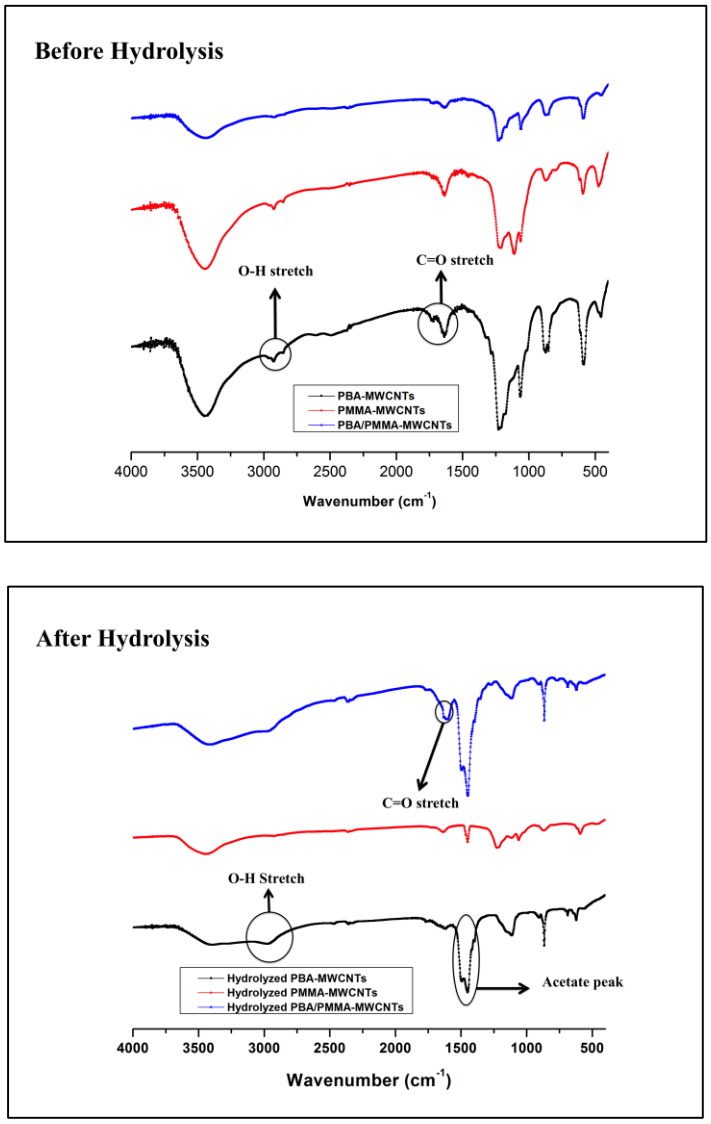


Figure 35. FTIR analysis of encapsulated MWCNTs before and after hydrolysis

From SEM micrographs, FTIR and EDS analysis, polymer formation on MWCNTs was confirmed. Thermo gravimetric analysis was implemented on samples to obtain the percentage of polymer content in polymer encapsulated MWCNTs. Figure 36 shows TGA curves of pristine MWCNTs, PBA-MWCNTs, PMMA-MWCNTs and

PBA/PMMA–MWCNTs before and after hydrolysis. The pristine carbon nanotubes have high thermal stability and almost negligible weight loss after heating to 900°C. In case of samples before hydrolysis, the weight loss observed due to polymer decomposition before 400°C signifies a 25-30% polymer content in the samples. Two stages of decomposition mechanism were observed in samples before hydrolysis. At

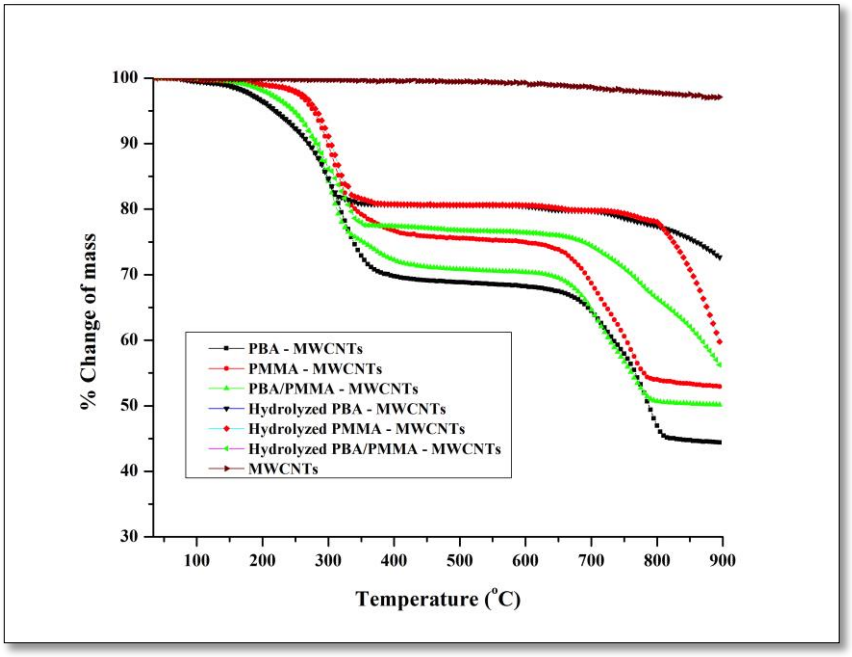


Figure 36. TG analysis of MWCNTs and encapsulated MWCNTs

around 650°C, there is an additional loss of around 25-30% indicating decomposition of higher molecular weight fragments formed during the first stage decomposition and leaving nanotubes thereafter. After hydrolysis, hydrolyzed PBA-MWCNTs and PMMA-MWCNTs have weight loss of approximately 20% compared to 25% for PBA/PMMA-MWCNTs. A difference of about 5-10% higher weight loss was found in samples after hydrolysis. The thermal stability of polymer formed after hydrolysis is higher than the thermal stability of polymer before hydrolysis. The butyl moiety has

higher mass than is present after hydrolysis, contributing to the larger weight loss. Formation of sodium salt of poly acrylic acid after hydrolysis affects the decomposition rate of polymer. Large ester groups on poly butyl acrylate polymers tend to form poly acrylic acid and corresponding olefins by a molecular ester decomposition mechanism[150] under thermal analysis but degradation of poly acrylic acid under thermal analysis occurs by decarboxylation mechanism[151, 152]. PBA-MWCNTs had higher polymer content than PMMA-MWCNTs because of relatively low hydrophobic properties of MMA monomer compared to BA monomer[127].

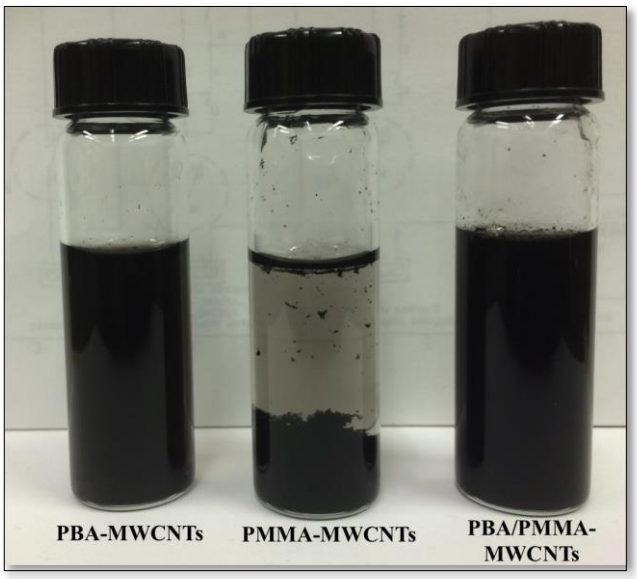


Figure 37. Encapsulated MWCNTs dispersed in water. Picture was taken after 3 days dispersion in water.

From above analytical techniques, polymer formation before and after hydrolysis was confirmed. To analyze the dispersion stability of the polymer formed on MWCNTs after hydrolysis, MWCNTs were dispersed in aqueous media and left aside for 3 days. In Figure 37, hydrolyzed PBA-MWCNTs and hydrolyzed PBA/PMMA - MWCNTs

were stable even after 3 days but PMMA-MWCNTs formed aggregates and settled at the bottom of the vial. Hydrolysis of PBA to form salts of poly acrylic acid increases the dispersion of nanotubes without any external means like sonication. Thus the formation of hydrophilic polymer after hydrolysis influences the dispersion stability of MWCNTs in aqueous media.

5.6 Conclusions

Admicellar polymerization was successfully employed to form copolymer of hydrophilic and hydrophobic characteristics around the surface of MWCNTs. Adsorption and adsolubilzation measurements were obtained for SDS surfactant and acrylate monomers. Presence of monomer has increased the peak adsorption of SDS on MWCNTs around CMC of surfactant. The ratio of monomer adsolubilized versus surfactant decreases with increasing surfactant concentration before beginning to level off at or near CMC of surfactant. For nanotubes, aggregation number of surfactants depends on the morphology of substrate. Aggregation numbers were estimated using a modified two-site adsolubilization model and sleeves as the structure formed on the MWCNTs surface. We examined the suitability of binary adsolubilization to predict the number of moles of monomer solid/liquid interface. Surface analytical techniques confirm the presence of copolymer of PBA and PMMA on the surface of nanotubes. Film thickness of around 5 nm was formed around surface of MWCNTs. The modified MWCNTs easily dispersed in aqueous media and remained stable even after 3 days.

Chapter 6

Formation of Copolymer on Multi-Walled Carbon Nanotubes using Admicellar Polymerization

6.1 Abstract

An emulsion like polymerization technique called admicellar polymerization (AP) was used to encapsulate a thin film of copolymer on the surface of multi-walled carbon nanotubes (MWCNTs). A water-soluble component sodium acrylate and a non-water soluble component methyl methacrylate were used to form thin films of copolymer on multi-walled carbon nanotubes. The hydrophilic nature will facilitate integration of nanotubes into a variety of composite materials by solubilization in aqueous media while the poorly water-soluble component should improve stability of the composite. Encapsulated MWCNTs were characterized using SEM, energy dispersive spectroscopy (EDS), thermal analysis and FT-IR. Analytical studies indicate the formation of copolymer on MWCNTs. Monomer conversion rate and copolymer reactivity ratios were analyzed using high performance liquid chromatography (HPLC) by Fineman-Ross and Kelen-Tüdos methods. The copolymer combination showed an alternating tendency and azeotropic composition at a composition of 0.6 of monomer. The encapsulated MWCNTs were stable in aqueous media with onset of aggregate formation beginning at 40 days.

6.2 Introduction

Carbon nanotubes have stirred broad interest across many economic sectors. Since the discovery of nanotubes, applications have been developed in fields such as energy conversion and storage, electrochemical devices, sensors, nanoscale electronic devices and biological applications[130, 153, 154]. Poor dispersion and stabilization of carbon nanotubes in common solvents impairs utilization of nanotubes in multiple fields. Modification of nanotubes either by grafting or encapsulation with organic molecules can improve the solubility of nanotubes in organic and aqueous media. Recently incorporation of carbon nanotubes to prepare polymer nanocomposites has generated considerable interest, by enhancing properties of materials [114, 116, 118, 119].

Formation of homogenous CNT/polymer composites, however, is difficult because of van der Waals forces between nanotubes[9]. To minimize the interaction and form homogenous composites, non-covalent or covalent bonding of functional groups between polymer matrix and CNTs surfaces is important. Several groups have developed different grafting or polymerization techniques to form polymer/CNT composites [124, 126, 134, 155, 156]. Development of polymer/CNT composites by grafting or polymerization requires complicated equipment and some treatments involve strong acids, which can degrade the electronic structure of nanotubes. To minimize the problem, researchers have employed surfactant assisted polymerization methods[9, 127, 136, 157]. Surfactants adsorb on the nanotube surface without disturbing the π system of the tube lattice and reduce van der Waals interactions between carbon nanotubes. Thin films of polymers like poly(methyl methacrylate)[136], poly (acrylic acid)[158], polyaniline[159] were formed on CNT surfaces using polymerization methods.

Encapsulation of MWCNTs with a strong hydrophilic polymer (e.g., polyacrylic acid or polyaniline) might dissolve away from the nanotubes. Alternatively if a weak hydrophilic polymer like poly(methyl methacrylate) is used, an unstable material would likely form in aqueous media. To solve this problem, copolymerization of strong hydrophilic component with a hydrophobic component is expected to form more stable and more readily redispersable nanotubes. Redispersable polymer/CNT composites can be used in different applications like electrochemical reactions[130], electrical devices[133], drug delivery methods[132, 135] and radiation therapies[131].

There has been prior work on copolymers and MWCNTs using different emulsion polymerization techniques. Surface-initiated atom transfer radical polymerization was employed to form a double layer hybrid nanocomposites of polystyrene and poly acrylic acid doped polyacrylonitrile on MWCNTs surface[133]. This polymerization method requires acid treatment and ultrasonication to introduce carboxylic functionalization to nanotubes before the formation of polymer, which might deteriorate the surface of nanotubes. Nguyen et al[160] employed reversible addition-fragmentation chain transfer emulsion polymerization mechanism to encapsulate carboxylic acid functionalized MWCNTs to form copolymer of butyl acrylate and methyl methacrylate at pH 6. Xia et al used in situ emulsion polymerization technique to form copolymer of butyl acrylate and methyl methacrylate on to carbon nanotubes by ultrasonication [136]. Throughout the polymerization process, ultrasonication is employed and nanotubes become thinner as well as shorter[161]. To overcome the aforementioned problems, admicellar polymerization(AP) an emulsion polymerization method can be employed as it can form thin films on surfaces without deteriorating the nanotubes. A robust method,

admicellar polymerization has been used to form thin films on different substrates like alumina[162], silica[1] and cotton[163].

In this paper, we focus on AP to form thin films on carbon nanotube surface. A thin polymer layer can be formed on CNTs with the adsorbed surfactant molecules functioning as a two-dimensional polymerization solvent. Admicellar polymerization follows three basic steps. First step is adsorption of surfactant molecules on to CNT surface. The second step is adsolubilization of monomer into adsorbed surfactant on CNT surface. The next step is to initiate reaction and once the polymer is formed, modified CNTs are rinsed for removal of excess surfactant.

To encapsulate multi-walled carbon nanotubes, we used the monomers sodium acrylate and methyl methacrylate for hydrophilic and hydrophobic polymeric components in combination with surfactant sodium dodecyl sulfate and a water insoluble initiator. Surface analytical techniques were used to analyze copolymer formation on nanotube surface. High performance liquid chromatography analytical studies were used to obtain monomer conversion rate, compositions of copolymer and monomer reactivity ratios by using Fineman-Ross and Kelen-Tüdos methods.

6.3 Experimental

6.3.1 Materials

All chemicals were used as received. Multi-walled carbon nanotubes (MWCNTs) were provided by Southwest Nano Technologies Inc. with a surface area of 295 m^2/g. The surfactant used was sodium dodecyl sulfate (SDS, Alfa Aesar USA). Monomers used to encapsulate MWCNTs were acrylic acid (AA) and methyl methacrylate (MMA) obtained from Sigma Aldrich USA. The initiator azobisisobutyronitrile (AIBN) was

purchased from Fisher Scientific USA. Sodium bicarbonate was purchased from EM Science USA.

6.3.2 Polymer Encapsulation

MWCNTs (6 mg) were placed in vials along with sodium dodecyl sulfate (6mM) solution. Samples were sonicated using a Fischer Scientific 550 Ultra sonic dismembrator (25 % power of 10 watts) at room temperature for 10 min. Combination of monomers with a total concentration of 4mM were added to vials and placed in a shaker bath at 30^{o}C for 14 hrs for adsorption and adsolubilization to take place. Initiator concentration with a ratio of 1:2 with monomers was added to vials and sodium bicarbonate (2mM) was added to increase the pH of solution to 8.5. The polymerization reaction was carried out for 14 hrs at 80^{o}C in a shaker bath at 80 rpm. The samples were removed from the shaker bath and vacuum dried at 80^{o}C overnight. The samples were washed with methanol to remove labile surfactant.

6.4 Characterization

6.4.1 Fourier Transform Infrared Spectroscopy (FTIR)

FTIR spectra of samples were recorded by the KBr pellet testing techniques using a Bruker Tensor 27 FTIR spectrophotometer in the wavenumber range from 4000 to 400 cm^{-1} for 128 scans with a resolution of 4 cm^{-1}. Samples were weighed and mixed with KBr in mortar and pestle. Specac's atlas manual hydraulic press was used to prepare KBr pellets for FTIR analysis.

6.4.2 Scanning Electron Microscopy (SEM)

The encapsulated nanotubes were examined by SEM using a Zeiss NEON high resolution SEM with a beam voltage of 5 keV. Samples for SEM were sputter coated with a thin layer of iridium.

6.4.3 Thermo Gravimetric Analysis (TGA)

Thermo gravimetric analysis (TGA) was performed using a NETZSCH STA 449F1 TG instrument. TGA studies were carried out as 10 mg samples in alumina crucibles. The flow rate of argon was 30 ml min^{-1} with a protective inert gas argon flow rate of 20 ml min^{-1}. Temperature was increased from ambient temperature to 900 ˚C at a heating rate of 10˚C min^{-1}.

6.4.4 Energy Dispersive Spectroscopy (EDS)

Energy dispersive spectroscopy (EDS) of samples was carried out using INCA Energy 250 Energy Dispersive X-ray SEM microanalysis system with analytical drift detector at beam energy of 5 keV. Elemental analyses provided an indication of carbon, oxygen, sodium and sulfur content on the surface of MWCNTs.

6.4.5 UV-Vis Spectrophotometry

Shimadzu scientific UV-3600 plus UV-Vis spectrophotometer was used to obtain absorbance spectra for encapsulated and pristine nanotubes. The samples were tested for UV-Visible region of wavelength range from 900 nm to 190 nm. Aqueous solutions of encapsulated nanotubes (1 mg/ml) were prepared for analysis. Pristine nanotubes were dissolved in ethanol (1mg/ml) and diluted to obtain the spectra.

6.4.6 Determination of % Monomer Conversion and Copolymer Composition

To study percent conversion and copolymerization of acrylic acid and methyl methacrylate, two sets of experiments were carried out. The first set of experiments was analyzed to know the % conversion of monomer. MWCNTs (0.6 mg) and sodium dodecyl sulfate solution (6mM) were added to 10ml vials. Samples were sonicated using an ultra sonic dismembrator (25% power of 10 watts) at room temperature for 10min. Adsorption, adsolubilization and reaction were carried out at a total monomer concentration of 4mM and shortened reaction times. The solutions were maintained at pH 8.5 and reaction temperature was 80^{o}C. After a pre-determined time, vials were removed from shaker bath and transferred to cooling bath to stop the polymerization reaction. After the vials were cooled to room temperature, Amicon Ultra-0.5 centrifugal filter devices were used to separate supernatant solution from the MWCNTs using centrifuge at 10000 rpm for 30 min. A small aliquot from the centrifuged vials was filtered with 0.45μm size filters for analysis by HPLC. The % conversion of monomer (equation 20) was determined from the initial and final concentration changes measured by using a C18 surfactant column (RESTEK) (dimensions of 250mm x 4.6mm) with a UV-Vis detector for monomers AA (200nm) and MMA (231mm). Mobile phases used for analysis were methanol and water in ratios of 85:15 for AA and MMA, respectively.

$$\%\ \mathbf{conversion} = \frac{\mathbf{C_{initial} - C_{final}}}{\mathbf{C_{initial}}} \times \mathbf{100} \qquad \textbf{Equation 20}$$

To study copolymerization composition of AA and MMA, experiments were carried out with MWCNTs (0.6 mg) and sodium dodecyl sulfate solution (6mM) in 10ml vials. Samples were sonicated using an ultra sonic dismembrator (25% power of 10 watts) for 10 min at room temperature. Combined total concentrations of 4mM of monomers AA

and MMA were added to vials for adsolubilization and react as before. To utilize the copolymer equation, the monomer conversion rate was restricted to less than 10%. From the conversion experiments, the time for polymerization was set to 1hr. After the set time, the reaction was stopped by cooling in an ice bath. After the vials were cooled to room temperature, Amicon Ultra-0.5 mL centrifugal filters were used to separate supernatant solution from the MWCNTs at 10000 rpm for 30 min. A small aliquot from the centrifuged vials was filtered further with 0.45μm size filters prior to analysis by HPLC. The copolymer composition was inferred from the initial and final concentration changes measured by using a C18 surfactant column (RESTEK) (dimensions of 250mm x 4.6mm) with a UV-Vis detector for monomers AA (200nm) and MMA (231mm). Mobile phases used for analysis were methanol and water in ratios of 85:15 for AA and MMA, respectively. Calibration curves were obtained for monomers followed by measurements for percent conversion and copolymer composition.

6.5 Results and Discussion

Commercially available pristine MWCNTs were encapsulated with sodium salt of poly acrylic acid and poly methyl methacrylate copolymers to obtain a semi water-soluble nanocomposites using AP. Samples were analyzed to confirm the interaction of polymer with carbon nanotubes. Pristine MWCNTs are used as obtained and encapsulated nanotubes are termed as PAA-MWCNTs, PMMA-MWCNTs and PAA/PMMA – MWCNTs.

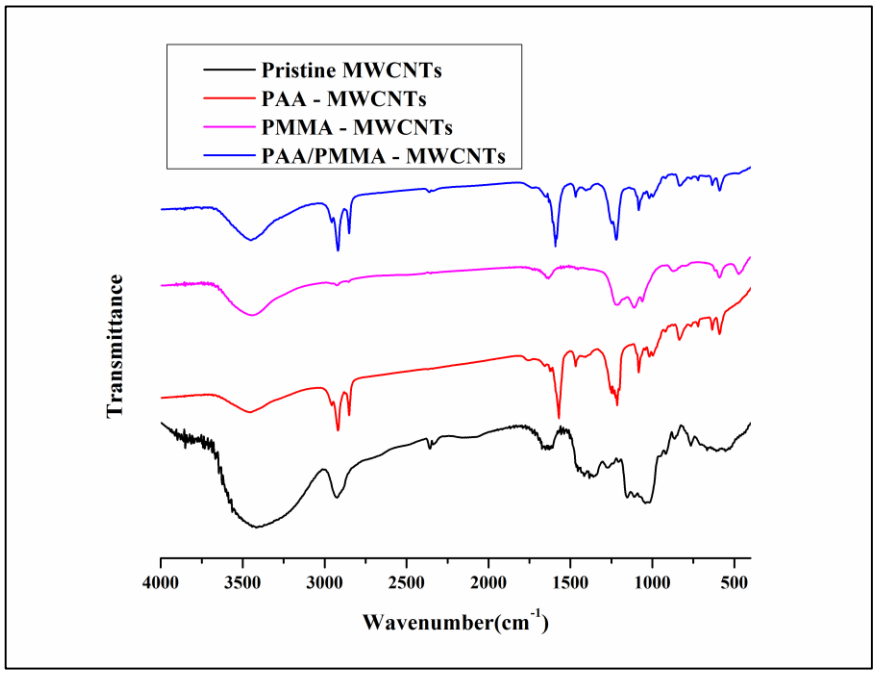


Figure 38. FTIR analysis of pristine MWCNTs and encapsulated MWCNTs

6.5.1 Analysis of Encapsulated MWCNTs

FTIR spectra of pristine MWCNTs, PAA-MWCNTs, PMMA-MWCNTs and PAA/PMMA-MWCNTs are displayed in Figure 38. The characteristic peaks of polymers can be observed in all the encapsulated samples. The peaks between 1000 cm^{-1} to 1200 cm^{-1} are attributed to stretching vibration of C-O group present in all encapsulated samples. In PMMA-MWCNTs, the characteristic peak for a C=O carbonyl group at 1733 cm^{-1} is clear in the spectra along with other characteristic peaks for PMMA. The peak at 1562 cm^{-1} corresponds to an anti-symmetric peak for carboxyl group (–COO) in PAA samples evident in PAA-MWCNTs and PAA/PMMA-MWCNTs. The peak at 2940 cm^{-1} corresponds to the stretching mode of C-H vibration of polymer evident in all samples. The interactions for PAA-MWCNTs and PAA/PMMA-MWCNTs at 2940 cm^{-1} are present even in MWCNTs indicating MWCNTs are undisturbed after PAA wrapping[149]. The peak at 1275 cm^{-1}

corresponds to a C-O symmetric peak for PAA interactions with the nanotube surface evident in both PAA-MWCNTs and PAA/PMMA-MWCNTs[152]. From the results, it suggests that physical interactions between MWCNTs and polymer exist. The strong peaks observed at the respective wavenumbers suggest that interactions are stronger between MWCNTs and polymer. The FTIR does not provide unambiguous evidence for the presence of PMMA, which could be inferred from conversion and TGA data (see below).

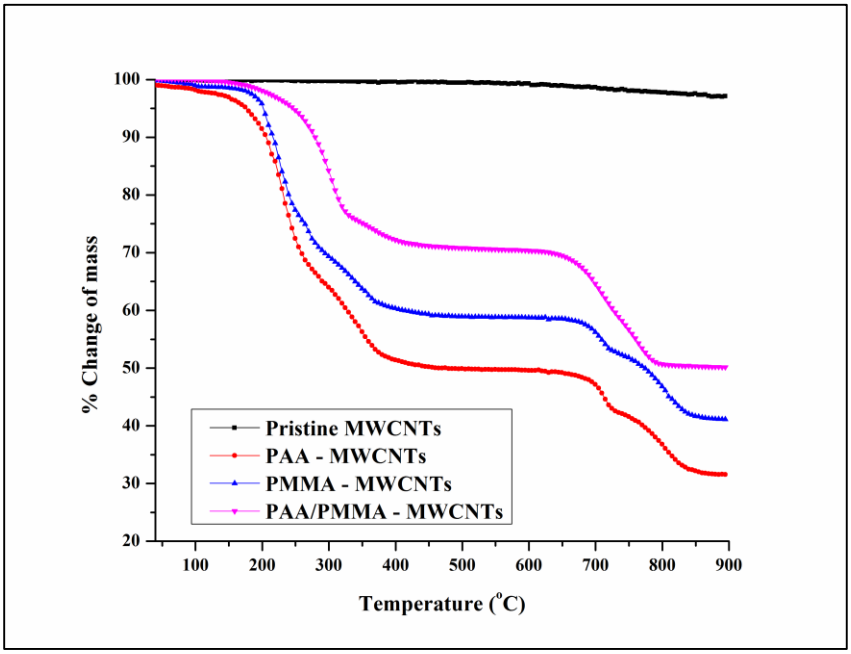


Figure 39. TGA of pristine MWCNTs and encapsulated MWCNTs

Results for thermo gravimetric analysis of pristine MWCNTs, PAA-MWCNTs, PMMA-MWCNTs, and PAA/PMMA-MWCNTs are plotted in Figure 39. Thermo gravimetric analysis provides data on polymer content. The rate of decomposition of polymer depends on molecular weight and tacticity which have a profound effect on decomposition rate [164]. The pristine carbon nanotubes have negligible weight loss even after heating to 900°C in an inert atmosphere because of high thermal stability. In

the case of PAA-MWCNTs around 50% weight loss was observed when the temperature reached 400^{o}C. In the case of PMMA-MWCNTs, when the temperature reached 400^{o}C there was a weight loss of about 30%. PMMA doesn't decompose until around 250^{o}C - 300^{o}C as the end chain mechanism do not occur due to lack of double bond[164]. The polymer content for the copolymer of PAA and PMMA was around 40% at 400^{o}C. At 600^{o}C an additional weight loss of about 20- 25%, occurs due to decomposition of higher weight fractions formed during the initial stage of decomposition at 250-300 ^{o}C. Thus the polymer content in the samples was added to around 70% for PAA, 60% for PAA/PMMA and 50% for PMMA encapsulated MWCNTs. The chemical cross-linked copolymer of PMMA was found to decompose by forming char rather than end chain scission resulting in a polymer with high thermal stability[164]. The thermal stability of the copolymer of PAA/PMMA increased as the decomposition temperature increased compared to PAA encapsulated MWCNTs. Moreover, TGA provides evidence in support of the presence of PMMA in the copolymer.

SEM images obtained for pristine MWCNTs, PAA-MWCNTs, PMMA-MWCNTs and PAA/PMMA-MWCNTs are represented in Figure 40. Encapsulation of thin films of polymer on nanotube surface increases the diameter of MWCNTs. The average diameters of pristine and encapsulated MWCNTs were measured using ImageJ image analysis program. Average diameters of encapsulated MWCNTs were around 13nm (Table 14) while the diameter of pristine MWCNTs were smaller compared to encapsulated nanotubes. The diameters (Table 14) for PAA-MWCNTs, PMMA-

MWCNTs and PAA/PMMA-MWCNTs were more or less equal. The average diameters confirm thickness of polymer of about 4nm around the surface of MWCNTs.

Table 14. Average diameter from SEM micrographs

Sample	Average diameter (nm)
Pristine MWCNTs	9.2
PAA - MWCNTs	13.2
PMMA - MWCNTs	12.6
PAA/PMMA - MWCNTs	13.2

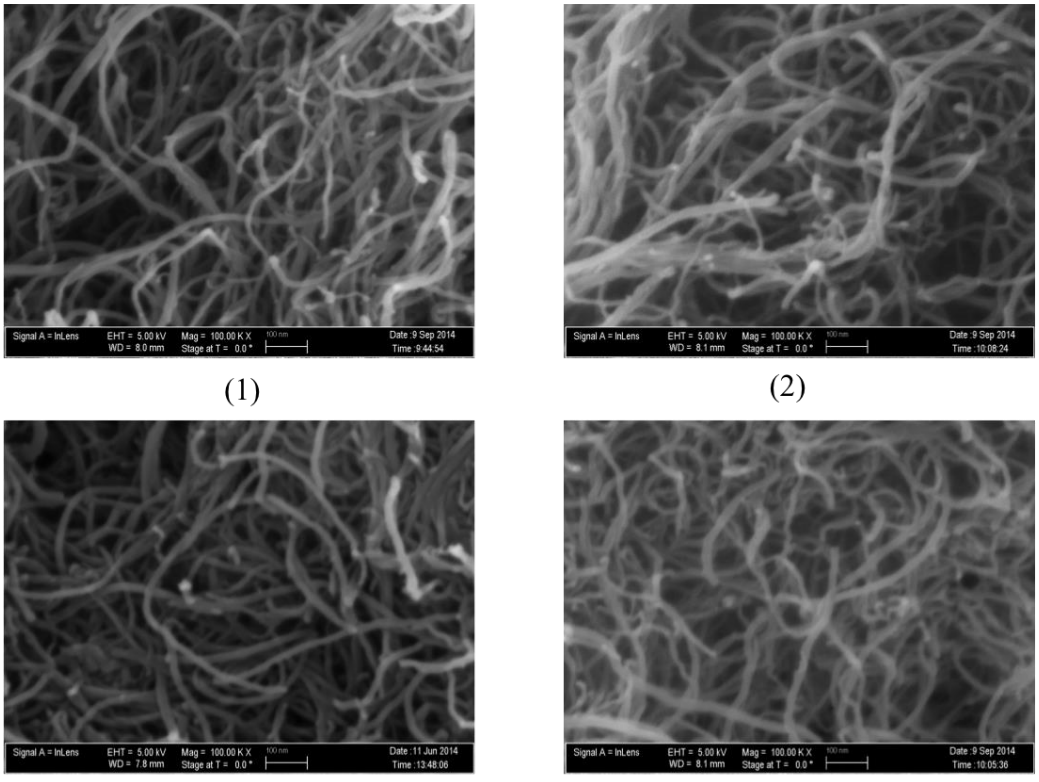


Figure 40. SEM micrographs (1) pristine MWCNTs (2) PAA – MWCNTs (3) PMMA – MWCNTs (4) PAA/PMMA – MWCNTs

Energy dispersive spectroscopy was conducted to obtain elemental composition of samples with the weight percentage of elements present in pristine MWCNTs and encapsulated MWCNTs shown in Table 15. Pristine MWCNTs contain mostly carbon as evidenced by the elemental analysis. Polymer formation around the surface of nanotubes decreases the percentage of carbon but increases the amount of oxygen and sodium. High percentages of carbon are observed in all encapsulated samples because the high energy X-ray beam can cause surface melting of polymer and expose the nanotubes during testing. The amount of sodium and sulphur in PMMA-MWCNTs, are contributed by trace amounts of surfactant on the nanotube surface even after washing the sample. Addition of sodium bicarbonate to control reaction pH increases the amount of sodium in PAA-MWCNTs and PAA/PMMA-MWCNTs, as the salts of polymer are present in the samples.

Table 15. EDS analysis for elemental composition of encapsulated MWCNTs

Sample	Carbon	Oxygen	Sodium	Sulphur
Pristine MWCNTs	97	2.8	0	0
PAA - MWCNTs	87.6	9.0	2.5	0.9
PMMA - MWCNTs	92.4	6.9	0.8	1.1
PAA/PMMA - MWCNTs	90.2	7.5	1.6	0.7

Figure 41 shows typical UV-Visible spectra obtained from dilute solutions of pristine multi-walled carbon nanotubes and encapsulated nanotubes. UV-Vis spectra were performed to observe any change in electronic structure of nanotube surface or interaction between polymer and nanotubes[158]. No significant peaks were observed for interactions between nanotubes and polymers. At around 220 nm, small bands were

observed in samples, which can be attributed to C=C interaction of MWCNTs. In addition several weak bands were observed at around 900 nm, might indicate a band-to-band transition of nanotubes in composite. No significant evidence is obtained to confirm the change in electronic structure of nanotubes from UV-Vis analysis.

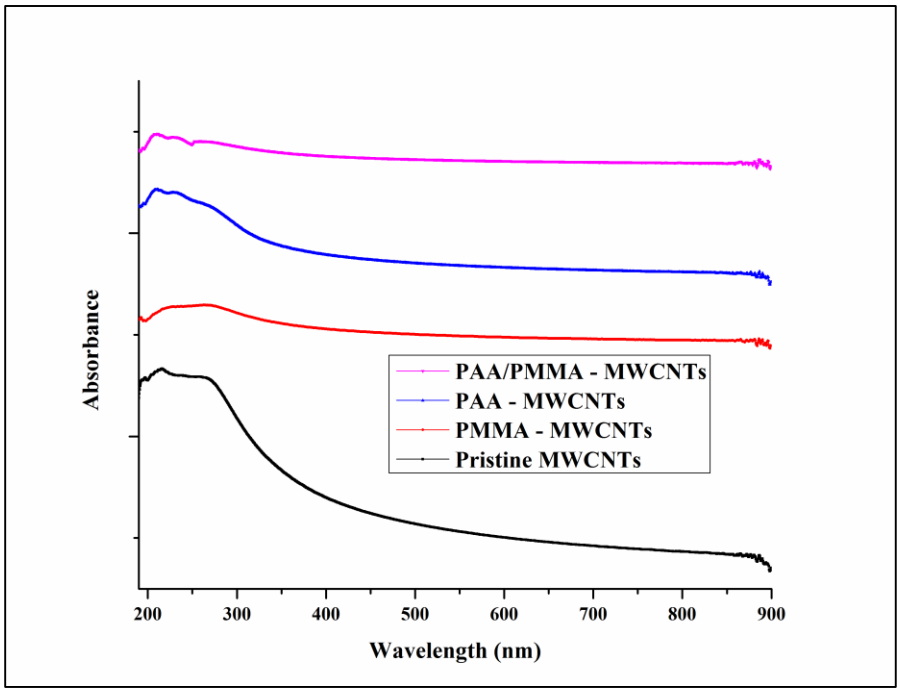


Figure 41. UV-Vis spectra of pristine MWCNTs and encapsulated MWCNTs

6.5.2 Determination of Monomer Conversion and Copolymer Composition

Conversions of monomers (AA, MMA) to form a copolymer on MWCNTs were plotted in Figure 42. Monomer conversion rate was calculated using equation 20. It is clear that the rate of conversion of AA was higher than that of MMA. As acrylic acid is smaller molecule than methyl methacrylate, diffusion of acrylic acid monomer from supernatant solution is higher than the MMA. When the polymerization reaction initiates, monomer diffuses from supernatant to surfactant micelles to compensate the loss during polymerization reaction[165]. Similarly, polymerization proceeds on the surface as the

monomer concentration is maintained at the equilibrium level by diffusion of monomer from solution. From Figure 42, the conversion rate increases with time and reaches around 80% conversion rate at 14 hrs and remains constant thereafter, indicating saturation of polymerization. Polymerization rate is unaffected once the monomer molecules have reached saturation in supernatant solution and polymer was saturated on the surface[166].

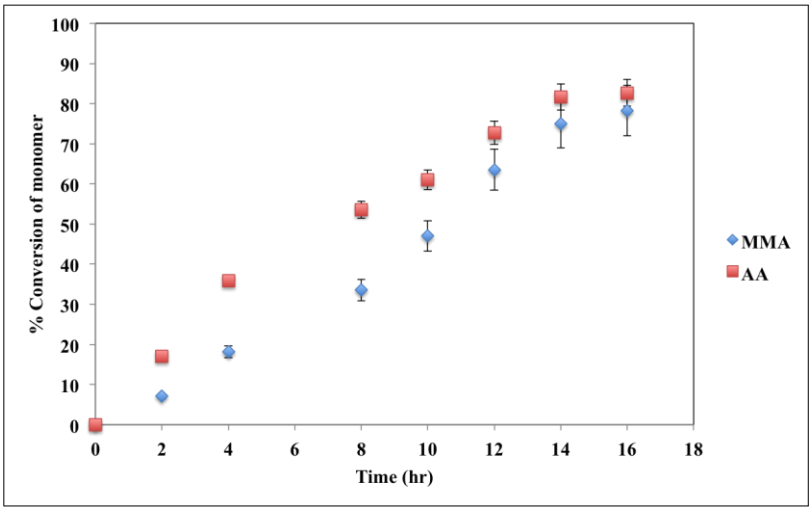


Figure 42. Conversion of monomers vs. time

We used high performance liquid chromatography to find the copolymer composition and monomer reactivity ratios r_1 and r_2. Mole fractions of monomers AA and MMA in the feed are given as F_1 and F_2. Mole fractions of co-monomer units in the copolymer (f_1 and f_2) found using analysis of the supernatant solution were also found using HPLC. Copolymerization reactions were carried out under low conversion conditions (<10%) to determine monomer reactivity ratios (r_1 and r_2) in the stationary kinetic stage by using known terminal models of Fineman-Ross and Kelen-Tüdos equations, (equations 21 and 22) respectively:

Table 16. Fineman-Ross and Kelen-Tüdos parameters for copolymerization of AA and MMA

Mole fraction of AA		Mole ratio of AA		Fineman-Ross		Kelen - Tüdos	
In feed F_1	In copolymer f_1	In feed X	In copolymer Y	$\frac{X^2}{Y}$	$\frac{X(Y-1)}{Y}$	ξ	η
0.15	0.215	0.176	0.275	0.113	-0.464	0.127	-0.640
0.30	0.335	0.428	0.504	0.363	-0.420	0.325	-0.430
0.45	0.495	0.818	0.980	0.682	-0.016	0.428	-0.012
0.60	0.603	1.500	1.520	1.480	0.513	0.694	0.245
0.75	0.731	3.000	2.721	3.306	1.897	0.992	0.484

$$\frac{X(Y-1)}{Y} = r_1\left(\frac{X^2}{Y}\right) - r_2 \qquad \textbf{Equation 21}$$

$$\eta = \left(r_1 + \frac{r_2}{\alpha}\right)\xi - \frac{r_2}{\alpha} \qquad \textbf{Equation 22}$$

Where X is the mole ration of monomers in feed, X = [AA/MMA]; Y is the mole ratio of co-monomer units in copolymers. ξ and η are parameters of Kelen-Tüdos and α is arbitrary constant.

$$Y = \frac{f_1}{f_2} \qquad \textbf{Equation 23}$$

$$\xi = \left(\frac{X^2}{Y}\right) \Big/ \left(\left(\frac{Y^2}{Y}\right) + \alpha\right) \qquad \textbf{Equation 24}$$

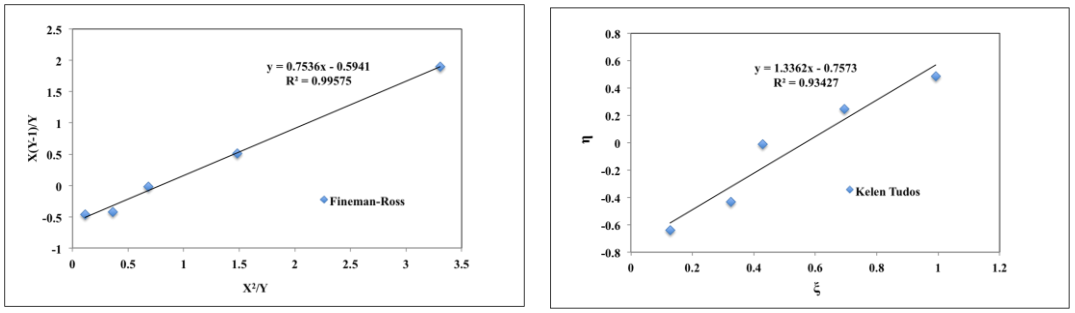
$$\eta = \left(\frac{X(Y-1)}{Y}\right) \Big/ \left(\frac{X^2}{Y} + \alpha\right) \qquad \textbf{Equation 25}$$

$$\alpha = \left[\left(\frac{X^2}{Y}\right)_{min}\left(\frac{X^2}{Y}\right)_{max}\right]^{1/2} \qquad \textbf{Equation 26}$$

Table 16 lists the parameters for Fineman-Ross and Kelen-Tüdos calculated using equations 21 and 22. To obtain monomer reactivity ratios by the Fineman-Ross method, equation 21 was plotted (Figure 43a) to obtain the slope and intercept. The slope and intercept gives the monomer reactivity ratios r_1 and r_2 as 0.7536 and 0.5941. From the Kelen-Tüdos plot (Figure 43b) of equation 22, monomer reactivity ratios were calculated giving r_1 as 0.5789 and r_2 as 0.4629. The reactivity ratios confirm that AA has higher polymerization rate than MMA[167]. The product of the monomer ratios (r_1r_2) was much lower than 1 indicating the copolymer system showed an alternating tendency and formed random copolymers. Fineman-Ross and Kelen-Tüdos methods gave similar trends of the monomer reactivity ratios. Because r_1 and r_2 values were less than 1 and from curve in Figure 44, AA and MMA system was found to exhibit azeotropic polymerization at a particular composition.

The azeotropic composition was calculated using equation 27.

$$F_A = \frac{1-r_2}{2-r_1-r_2} \qquad \textbf{Equation 27}$$



(a) (b)

Figure 43. Fineman-Ross (a) and Kelen-Tüdos (b) plots for copolymer of AA and MMA with a total concentration of 4mM and mole fraction of AA in co-monomer feed varied from 0.15 to 0.75

The azeotropic composition calculated from the Fineman-Ross and Kelen-Tüdos methods were 0.62 and 0.56 respectively, which were close to that of 0.6 as plotted in Figure 44. When the mole fraction of AA in the feed (F_1) was 0.6, the copolymer formed would have the same composition as that of the feed. When F_1 was lower than 0.6, AA in the copolymer composition was higher than that in the feed. When F_1 was above 0.6, the copolymer was richer in MMA units. Although the system showed a tendency toward an alternating copolymer ($r_1 \cdot r_2 < 1$), there was a small range of feed composition (0.6-1.0) in which the resulting copolymer was richer in MMA units. Thus, formation of an alternating copolymer occurred preferentially with AA monomer.

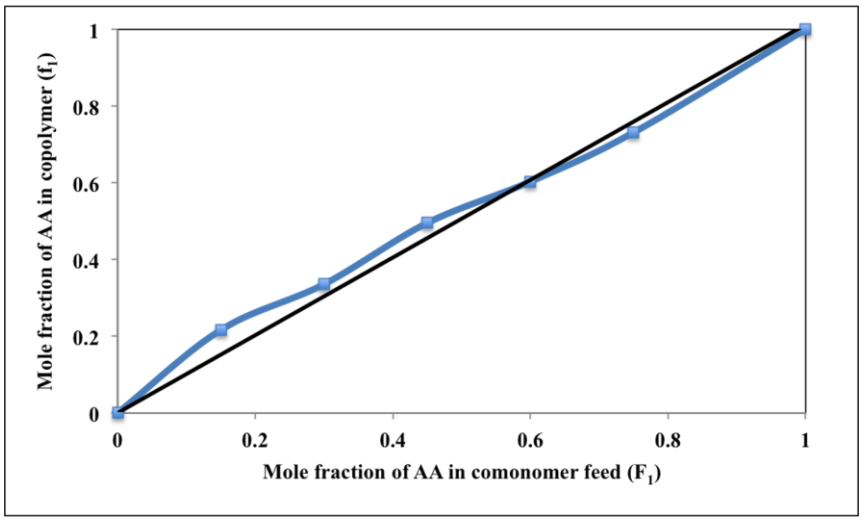
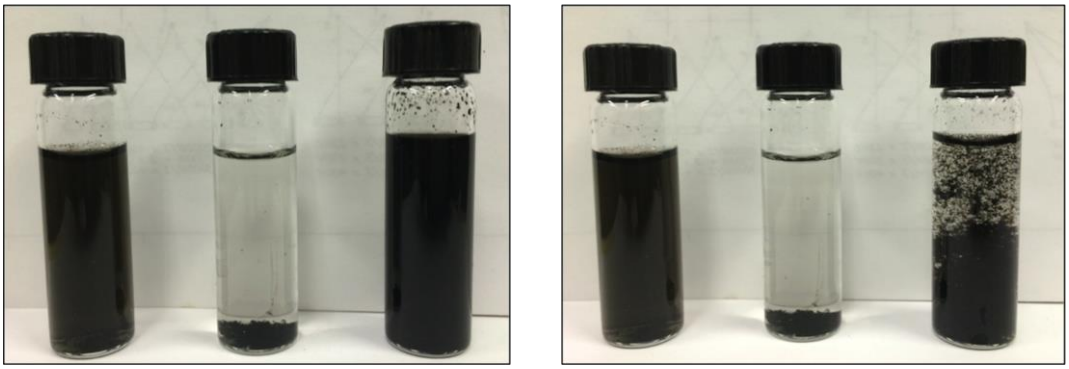


Figure 44. Comparison mole fraction of AA in co-monomer feed and the mole fraction in copolymer feed**.**

6.5.3 Dispersion Stability of Encapsulated MWCNTs:



(1) (2)

Figure 45. Solubility of encapsulated MWCNTs in aqueous media at different time frames (1) 3 days (2) 40 days

To analyze the dispersion stability of encapsulated polymers on MWCNTs, samples were dissolved in aqueous media (Figure 45). Encapsulation of hydrophilic polymer has a significant effect on dispersion of the MWCNTs, as the PAA-MWCNTs remain stable even after 40 days. The carboxyl group in PAA surrounding the MWCNTs should

decrease the van der Waals force between the nanotubes thus making the encapsulated MWCNTs dispersible in aqueous media. PMMA-MWCNTs formed aggregates and settled at the bottom of vial in less than 3 days, as the PMMA is hydrophobic. Copolymer of PAA/PMMA-MWCNTs was stable for 40 days, although the dispersion was not stable after 40 days and showed a tendency to form aggregates. This indicates the formation of hydrophobic PMMA in encapsulated MWCNTs does affect the stability of dispersion in aqueous media. Therefore a copolymer formation of hydrophobic and hydrophilic content does affect the stability of dispersion. The advantage of using polymerization mechanism is that, we can form a thin film of polymeric encapsulation without disturbing the surface heterogeneity of carbon nanotubes. The formed thin film of copolymer is stable for up to 40 days.

6.6 Conclusion

In this work, we demonstrated the application of admicellar polymerization to obtain thin films on MWCNTs. A thin film of copolymer on the surface was effectively developed using PAA and PMMA. FTIR results confirmed the presence of copolymer in the samples. Around 4nm thick films of polymer were formed due to admicellar polymerization. The monomers AA and MMA showed an alternating tendency in copolymer formation on the surface and exhibited an azeotropic composition around 0.6 of monomer AA. The PAA-MWCNTs formed a stable dispersion even after 40 days but copolymers of PAA/PMMA-MWCNTs were stable for up to 40 days and after which the copolymer began to form aggregates.

Chapter 7

Conclusions

In this dissertation, application of admicellar polymerzation to develop the properties on the substrate surface has been explained. Formulations were developed to obtain thin film coatings on the surfaces of cotton and multiwalled carbon nanotubes to obtain the respective properties.

7.1 Summmary from Part I

- Developed formulations to obtain thin film coatings on susbstrate surface using admicellar polymerization.
- Adsorption and adsolubilization data were obtained for a cationic surfactant (FS1620) and zwitterionic surfact (FS230) with TFEM, OFPM fluoromonomers.
- Aggregation numbers of fluorosurfactants were calculated using two-site adsolubilization model to analyze the polymer formation on the surface.
- PA1 and PA2 formulations were developed to obtain stain resistance/stain release properties.
- The performance of the fabric was compared to commercially available samples to evaluate the quality of the treatment.
- Formulations were scaled up from laboratory scale of 20ml vial size to pilot scale unit size of 68L.

7.2 Summary from Part II

- Formulations were developed to obtain thin film coatings on the surface of multi-walled carbon nanotubes.
- Two different formulations were developed to obtain semi-hydrophilic properties.
- Developed adsorption isotherms and adsolubilization data to obtain the optimal formulation.
- Modifed two-site adsolubilization model to obtain the aggregation numbers of surfactants on the MWCNTs surface.
- Thin films formed on the MWCNTs were stable even after 3 days.

Bibilography

1. O'Haver, J.H.; Harwell, J.H.; O'Rear, E.A.; Snodgrass, L.J.; Waddell, W.H. *In situ Formation of Polystyrene in Adsorbed Surfactant Bilayers on Precipitated Silica.* Langmuir, 1994. **10**(8): p. 2588-2593.

2. Wang, S.; Russo, T.; Qiao, G.; Soloman, D.; Shanks, R. *Admicellar polymerization of styrene with divinyl benzene on alumina particles: the synthesis of white reinforcing fillers.* Journal of Materials Science, 2006. **41**(22): p. 7474-7482.

3. Karlsson, P.M.; Esbjornsson, N.B.; Holmberg, K. *Admicellar polymerization of methyl methacrylate on aluminum pigments.* Journal of Colloid and Interface Science, 2009. **337**(2): p. 364-368.

4. Pongprayoon, T.; O'Rear, E.A.; Yanumet, N.; Yuan, W.L. *Wettability of cotton modified by admicellar polymerization.* Langmuir, 2003. **19**(9): p. 3770-3778.

5. Pongprayoon, T., Yanumet, N.; O'Rear, E.A. *Admicellar polymerization of styrene on cotton.* Journal of Colloid and Interface Science, 2002. **249**(1): p. 227-234.

6. Barraza, H.J.; Hwa, M.J.; Blakely, K.; O'Rear E.A.; Grady, B.P. *Wetting Behavior of Elastomer-Modified Glass Fibers.* Langmuir, 2001. **17**(17): p. 5288-5296.

7. Matarredona, O.M.; Mach, K.; Rieger M.M; O'Rear, E.A. *Alteration of wettability and inhibition of corrosion in narrow aluminium 7075 gaps by thin polymer films.* Corrosion Science, 2003. **45**(11): p. 2541-2562.

8. Yuan, W.L.; O'Rear, E.A.; Grady, B.P.; Glatzhofer, D.T. *Nanometer-Thick Poly(pyrrole) Films Formed by Admicellar Polymerization under Conditions of Depleting Adsolubilization.* Langmuir, 2002. **18**(8): p. 3343-3351.

9. Poochai, C.; Pongprayoon, T. *Enhancing dispersion of carbon nanotube in polyacrylonitrile matrix using admicellar polymerization.* Colloids and Surfaces A: Physicochemical and Engineering Aspects, 2014. **456**(0): p. 67-74.

10. Pomthong, M.; Siriporn, R.; Savanit, J.; O'haver, J.H. *Surfactant adsortion and adsolubilization of organic compounds in single and mixed surfactant systems of cationic -nonionic surfactants adsorbed on precipitated silica.* Asahi glass foundation, 2009: p. 2-11.

11. Kitiyanan, B.; O'Haver, J.H.; Jeffrey, J.H.; Osuwan, S. *Absolubilization of Styrene and Isoprene in Cetyltrimethylammonium Bromide Admicelle on Precipitated Silica.* Langmuir, 1996. **12**(9): p. 2162-2168.

12. Dickson, J.; O'Haver, J.H. *Adsolubilization of Naphthalene and α-Naphthol in CnTAB Admicelles.* Langmuir, 2002. **18**(24): p. 9171-9176.

13. Lai, C.L.; Harwell, J.H.; O'Rear, E.A.; Komatsuzaki, S.; Arai, J.; Nakakawaji, T.; Ito, Y. *Adsorption isotherms of perfluorocarbon surfactants from aqueous and non-aqueous solutions and friction measurements of perfluorosurfactant-adsorbed alumina.* Colloids and Surfaces A: Physicochemical and Engineering Aspects, 1995. **104**(2-3): p. 231-241.

14. Barton, J.W.; Fitzgerald, T.P.; Lee, C.; O'Rear, E.A.; Harwell, J.H. *Admicellar Chromatography: Separation and Concentration of Isomers Using Two-Dimensional Solvents.* Separation Science and Technology, 1988. **23**(6-7): p. 637-660.

15. Esumi, K.; Maedomari, N.; Torigoe, K. *Mixed Surfactant Adsolubilization of 2-Naphthol on Alumina.* Langmuir, 2000. **16**(24): p. 9217-9220.

16. Wu, J.; Harwell, J.H.; O'Rear, E.A. *Two-dimensional reaction solvents: surfactant bilayers in the formation of ultrathin films.* Langmuir, 1987. **3**(4): p. 531-537.

17. Lai, C.L.; O'Rear, E.A.; Harwell, J.H.; Hwa, M.J. *Adsolubilization of Fluorocarbon Alcohols into Perfluoroheptanoate Admicelles Formed on Alumina.* Langmuir, 1997. **13**(16): p. 4267-4272.

18. Paria, S.; Manohar, C.; Khilar, K.C. *Adsorption of anionic and non-ionic surfactants on a cellulosic surface.* Colloids and Surfaces A: Physicochemical and Engineering Aspects, 2005. **252**(2-3): p. 221-229.

19. Somasundaran, P.; Krishnakumar, S. *Adsorption of surfactants and polymers at the solid-liquid interface.* Colloids and Surfaces a-Physicochemical and Engineering Aspects, 1997. **123**: p. 491-513.

20. Nayyar, S.P.; Sabatini, D.A.; Harwell, J.H. *Surfactant Adsolubilization and Modified Admicellar Sorption of Nonpolar, Polar, and Ionizable Organic Contaminants.* Environmental Science & Technology, 1994. **28**(11): p. 1874-1881.

21. Jansen, J.; Treiner, C.; Vaution, C. *Coadsorption of Steroids and Nonionic Surfactants on Polystyrene Latex Particles from Aqueous Solutions.* Journal of Colloid and Interface Science, 1996. **179**(2): p. 578-586.

22. Hari, A.C.; Paruchuri, R.A.; Sabatini, D.A.; Kibbey, T.C.G. *Effects of pH and Cationic and Nonionic Surfactants on the Adsorption of Pharmaceuticals to a*

Natural Aquifer Material. Environmental Science & Technology, 2005. **39**(8): p. 2592-2598.

23. Sakhalkar, S.S.; Hirt, D.E. *Admicellar Polymerization of Polystyrene on Glass Fibers.* Langmuir, 1995. **11**(9): p. 3369-3373.

24. Pongprayoon, T.; O'Rear, E.A.; Yanumet, N.; Yuan, W.L. *Wettability of cotton modified by admicellar polymerization.* Langmuir, 2003. **19**(9): p. 3770-3778.

25. Jang, I.B.; Sung, J.H.; Choi, H.J.; Chin, I. *Synthesis and characterization of TiO2/polystyrene hybrid nanoparticles via admicellar polymerization.* Journal of Materials Science, 2005. **40**(11): p. 3021-3024.

26. Karlsson, P.M.; Esbj√∂rnsson, N.B.; Holmberg, K. *Admicellar polymerization of methyl methacrylate on aluminum pigments.* Journal of Colloid and Interface Science, 2009. **337**(2): p. 364-368.

27. Lei, L.; Qiu, J.; Sakai, E. *Preparing conductive poly(lactic acid) (PLA) with poly(methyl methacrylate) (PMMA) functionalized graphene (PFG) by admicellar polymerization.* Chemical Engineering Journal, 2012. **209**(0): p. 20-27.

28. Sakai, K.; Nakajima, E.; Takamatsu, Y.; Sharma, S.C.; Torgie, K.; Esumi, K.; Abe, M. *Adsorption of Cationic Monomeric and Gemini Surfactants on Montmorillonite and Adsolubilization of Vitamin E.* Journal of Oleo Science, 2008. **57**(8): p. 423-429.

29. Koner, S.; Pal, A.; Adak, A. *Utilization of silica gel waste for adsorption of cationic surfactant and adsolubilization of organics from textile wastewater: A case study.* Desalination, 2011. **276**(1-3): p. 142-147.

30. Koner, S.; Pal, A.; Adak, A. *Cationic surfactant adsorption on silica gel and its application for wastewater treatment.* Desalin. Water Treat., 2010. **22**(Copyright (C) 2012 American Chemical Society (ACS). All Rights Reserved.): p. 1-8.

31. Moral, A.; Sicilia, M.D.; Rubio, S.; Dolores, P.B. *Sodium dodecyl sulphate-coated alumina for the extraction/preconcentration of benzimidazolic fungicides from natural waters prior to their quantification by liquid chromatography/fluorimetry.* Analytica Chimica Acta, 2006. **569**(1‚Äì2): p. 132-138.

32. Garcia-Prieto, A.; Lunar, L.; Rubio, S.; Dolores, P.B. *Hemimicelle-based solid-phase extraction of estrogens from environmental water samples.* Analyst, 2006. **131**(3): p. 407-414.

33. Yu, C.C.; Wong, D.W.; Lobban, L.L. *Catalysis of the hydrolysis of trimethyl orthobenzoate by adsorbed sodium dodecyl sulfate.* Langmuir, 1992. **8**(10): p. 2582-2584.

34. Meguro, K.; Yabe, T.; Ishioka, S.; Kato, K.; Esumi, K. *Polymerization of Styrene Adsolubilized in Surfactant Adsorbed Bilayer on Pigments.* Bulletin of the Chemical Society of Japan, 1986. **59**(10): p. 3019-3021.

35. Ren, X.; Kou, L.; Kocer, K.H.; Worley, S.D.; Huang, T.S. *Antimicrobial modification of polyester by admicellar polymerization.* Journal of Biomedical Materials Research Part B: Applied Biomaterials, 2009. **89B**(2): p. 475-480.

36. Maldonado, F.; Bauitista, E.; Manich, A.M.; Marsal, A. *Adsolubilisation of organic compounds onto collagen fibres.* Journal of Colloid and Interface Science, 2010. **351**(2): p. 466-471.

37. O'Haver, J.H.; Lobban, L.L.; Harwell, J.H.; O'Rear, E.A. *Solubilization in Surfactant Aggregates* in *Surfactant Science Series*, J.F.S. Sherril D. Christian, Editor. 1995, Marcel Dekker Inc.: New york. p. P. 277.

38. Tsurumi, D.; Sakai, K.; Yoshimura, T.; Esumi, K. *Adsolubilization of 2-naphthol into adsorbed layers of triblock PEO-PPO-PEO copolymers on hydrophobic silica particles.* Journal of Colloid and Interface Science, 2006. **302**(1): p. 82-86.

39. Nunn, C.C.; Schechter, R.S.; Wade, W.H. *Visual evidence regarding the nature of hemimicelles through surface solubilization of pinacyanol chloride.* The Journal of Physical Chemistry, 1982. **86**(16): p. 3271-3272.

40. Pradubmook T.; O'Haver, J.H.; Malakul, P.; Harwell, J.H. *Effect of pH on adsolubilization of toluene and acetophenone into adsorbed surfactant on precipitated silica.* Colloids and Surfaces a-Physicochemical and Engineering Aspects, 2003. **224**(1-3): p. 93-98.

41. Esumi, K.; Shibayama, M.; Meguro, K. *Adsolubilization of Alcohols in Surfactant Bilayers Formed on Alumina.* Langmuir, 1990. **6**(4): p. 826-829.

42. Aloulou, F.; Bourfi, S.; Belgacem, N.; Gandini, A. *Adsorption of cationic surfactants and subsequent adsolubilization of organic compounds onto cellulose fibers.* Colloid & Polymer Science, 2004. **283**(3): p. 344-350.

43. Esumi, K. *Interactions between Surfactants and Particles: Dispersion, Surface Modification, and Adsolubilization.* Journal of Colloid and Interface Science, 2001. **241**(1): p. 1-17.

44. Li, L.; Wang, L.S.; Du, X.G.; Lu., Y.; Yang, Z.Y. *Adsolubilization of dihydroxybenzenes into CTAB layers on silica particles.* Journal of Colloid and Interface Science, 2007. **315**(2): p. 671-677.

45. Harwell, J.H.; Hoskins, J.C.; Schechter, R.S.; Wade, J.H. *Pseudophase separation model for surfactant adsorption: isomerically pure surfactants.* Langmuir, 1985. **1**(2): p. 251-262.

46. Lee C.; Yeskie, M.A.; Harwell, J.H.; O''Rear, E.A. *2-Site Adsolubilization Model of Incorporation of Alcohols into Adsorbed Surfactant Aggregates.* Langmuir, 1990. **6**(12): p. 1758-1762.

47. See, C.H.; O'Haver, J.H. *Two-dimensional phase transition of styrene adsolubilized in cetyltrimethylammonium bromide admicelles on mica.* Colloids and Surfaces A: Physicochemical and Engineering Aspects, 2004. **243**(1,Äì3): p. 169-183.

48. Behrends, T.; Holzheu, S.; Herrmann, R. *A three-site model to describe the adsolubilization of aromatic compounds at surfactant covered silica.* Acta Hydrochimica Et Hydrobiologica, 1999. **27**(6): p. 422-429.

49. Misra, P.K.; Somasundaran, P. *Fluorescence probing of the surfactant assemblies in solutions and at solid-liquid interfaces.* Adv. Polym. Sci., 2008. **218**(Copyright (C) 2013 American Chemical Society (ACS). All Rights Reserved.): p. 143-188.

50. Lai C.L.; O'Rear, E.A.; Harwell, J.H.; Hwa, M.J.; *Adsolubilization of fluorocarbon alcohols into perfluoroheptanoate admicelles formed on alumina.* Langmuir, 1997. **13**(16): p. 4267-4272.

51. Hanumansetty, S.; Maity, J.; Foster, R.; O'Rear, E.A. *Stain Resistance of Cotton Fabrics before and after Finishing with Admicellar Polymerization.* Applied Sciences, 2012. **2**(1): p. 192-205.

52. Cases, J.M.; Villieras, F. *Thermodynamic model of ionic and nonionic surfactants adsorption-abstraction on heterogeneous surfaces.* Langmuir, 1992. **8**(5): p. 1251-1264.

53. Esumi, K.; Ono, Y.; Ishizuka, M.; Merugo, K. *Interaction between hydrocarbon and fluorocarbon surfactants on monodispersed ferric hydro sols.* Colloids and Surfaces, 1988. **32**(0): p. 139-147.

54. Matsuoka, K.; Moroi, Y. *Micellization of fluorinated amphiphiles.* Current Opinion in Colloid & Interface Science, 2003. **8**(3): p. 227-235.

55. Cases, J.M.; Villieras, F.; Michot, L.J.; Bersillon, J.L. *Long chain ionic surfactants: the understanding of adsorption mechanisms from the resolution of adsorption isotherms.* Colloids and Surfaces A: Physicochemical and Engineering Aspects, 2002. **205**(1–2): p. 85-99.

56. Wakelin, J.H.; Virgin, H.S.; Crystal, E. *Development and Comparison of Two X- Ray Methods for Determining the Crystallinity of Cotton Cellulose.* Journal of Applied Physics, 1959. **30**(11): p. 1654-1662.

57. Kothary, P. *Optimization of admicellar polymerizatio for formation of hydrophobic thin films on cotton*, in *Chemical Bio and Materials Engineering Department*. 2009, University of Oklahoma. p. 131.

58. Cakara, D.; Fras, L.; Bracic, M.; Kleinschek, K.S. *Protonation behavior of cotton fabric with irreversibly adsorbed chitosan: A potentiometric titration study.* Carbohydrate Polymers, 2009. **78**(1): p. 36-40.

59. Myers, D. *Surfactant Science and Technology*. 1988, New York: VCH.

60. Yeskie, M.A., *Various Aspects of Surfactant Aggregates Adsorbed on an Oxide Surface: The Hemimicelle/Admicelle Transition and the Interaction of Alcohols and Alkanes*, in *Chemical, Bio and Materials Engineering Department*. 1988, University of Oklahoma: Norman.

61. Tan, Y.Q.; O'Haver, J.H. *Use of the BET adsorption isotherm equation to examine styrene adsolubilization by nonionic surfactants at the water-silica interface.* Journal of Colloid and Interface Science, 2004. **279**(2): p. 289-295.

62. Saphanuchart, W.; Saiwan, C.; O'Haver, J.H. *Temperature effects on adsolubilization of aromatic solutes partitioning to different regions in cationic admicelles.* Colloids and Surfaces a-Physicochemical and Engineering Aspects, 2008. **317**(1-3): p. 303-308.

63. Funkhouser, G.P.; Arevalo, M.P.; Glatzofer, D.T.; O'Rear, E.A. *Solubilization and Adsolubilization of Pyrrole by Sodium Dodecyl-Sulfate - Polypyrrole Formation on Alumina Surfaces.* Langmuir, 1995. **11**(5): p. 1443-1447.

64. Dickson, J.; O'haver, J. *Adsolubilization of naphthalene and alpha-naphthol in C(n)TAB admicelles.* Langmuir, 2002. **18**(24): p. 9171-9176.

65. Monticone, V.; Mannebach, M.H.; Treiner, C. *Coadsorption of 2-Naphthol and Cetylpyridinium Chloride at a Silica/Water Interface in Relation with the Micellar Solubilization Effect.* Langmuir, 1994. **10**(7): p. 2395-2398.

66. Rosen, M.J. *Micelle Formation by Surfactants*, in *Surfactants and Interfacial Phenomena*. 2004, John Wiley & Sons, Inc. p. 105-177.

67. Eastoe, J.; Rogers, S.E.; Martin, L.J.; Paul, A.; Guittard, F.; Guittard, E.; Heenan, R.K.; Webster, J.R.P. *Fluorosurfactants at Structural Extremes: Adsorption and Aggregation.* Langmuir, 2006. **22**(5): p. 2034-2038.

68. Evenäs L.; Furo, I.; Stilbs, P.; Valiullin, R. *Adsorption Isotherm and Aggregate Properties of Fluorosurfactants on Alumina Measured by 19F NMR.* Langmuir, 2002. **18**(21): p. 8096-8101.

69. Holme, I. *Innovative technologies for high performance textiles.* Coloration Technology, 2007. **123**(2): p. 59-73.

70. Sawhney, A.P.S.; Condon, B.; Singh, K.V.; Pang, S.S.; Li, G.; Hui, D. *Modern Applications of Nanotechnology in Textiles.* Textile Research Journal, 2008. **78**(8): p. 731-739.

71. Vazquez, F. *silicone softeners for stain repellent and stain resistance fabric finishing.* dyes and chemicals, 2004.

72. Kathirvelu, S.; D'Souza, L.; Dhurai, B. *Study of stain-eliminating textiles using ZnO nanoparticles.* Journal of the Textile Institute, 2010. **101**(6): p. 520-526.

73. Badyal, J.P. *Beyond the surface cold plasmas are streaming the surface coatings.* chemistry in britain, 2001. **37**(1): p. 45-46.

74. Bubert, H. *Surface and thin film analysis.* Ullmann's Encyclopedia of Industrial Chemistry, 2011.

75. Ma, M.L.; Gupta, M.; Zhai, L.; Gleason, K. K.; Cohen, R. E.; Rubner, M. F.; Rutledge, G. C. *Decorated Electrospun Fibers Exhibiting Superhydrophobicity.* Advanced Materials, 2007. **19**(2): p. 255-259.

76. Maity, J.; Jacob, C.; Das, C.K.; Singh, R.P. *Direct fluorination of Twaron fiber and investigation of mechanical thermal and morphological properties of high density polyethylene and Twaron fiber composites.* Journal of Applied Polymer Science, 2008. **107**(6): p. 3739-3749.

77. Tarimala, S.; Kothari, N.; Abidi, N.; Hequet, E.; Fralick, J.; Dai, L.L. *New approach to antibacterial treatment of cotton fabric with silver nanoparticle–doped silica using sol–gel process.* Journal of Applied Polymer Science, 2006. **101**(5): p. 2938-2943.

78. Yeh, J.T.; Chen, C.L.; Huang, K.S. *Preparation and application of fluorocarbon polymer/SiO2 hybrid materials, part 2: Water and oil repellent processing for cotton fabrics by sol–gel method.* Journal of Applied Polymer Science, 2007. **103**(5): p. 3019-3024.

79. Wang, T.; Hu, X.; Dong, S. *A general route to transform normal hydrophilic cloths into superhydrophobic surfaces.* Chemical Communications, 2007(18): p. 1849-1851.

80. Hoefnagels, H.F.; Wu, D.; de With, G.; Ming, W. *Biomimetic Superhydrophobic and Highly Oleophobic Cotton Textiles.* Langmuir, 2007. **23**(26): p. 13158-13163.

81. Xue, C.H.; Jia, S.T.; Chen, H.Z.; Wang, M. *Superhydrophobic cotton fabrics prepared by sol–gel coating of TiO 2 and surface hydrophobization.* Science and Technology of Advanced Materials, 2008. **9**(3): p. 035001.

82. Wang, H.; Fang, J.; Cheng, T.; Ding, J.; Qu, L.; Dai, L.; Wang, X.; Lin, T. *One-step coating of fluoro-containing silica nanoparticles for universal generation of surface superhydrophobicity.* Chemical Communications, 2008(7): p. 877-879.

83. Leng, B.; Shao, Z.Z.; de With, G.; Ming, W. *Superoleophobic Cotton Textiles.* Langmuir, 2009. **25**(4): p. 2456-2460.

84. Zhao, Y.; Tang, Y.W.; Wang, X.G.; Lin, T. *Superhydrophobic cotton fabric fabricated by electrostatic assembly of silica nanoparticles and its remarkable buoyancy.* Applied Surface Science, 2010. **256**(22): p. 6736-6742.

85. Luna-Xavier, J.-L.; Guyot, A.; Bourgeat-Lami, E. *Synthesis and Characterization of Silica/Poly (Methyl Methacrylate) Nanocomposite Latex Particles through Emulsion Polymerization Using a Cationic Azo Initiator.* Journal of Colloid and Interface Science, 2002. **250**(1): p. 82-92.

86. Maity, J.; Kothary, P.; O'Rear, E.A.; Jacob, C. *Preparation and Comparison of Hydrophobic Cotton Fabric Obtained by Direct Fluorination and Admicellar Polymerization of Fluoromonomers.* Industrial & Engineering Chemistry Research, 2010. **49**(13): p. 6075-6079.

87. Siriviriyanun, A.; O'Rear, E.A.; Yanumet, N. *Improvement in the flame retardancy of cotton fabric by admicellar polymerization of 2-acryloyloxyethyl diethyl phosphate using an anionic surfactant.* Journal of Applied Polymer Science, 2008. **109**(6): p. 3859-3866.

88. Tragoonwichian, S.; O'Rear, E.A.; Yanumet, N. *Broad ultraviolet protection by copolymerization of 2-[3-(2H-benzotriazol-2-yl)-4-hydroxyphenyl]ethyl methacrylate and 2-hydroxy-4-acryloyloxybenzophenone on cotton via admicellar polymerization.* Journal of Applied Polymer Science, 2008. **108**(6): p. 4004-4013.

89. Nontasorn, P.; Chavadej, S.; Rangsumvigit, P.; O'Haver, J. *Admicellar polymerization modified silica via a continuous stirred-tank reactor system: Comparative properties of rubber compounding.* Chemical Engineering Journal, 2005. **108**(3): p. 213-218.

90. Sangthong, S.; Pongprayoon, T.; Yanumet, N. *Mechanical property improvement of unsaturated polyester composite reinforced with admicellar-treated sisal fibers.* Composites Part a-Applied Science and Manufacturing, 2009. **40**(6-7): p. 687-694.

91. Barraza, H.J.; Olivero, K.; Hamidi, Y.; O'Rear, E.A.; Altan, M.C. *Elastomeric sizings for glass fibers and their role in fiber wetting and adhesion in resin transfer molded composites.* Composite Interfaces, 2002. **9**(6): p. 477-507.

92. Nishio, K.; Masaike, Y.; Ikeda, M.; Narimatsu, H.; Gokon, N.; Tsubouchi, S.; Hatakeyama, M.; Sakamoto, S.; Hanyu, N.; Sandhu, A.; Kawaguchi, H.; Abe, M.; Handa, H. *Development of novel magnetic nano-carriers for high-performance affinity purification.* Colloids and Surfaces B-Biointerfaces, 2008. **64**(2): p. 162-169.

93. Sandhu, A.; Handa, H.; Abe, M. *Synthesis and applications of magnetic nanoparticles for biorecognition and point of care medical diagnostics.* Nanotechnology, 2010. **21**(44): p. 442001/(1-22).

94. Siriviriyanun, A.; O'Rear, E.A.; Yanumet, N. *Self-extinguishing cotton fabric with minimal phosphorus deposition.* Cellulose, 2008. **15**(5): p. 731-737.

95. Tragoonwichian, S.; O'Rear, E.A.; Yanumet, N. *Admicellar polymerization of 2-hydroxy-4-acryloyloxybenzophenone: The production of UV-protective cotton.* Colloids and Surfaces a-Physicochemical and Engineering Aspects, 2008. **329**(1-2): p. 87-94.

96. Layer, R.W. *Reaction of epoxides with 2,6-di-tert-butylphenol.* Journal of Organic Chemistry, 1981. **46**(25): p. 5224-5225.

97. Castellanos, E.; Diaz, R.; Neumann, H. *Coke characteristics in relation to the colloidal matter of petroleum for thermal-processes.* Fuel Science & Technology International, 1994. **12**(4): p. 543-565.

98. Pastor, G.R.; Angelovi. J.M.; Silver, H.F. *Study of interaction of solvent and catalyst in coal hydrogenation.* Industrial & Engineering Chemistry Process Design and Development, 1970. **9**(4): p. 609.

99. Montgomery, J.B.; Hoffmann, A.N.; Glasebrook, A.L.; Thigpen, J.I. *Catalytic perhydrogenation of rosin.* Industrial and Engineering Chemistry, 1958. **50**(3): p. 313-316.

100. Ryoo, D.; Murphy, V.G.; Karim, M.N.; Tengerdy, R.P. *Evaporative temperature and moisture control in a rocking reactor for solid substrate fermentation*. Biotechnology Techniques, 1991. **5**(1): p. 19-24.

101. Glazyrina, J.; Materne, E.; Dreher, T.; Storm, D.; Junne. S.; Adams. T.; Greller, G.; Neubauer, P. *High cell density cultivation and recombinant protein production with Escherichia coli in a rocking- motion- type bioreactor*. Microbial Cell Factories, 2010. **9**.

102. Eibl, R.; Eibl, D. *Application of Disposable Bag Bioreactors in Tissue Engineering and for the Production of Therapeutic Agents*, in *Bioreactor Systems for Tissue Engineering*, C. Kasper, M. VanGriensven, and R. Portner, Editors. 2009. p. 183-207.

103. Eibl, R.; Werner, S.; Eibl, D. *Disposable bioreactors for plant liquid cultures at Litre-scale.* Engineering in Life Sciences, 2009. **9**(3): p. 156-164.

104. Hoffmann, A.N.; Montgomery, J.B.; Moore, J.K. *Agitation in experimental rocking-type autoclaves.* Industrial and Engineering Chemistry, 1948. **40**(9): p. 1708-1710.

105. Snyder, J.R.; Hagerty, P.F.; Molstad, M.C. *Operation and performance of bench scale reactors.* Industrial and Engineering Chemistry, 1957. **49**(4): p. 689-695.

106. Murzin, D.Y.; Konyukhov, V.Y.; Kulkova, N.V.; Temkin, M.I. *Diffusion from the surface of suspended particles and specific mixing power in rocking reactors.* Kinetics and Catalysis, 1992. **33**(3): p. 586-589.

107. Nyoka, M.; Akdogan, G.; Eric, R.H.; Sutcliffe, N. *Mixing and solid-liquid mass-transfer rates in a Creusot-Loire Uddeholm vessel: A water model case study.* Metallurgical and Materials Transactions B-Process Metallurgy and Materials Processing Science, 2003. **34**(6): p. 833-842.

108. Temkin, M.I. *Transfer of a solute between a turbulently flowing liquid and particles suspended in it.* Kinetics and Catalysis, 1977. **18**(2): p. 413-416.

109. Konyukhov, V.; Kulkova, N.; Temkin, M. *Determination of the coefficients of mass-transfer toward particles suspended in a mixed-solution.* kinetics and catalysis, 1982. **23**(2): p. 425-428.

110. Hajek, J.; Murzin, D.Y. *Liquid-phase hydrogenation of cinnamaldehyde over a Ru-Sn sol-gel catalyst. 1. Evaluation of mass transfer via a combined experimental/theoretical approach.* Industrial & Engineering Chemistry Research, 2004. **43**(9): p. 2030-2038.

111. Noulty, R.A.; Leaist, D.G. *Diffusion-coefficient of aqueous benzoic-acid at 25-degrees-c.* Journal of Chemical and Engineering Data, 1987. **32**(4): p. 418-420.

112. Velasco, C. S.; Martinez, H.A.L.; Fisher, F.T.; Ruoff, R.; Castano, V.M. *Improvement of Thermal and Mechanical Properties of Carbon Nanotube Composites through Chemical Functionalization.* Chemistry of Materials, 2003. **15**(23): p. 4470-4475.

113. Wang, J.; Fang, Z.; Gu, A.; Xu, L.; Liu, F. *Effect of amino-functionalization of multi-walled carbon nanotubes on the dispersion with epoxy resin matrix.* Journal of Applied Polymer Science, 2006. **100**(1): p. 97-104.

114. Sung, Y.T.; Hang, M.S.; Song, K.H.; Jung, J.W.; ee, H.S.; Kum, C.K.; Joo, J.; Kim, W.N. *Rheological and electrical properties of polycarbonate/multi-walled carbon nanotube composites.* Polymer, 2006. **47**(12): p. 4434-4439.

115. Jingjing, Q.; Chuck, Z.; Bee, W.; Richards, L. *Carbon nanotube integrated multifunctional multiscale composites.* Nanotechnology, 2007. **18**(27): p. 275708.

116. Zou, W.; Du, Z.J.; Liu, Y.X.; Yang, X.; Li, H.Q.; Zhang, C. *Functionalization of MWNTs using polyacryloyl chloride and the properties of CNT–epoxy matrix nanocomposites.* Composites Science and Technology, 2008. **68**(15–16): p. 3259-3264.

117. Meng, H.; Sui, G.X.; ang, P.F.; Yang, R. *Effects of acid- and diamine-modified MWNTs on the mechanical properties and crystallization behavior of polyamide 6.* Polymer, 2008. **49**(2): p. 610-620.

118. Wu, D.; Wu, L.; Zhang, M.; Zhao, Y. *Viscoelasticity and thermal stability of polylactide composites with various functionalized carbon nanotubes.* Polymer Degradation and Stability, 2008. **93**(8): p. 1577-1584.

119. Song, P.A.; Xu, L.; Guo, Z.; Zhang, Y.; Fang, Z. *Flame-retardant-wrapped carbon nanotubes for simultaneously improving the flame retardancy and mechanical properties of polypropylene.* Journal of Materials Chemistry, 2008. **18**(42): p. 5083-5091.

120. Park, S.J.; Cho, M.S.; Lim, S.T.; Choi, H.J.; Jhon, M.S. *Synthesis and Dispersion Characteristics of Multi-Walled Carbon Nanotube Composites with Poly(methyl methacrylate) Prepared by In-Situ Bulk Polymerization.* Macromolecular Rapid Communications, 2003. **24**(18): p. 1070-1073.

121. Barraza, H.J.; Pompeo, F.; O'Rear, E.A.; Resasco, D.E. *SWNT-Filled Thermoplastic and Elastomeric Composites Prepared by Miniemulsion Polymerization.* Nano Letters, 2002. **2**(8): p. 797-802.

122. Blond, D.; Baron, V.; Ruether, M.; Ryan, K.P.; Nicolsi, V.; Blau, W.J.; Coleman, J.N. *Enhancement of Modulus, Strength, and Toughness in Poly(methyl methacrylate)-Based Composites by the Incorporation of Poly(methyl methacrylate)-Functionalized Nanotubes.* Advanced Functional Materials, 2006. **16**(12): p. 1608-1614.

123. Regev, O.; Elkati, P.N.B.; Loos, J.; Koning, C.E. *Preparation of Conductive Nanotube–Polymer Composites Using Latex Technology.* Advanced Materials, 2004. **16**(3): p. 248-251.

124. Guo, G.; Yang, D.; Wang, C.; Yang, S. *"Fishing" Polymer Brushes on Single-Walled Carbon Nanotubes by in-Situ Free Radical Polymerization in a Poor Solvent.* Macromolecules, 2006. **39**(26): p. 9035-9040.

125. Kim, T.H.; Doe, C.; Kline, S.R.; Choi, S.M. *Organic Solvent-Redispersible Isolated Single Wall Carbon Nanotubes Coated by in-Situ Polymerized Surfactant Monolayer.* Macromolecules, 2008. **41**(9): p. 3261-3266.

126. Cheng, Z.; Pan, Q.; Rempel, G.L. *Modification of multiwall carbon nanotubes via soap-free emulsion polymerization of acrylonitrile.* Journal of Polymer Science Part A: Polymer Chemistry, 2010. **48**(10): p. 2057-2062.

127. Xia, H.; Wang, Q.; Qiu, G. *Polymer-Encapsulated Carbon Nanotubes Prepared through Ultrasonically Initiated In Situ Emulsion Polymerization.* Chemistry of Materials, 2003. **15**(20): p. 3879-3886.

128. Huang, F.; Vanhaecke, E.; Chen, D. *In situ polymerization and characterizations of polyaniline on MWCNT powders and aligned MWCNT films.* Catalysis Today, 2010. **150**(1–2): p. 71-76.

129. Zhong, W.; Zeuna, J.N. Claverie, J.P. *A versatile encapsulation method of noncovalently modified carbon nanotubes by RAFT polymerization.* Journal of Polymer Science Part A: Polymer Chemistry, 2012. **50**(21): p. 4403-4407.

130. Urbanová, V.; Allai, N.; Ghach, W.; Mamane, V.; Etienne, M.; Walcarius, A. *Functionalized carbon nanotubes for bioelectrochemical applications: Critical influence of the linker.* Journal of Electroanalytical Chemistry, 2013. **707**(0): p. 129-133.

131. Jiang, B.P.; Hu, L..; Shen, X.C.; Ji, S.C.; Shi, Z.; Zhang, L.; Liang, H. *One-Step Preparation of a Water-Soluble Carbon Nanohorn/Phthalocyanine Hybrid for Dual-Modality Photothermal and Photodynamic Therapy.* ACS Applied Materials & Interfaces, 2014. **6**(20): p. 18008-18017.

132. Moore, T.L.; Grimes, S.W.; Lewis, R.L.; Alex, F. *Multilayered Polymer-Coated Carbon Nanotubes To Deliver Dasatinib.* Molecular Pharmaceutics, 2013. **11**(1): p. 276-282.

133. Mu, B.; Lu, P.; Yu, X.; Pan, F.; Gao, Z.; Liu, X. *Preparation and characterization of conductor–insulator–semiconductor sandwich-structured MWCNT/double-layer polymer hybrid nanocomposites.* Synthetic Metals, 2010. **160**(21–22): p. 2329-2335.

134. Wang, G.; Yang, J.; Wang, Y.; Liu, Y. *Self-assembly behavior of carbon nanotubes modified by amphiphilic block copolymer.* Colloid and Polymer Science, 2010. **288**(18): p. 1677-1685.

135. Zou, P.; Shi, G.Y.; Pan, C.Y. *Large-compound vesicle-encapsulated multiwalled carbon nanotubes: A unique route to nanotube composites.* Journal of Polymer Science Part A: Polymer Chemistry, 2009. **47**(14): p. 3669-3679.

136. Xia, H.; Qiu, G.; Wang, Q. *Polymer/carbon nanotube composite emulsion prepared through ultrasonically assisted in situ emulsion polymerization.* Journal of Applied Polymer Science, 2006. **100**(4): p. 3123-3130.

137. Lee C.; Yeskie, M.A.; Harwell, J.H.; O"Rear, E.A. *Two-site adsolubilization model of incorporation of alcohols into adsorbed surfactant aggregates.* Langmuir, 1990. **6**(12): p. 1758-1762.

138. Hanumansetty, S.; O'Rear, E.A. *Two-Site Adsolubilization Model of Incorporation of Fluoromonomers into Fluorosurfactants Formed on Cotton Fabric.* Langmuir, 2014. **30**(13): p. 3665-3672.

139. Duan, W.H.; Wang, Q.; Collins, F. *Dispersion of carbon nanotubes with SDS surfactants: a study from a binding energy perspective.* Chemical Science, 2011. **2**(7): p. 1407-1413.

140. Maeder, A. Salts of hydrolyzed polyacrylate esters and solutions thereof. U.S. Patent 2,897,172, July 28, 1959.

141. Theodorou, V.; Skobridis, K.; Tzakos, A.G.; Ragoussis, V. *A simple method for the alkaline hydrolysis of esters.* Tetrahedron Letters, 2007. **48**(46): p. 8230-8233.

142. Matarredona, O.; Rhoads, H.; Li, Z.; Harwell, J.H.; Balzano, L.; Resasco, D.E. *Dispersion of Single-Walled Carbon Nanotubes in Aqueous Solutions of the Anionic Surfactant NaDDBS.* The Journal of Physical Chemistry B, 2003. **107**(48): p. 13357-13367.

143. Esumi, K.; Yamamoto, S. *Adsorption of sodium dodecyl sulfate on hydrotalcite and adsolubilization of 2-naphthol.* Colloids and Surfaces A: Physicochemical and Engineering Aspects, 1998. **137**(1–3): p. 385-388.

144. Berthod, A.; Girard, I.; Gonnet, C. *Micellar liquid chromatography, adsorption isotherms of two ionic surfactants on five stationary phases.* Anal. Chem., 1986. **58**(7): p. 1356-8.

145. Mohamed, M.M. *Adsorption properties of ionic surfactants on molybdenum-modified silica gels.* Colloids and Surfaces A: Physicochemical and Engineering Aspects, 1996. **108**(1): p. 39-48.

146. Wang, W.; Kwak, J.C.T. *Adsorption at the alumina–water interface from mixed surfactant solutions.* Colloids and Surfaces A: Physicochemical and Engineering Aspects, 1999. **156**(1–3): p. 95-110.

147. Sakagami, K.; Yoshimura, T. Esumi, K. *Simultaneous Adsorption of Poly(1-vinylpyrrolidone-co-acrylic acid) and Sodium Dodecyl Sulfate at Alumina/Water Interface.* Langmuir, 2002. **18**(16): p. 6049-6053.

148. Yeskie, M.A. *Various aspects of surfactant aggregates adsorbed on an oxide surface: The hemimicelle/admicelle transition, and the interaction of alcohols and alkanes*. 1988, The University of Oklahoma: Ann Arbor. p. 193-193.

149. Alavi, M.H.S.; Habibi, M.; Amrollahi, R.; Taromi, F.A. *A Study on Plasma Polymerization of Acrylic Acid Using APF Plasma Focus Device.* J. Fusion Energy, 2011. **30**(2): p. 184-189.

150. Hu, Y.H.; Chen, C.Y.; Wang, C.C. *Thermal degradation kinetics of poly(n-butyl acrylate) initiated by lactams and thiols.* Polymer Degradation and Stability, 2004. **84**(3): p. 505-514.

151. McNeill, I.C.; Sadeghi, S.M.T. *Thermal stability and degradation mechanisms of poly(acrylic acid) and its salts: Part 1—Poly(acrylic acid).* Polymer Degradation and Stability, 1990. **29**(2): p. 233-246.

152. Dubinsky, S.; Grader, G.S.; Shter, G.E.; Silverstein, M.S. *Thermal degradation of poly(acrylic acid) containing copper nitrate.* Polymer Degradation and Stability, 2004. **86**(1): p. 171-178.

153. Haddon, R.C. *Carbon Nanotubes.* Accounts of Chemical Research, 2002. **35**(12): p. 997-997.

154. De Volder, M.F.L.; Tawfick, S.H.; Baughman, R.H.; Hart, A.J. *Carbon Nanotubes: Present and Future Commercial Applications.* Science, 2013. **339**(6119): p. 535-539.

155. Liu, Y.; Wang, G.J.; Wu, Y.J. *Amphiphilicity and self-assembly behaviors of polystyrene-grafted multi-walled carbon nanotubes in selective solvents.* Colloid and Polymer Science, 2014. **292**(1): p. 185-196.

156. Mallakpour, S.; Zadehnazari, A. *Functionalization of multiwalled carbon nanotubes with S-valine amino acid and its reinforcement on amino acid-containing poly(amide-imide) bionanocomposites.* High Performance Polymers, 2013. **25**(8): p. 966-979.

157. Dufresne, A.; Paillet, M.; Putaux, J.L.; Canet, R.; Carmona, F.; Delhaes, P.; Cui, S. *Processing and characterization of carbon nanotube/poly(styrene-co-butyl acrylate) nanocomposites.* Journal of Materials Science, 2002. **37**(18): p. 3915-3923.

158. Liu, A.; Honma, I.; Ichihara, M.; Zhou, H. *Poly(acrylic acid)-wrapped multi-walled carbon nanotubes composite solubilization in water: definitive spectroscopic properties.* Nanotechnology, 2006. **17**(12): p. 2845-2849.

159. Jeevananda, T.S.; Kim, N.H.; Heo, S.B.; Lee, J.H.; *Synthesis and characterization of polyaniline-multiwalled carbon nanotube nanocomposites in the presence of sodium dodecyl sulfate.* Polymers for Advanced Technologies, 2008. **19**(12): p. 1754-1762.

160. Nguyen, D.; Such, C.H.; Hawkett, B.S. *Polymer coating of carboxylic acid functionalized multiwalled carbon nanotubes via reversible addition-fragmentation chain transfer mediated emulsion polymerization.* Journal of Polymer Science Part A: Polymer Chemistry, 2013. **51**(2): p. 250-257.

161. Lu, K.L.; Lago, R.M.; Chen, Y.K.; Green, M.L.H.; Harris, P.J.F.; Tsang, S.C. *Mechanical damage of carbon nanotubes by ultrasound.* Carbon, 1996. **34**(6): p. 814-816.

162. Wang, S.; Russo, T.; Qiao, G.; Solomon, D.; Shanks, R. *Admicellar polymerization of styrene with divinyl benzene on alumina particles: the synthesis of white reinforcing fillers.* Journal of Materials Science, 2006. **41**(22): p. 7474-7482.

163. Hanumansetty, S.; Maity, J.; Foster, R.; O'Rear, E.A. *Stain Resistance of Cotton Fabrics before and after Finishing with Admicellar Polymerization.* Applied Sciences, 2012. **2**(1): p. 192-205.

164. Beyler, C.L.; Hirschler, M.M. Thermal decomposition of polymers. In *SFPE Handbook of Fire Protection Engineering*, Third Ed. 2001, 1-110, Sect. 1, Chap. 7.

165. Wu, J.; Harwell, J.H.; O'Rear, E.A. *Two-dimensional solvents: kinetics of styrene polymerization in admicelles at or near saturation.* The Journal of Physical Chemistry, 1987. **91**(3): p. 623-634.

166. Odian, G. *Emulsion Polymerization*, in *Principles of Polymerization*. 2004, John Wiley & Sons, Inc. p. 350-371.

167. Konaganti, V.K.; Madras, G. *Photocatalytic and Thermal Degradation of Poly(methyl methacrylate), Poly(butyl acrylate), and Their Copolymers.* Ind. Eng. Chem. Res., 2009. **48**(4): p. 1712-1718.

168. Debashish, R.; Semsarilar, M.; Guthrie, J.T.; Perrier, S. Cellulose modification by polymergrafting; a review. Chemical Society Reviews, 2009,. **38**: p. 2046-2064.

Appendix -A: Extended work for adsorption and adsolubilization of C6 fluoromonomer

Apart from the chemicals used in Chapter 2, 1H, 1H, 2H, 2H-Perfluorooctyl acrylate, was also analyzed to obtain the adsorption and adsolubilization data.

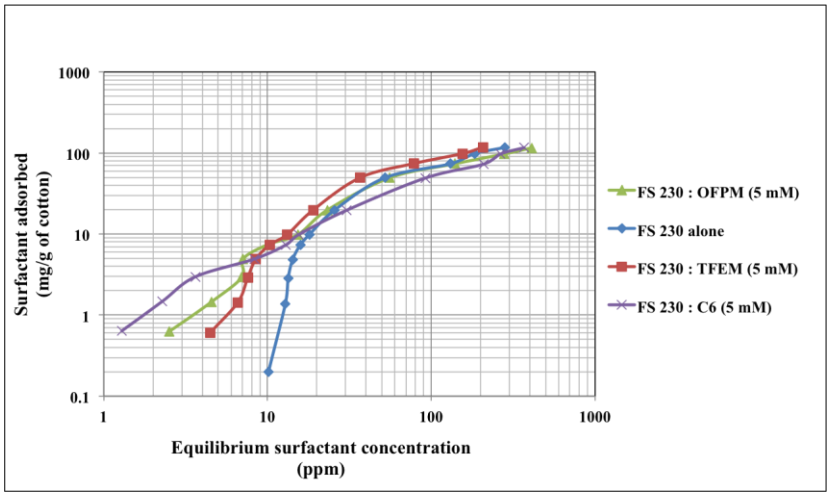
Materials:

The monomer 1H, 1H, 2H, 2H-Perfluorooctyl acrylate (C6) was purchased from Synquest labs, USA. The remaining chemicals were described in Chapter 2.3.1.

Experimental Analysis

The experiments were conducted with the monomer as described in Chapter 2.3.2.

Results:



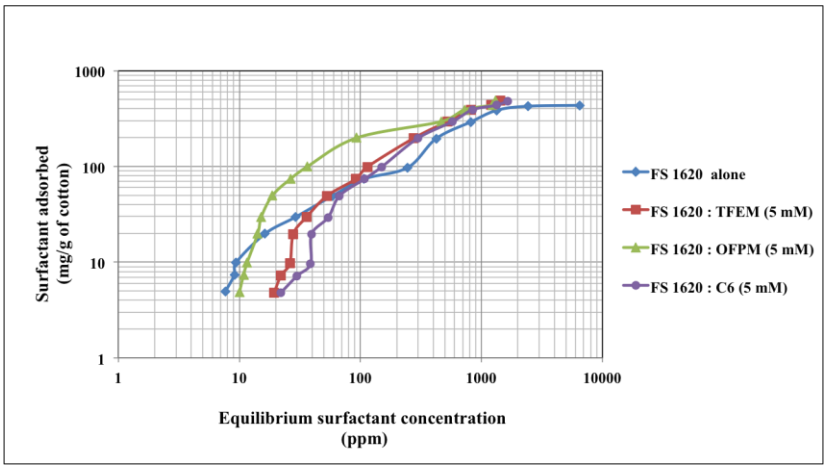


Figure A.1: Adsorption isotherm of surfactants alone and in the presence of monomers

(a) FS 230 (b) FS 1620

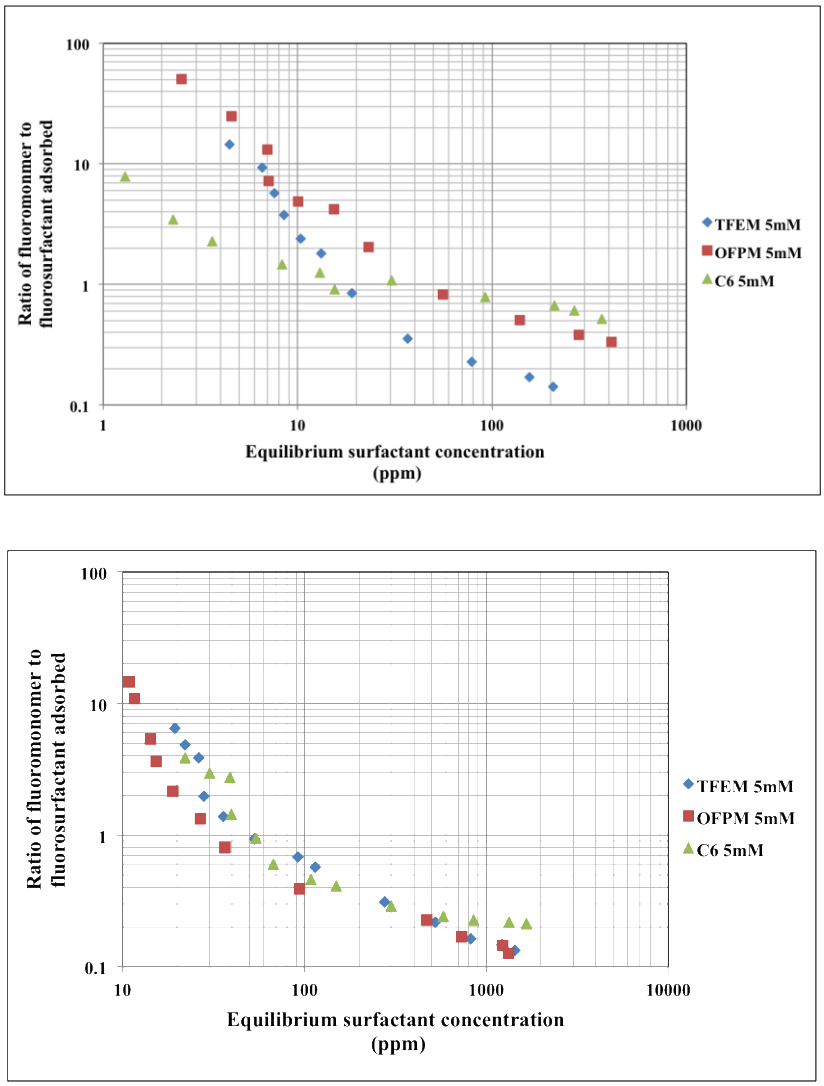
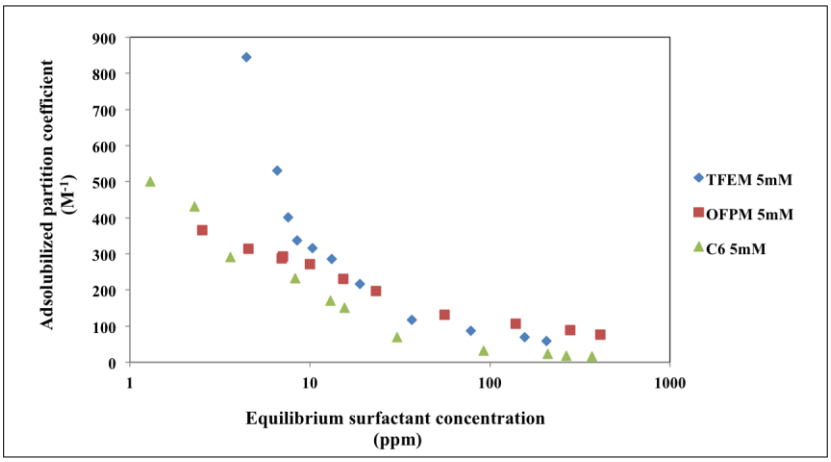


Figure A.2: Ratio of adsolubilized fluorormonomer to adsorbed fluorosurfactant

(a) FS 230 (b) FS1620



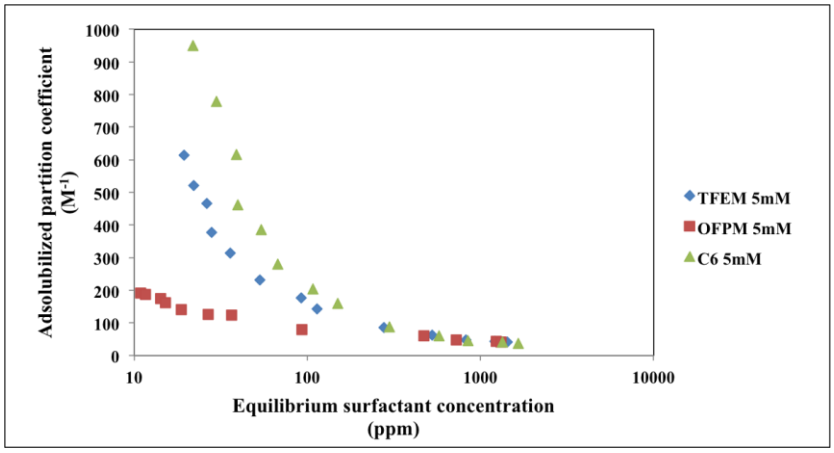
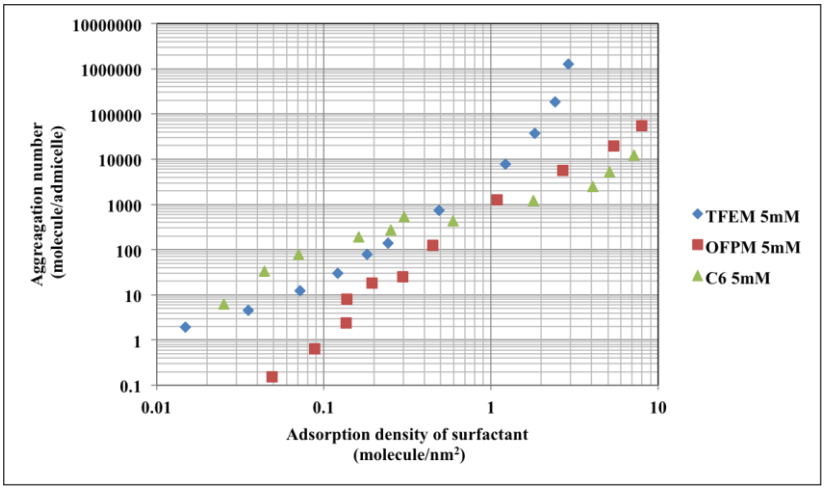


Figure A.3: Ratio of adsolubilized fluorormonomer to adsorbed fluorosurfactant

(a) FS 230 (b) FS1620



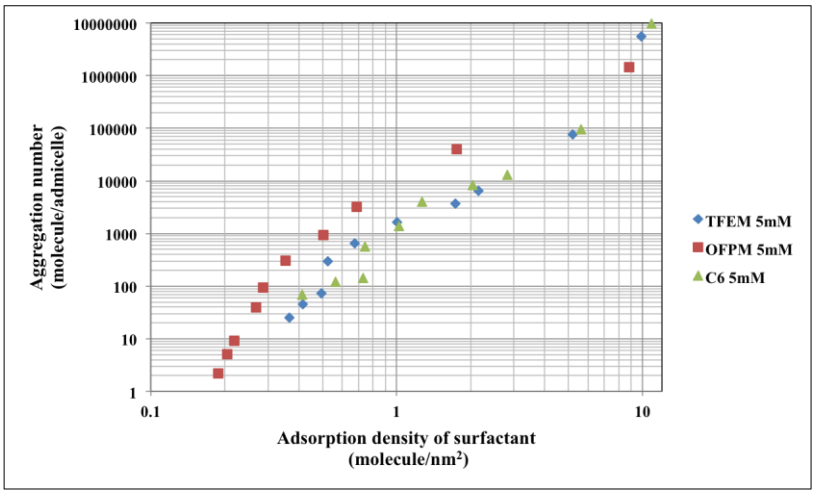
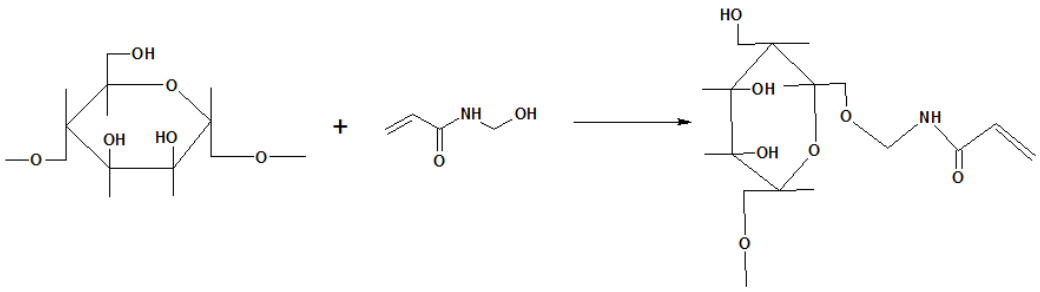


Figure A.4: Aggregation number for fluorosurfactants in presence of fluoromonomers

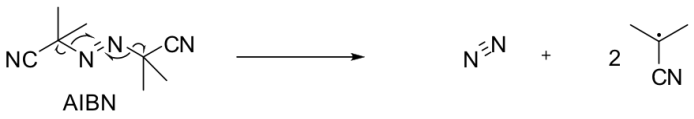
(a) FS 230 (b) FS1620

Appendix –B: Analytical tests and equipments used to develop formulations

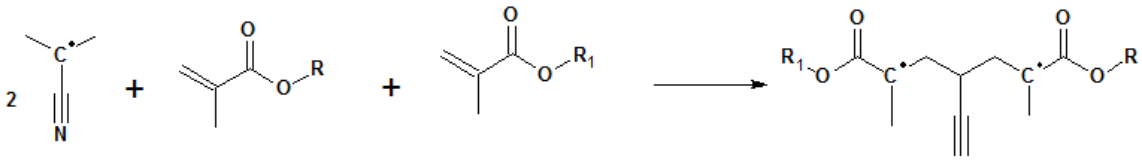
Mechanism of reaction:



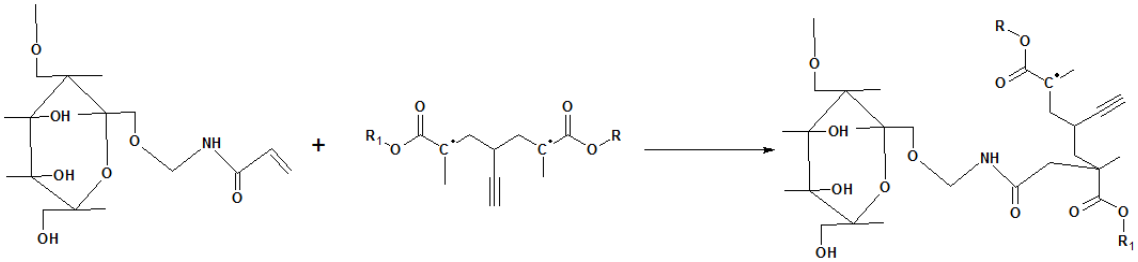
Binding agent interaction on cellulose (mechanism obtained from Chem. Soc. Rev. 2009, 38, 2046-2064 and Polym. Degrade. Stabil. 109, 2014, 137-146)



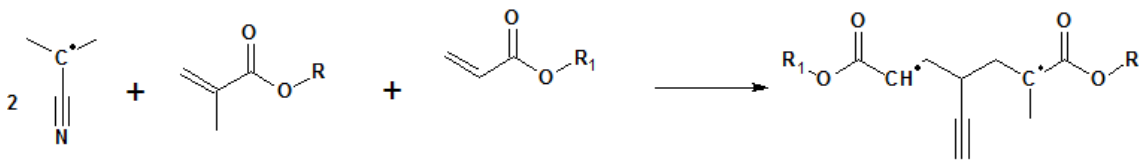
Initiation of reaction



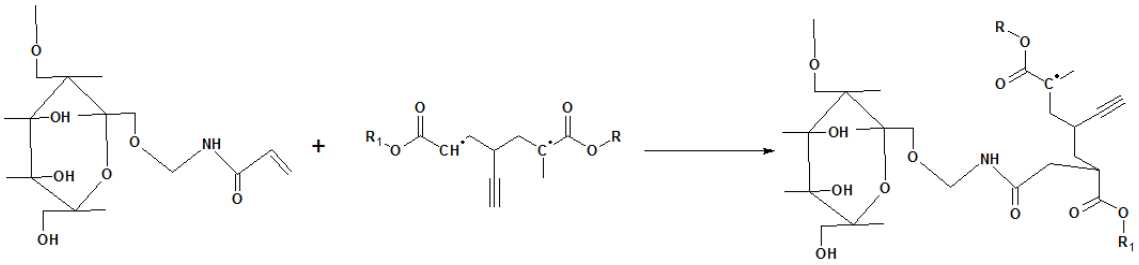
Reaction of initiator with TFEM and OFPM (R = CF_3 and R_1 = CH_2 $(CF_2)_4H$)



Formation of fluoropolymer with binding agent on cotton surface with PA1 formulation



Reaction of initiator with TFEM and C6 (R = CF_3 and R_1 = CH_2CH_2 $(CF_2)_5CF_3$)



Formation of fluoropolymer with binding agent on cotton surface with PA2 formulation

Analytical tests:

1. ***Contact angle***

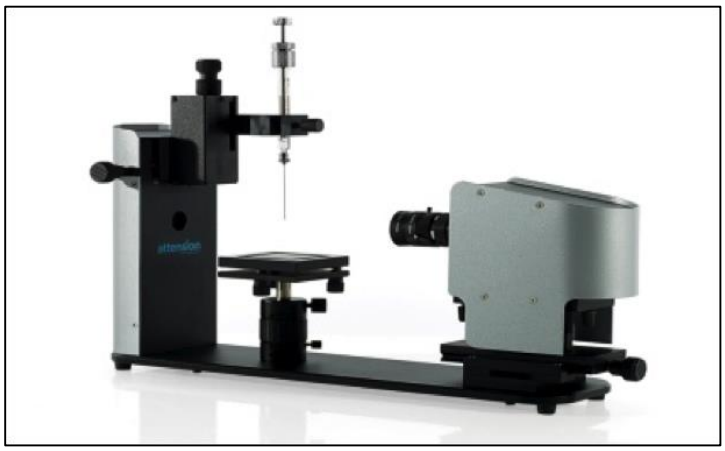


Figure B.1: Optical tensiometer by KSV instruments

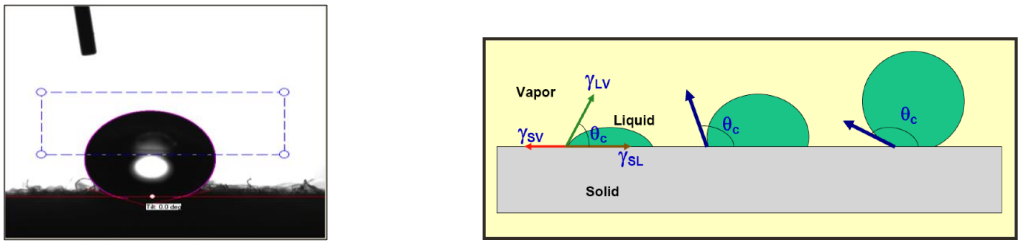


Figure B.2: (a) Measurement of contact anlge (b) variation of contact angle from hydrophilic to super hydrophobic

2. Spray test

The treated fabrics are characterized with AATCC test method 22 called as spray test.

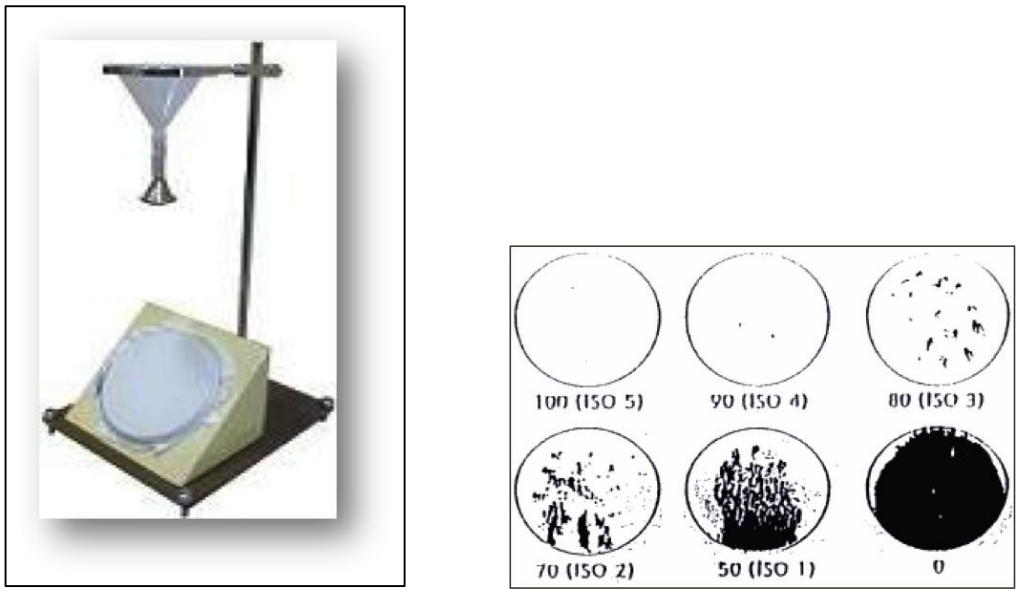


Figure B.3: (a) Spray test apparatus (b) Standard spray test ratings picture

Table B.1: Spray test ratings

100	No sticking on wetting of upper surface
90	Slight random sticking or wetting of upper
80	Wetting of upper surface at spray points
70	Partial wetting of whole of upper surface
50	Complete wetting of whole of upper surface
0	Complete wetting of whole upper and lower

3. Mechanical Characterization:



Figure B.4: SSTM tester according to ASTM D1708

4. Stain resistance and stain repellency tests

Reflectance measurements were measured Ultra scan colorimeter by Hunter lab



Figure B.5: Ultra scan colorimeter

5. Pictures of fabric for stain recovery and stain release tests:

Samples were treated with Crisco vegetable oil, Hellmann's mayonnaise, Heinz ketchup, coffee, French's mustard, fresh grease.

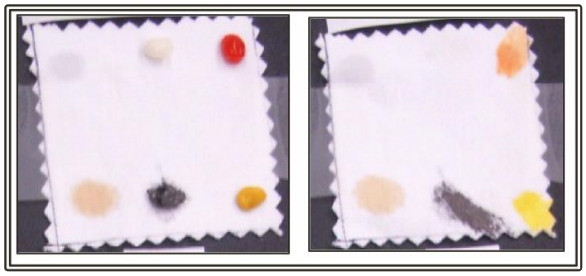


Figure B.6: Untreated Interlock fabric (a) with stains (b) after wiping stains



Figure B.7: Formulation PA2 treated fabric (a) with stains (b) after wiping stains

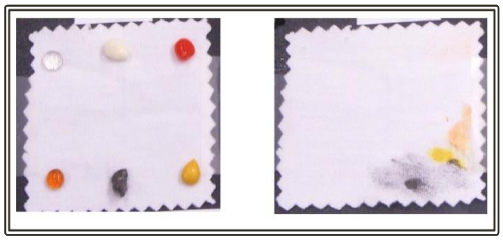


Figure B.8: Reference sample 1 (a) with stains (b) after wiping stains

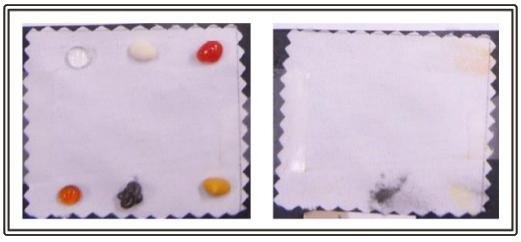


Figure B.9: Reference sample 2 (a) with stains (b) after wiping stains

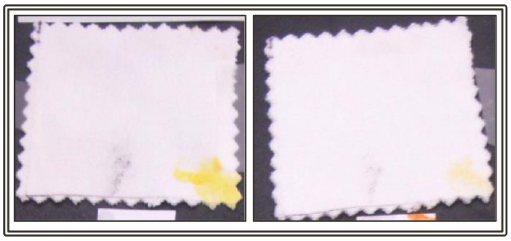


Figure B.10: Formulation PA2 reated fabric (a) after wiping stains (b) after 1 home laundering wash

6. Scale up of Process:

Initial experiments were performed in 20 ml vials in shaker bath (Fig.B.11) for laboratory scale. pH of solution maintained at 4. The fabric used was interlock knit cotton fabric. After the treatment for 4hrs the fabric was dried overnight. The sample was then tested to analyze its characteristics using water repellency and oil repellency tests.



Figure B.11: Shaker bath

After passing 5 HL (home launderings), the formulation was scaled up to pilot level with the reactor size being increased from 20mL to 1L. The formulation and conditions

were kept constant and the trial was carried out in a Werner Mathis Labomat unit (Fig. B.12). The sample was then subjected to tests for analyzing repellency characteristic based on water repellency and oil repellency. Additionally, the Spray Test (AATCC Test Method 35) was also carried out on the pilot trial samples since the sample size now permitted this test.



Figure B.12: Werner Mathis Labomat Unit

After successful scale up for 1lt in Werner Mathis Labomat unit, we obtained a pilot scale version of equipment of Werner Mathis JF unit (Fig B.13) used in industry having a volume of 3L. The formulation and conditions were kept constant and the trial runs were carried. As evident from the Figure B.13, the mixing mechanism in the unit resembles mixing in a front-loading washing machine, and is found in several industrially used dyeing units. Various processing conditions were studied in order to obtain the optimum conditions for getting a good finish. The optimum fill volume was found to be approximately 90% of the total volume of the chamber. The samples were then subjected to tests for analyzing repellency characteristic based on water repellency and oil repellency.



Figure B.13: Werner Mathis JF unit

After scaling up to 3L, we obtained exhaust-dyeing unit of capacity 68L from Unimac. As shown in Figure B.14, the equipment is similar to frontloading washing machine as JF unit. The formulation and conditions were kept constant and the trial runs were carried. The samples obtained were subject to tests for analyzing water and oil repellency characteristics.



Figure B.14: Unimac exhaust dyeing unit

The performance obtained on cotton knit fabric is hydrophobic and oleophobic and comparable to results obtained from pilot scale units used. After successful scale up of process to 68L, we developed operating procedure to run the experiments with Unimac exhaust dyeing unit.

Operating procedure for Unimac exhaust dyeing unit:

- Ensure that the drain valves are closed.
- Turn the Main switch ON located on the back panel of the Unimac.
- Turn the main power ON located on the controller console.
- Turn the water inlet ON. Collect the water in the holding tank and turn Water Inlet OFF after required amount of water is collected in the holding tank.
- Turn the pump ON from the controller console.
- After the pump is running for approximately 5 minutes, turn the valve ON for enabling the water to flow through the Unimac.
- Let the flow continue for 5 minutes.
- Add all the chemicals for Formulation 1 to the holding tank and let the flow action mix the chemicals for 10 minutes.
- Set the temperature to 176 F at the controller console and turn the heater ON.
- Maintain a very close watch on the heater and ensure that no smoke or a burning smell is emanated from the heater.
- Load the required weight of fabric in the Unimac and shut the door tight.

- Let the temperature reach 145 F before proceeding to the next step.
- Add Formulation 2.
- Turn the key to RUN mode and select Cycle 53 from the Cycle menu. Load the cycle onto the Unimac.
- Keep monitoring regularly (at least every 15 minutes) to ensure safety of the equipment.
- Once the cycle is complete and reaction solution drained, take the fabric out and carry out required post reaction treatment.
- Turn the heater off from the controller console.
- Let the solution still be in circulation till it reaches approximately 40 deg C (104 deg F) and then turn the pump OFF from the controller console.
- Drain the solution in waste containers or retain for next run as per requirement. NEVER DRAIN THE SOLUTION INTO BUILDING DRAINS.

Formulation 1:

Formulation 1 should be pre mixed before addition to the holding tank.

43g FS 230	dissolved in 2.5L water
7g FS 1620	dissolved in 1L water
200g C6	dissolved in 1.5L IPA
80g TFEM	dissolved in 1.5L IPA
0.26g of acrylamide (BA)/ g of fabric	to be added directly

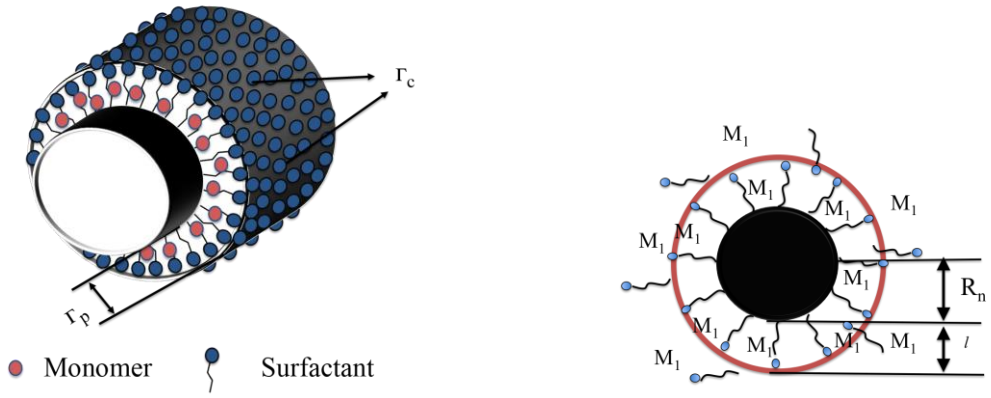
Formulation 2:

77g AIBN dissolved in 2L IPA

Emergency shut down procedure for equipment:

- PULL EMERGENCY KNOB LOCATED ON FRONT PANEL OF UNIMAC IN CASE OF AN EMERGENCY.
- WHEN AN EMERGENCY IS RECOGNIZED, DO NOT WAIT FOR SYSTEM TO STABILIZE AND PULL EMERGENCY SWITCH IMMEDIATELY. SAFETY FIRST.

Appendix –C Modified two-site Adsolubilzation for calculation of adsolubilization of MWCNTs



(a) (b)

Figure C.1: Schematic view of modified two-site adsolubilization model (a) Sleeve model showing monomer at the peripheral site (b) Cross-sectional view with monomer in the core

Figure C.1 shows an illustration of the modified two-site adsolubilization model for monomer adsolublized into surfactant hemimicelle. One site for adsolubilization is in the palisade layer of the hemimicelle core between headgroups of surfactant molecules represented as Γ_c. The other site for adsolubilizates with a hydrophobic moeity is on hydrophobic perimeter of sleeve shaped hemimicelle represented as Γ_p. The total adsolubilized amount of monomer (Γ_a) can be expressed as

$$\Gamma_a = \Gamma_c + \Gamma_p \qquad (1)$$

The partition coefficient (K) of monomer between hemimicellar and bulk phases is defined as follows:

$$K = X_c / C_a \quad (2)$$

$$\Gamma_c = X_c(\Gamma_s + \Gamma_c) \quad (3)$$

Where X_c is ratio of adsolubilized monomer (Γ_c) per adsorbed amount of surfactant (Γ_s), C_a is equilibrium concentration of monomer in supernatant. We assume there are no micelles present in supernatant at equilibrium. At coverages close to saturation, partition coefficient K can be considered as experimentally measured partition coefficient K_b.

$$\Gamma_c = \left(\frac{K_b C_a}{1-(K_b C_a)}\right)\Gamma_s \quad (4)$$

Now, we need to develop an expression for the adsolubilized amount of monomer on perimeter of surfactant aggregates. Assuming the surfactant aggregates form a sleeve on the nanotube, hydrophobic surface area of cylinder A_h, can be calculated from

$$A_h = 2\pi((R_n + l)^2 - R_n^2) \quad (5)$$

where *l* is the length of tail of surfactant molecule and R_n is radius of nanotube. From an assumption that the hydrophobic surface area (A_h) resembles an oil/water interface to the monomer molecules, one can obtain the value of adsorbed molecules for a monomer monolayer, A_h/A_A in which A_A is cross-sectional area per monomer molecule (Table 1). After multiplying this value by the number of cylinder-shaped surfactant aggregates (Γ_s/N_{avg}), adsolubilized amounts of monomer on hydrophobic perimeter of sleeve-shaped hemimicelle can be estimated as

$$\Gamma_p = \frac{A_h \Gamma_s}{A_A N_{avg}} \quad (6)$$

The combination of equation from 1 and 3-7 yields average aggregation number in terms of known quantities as

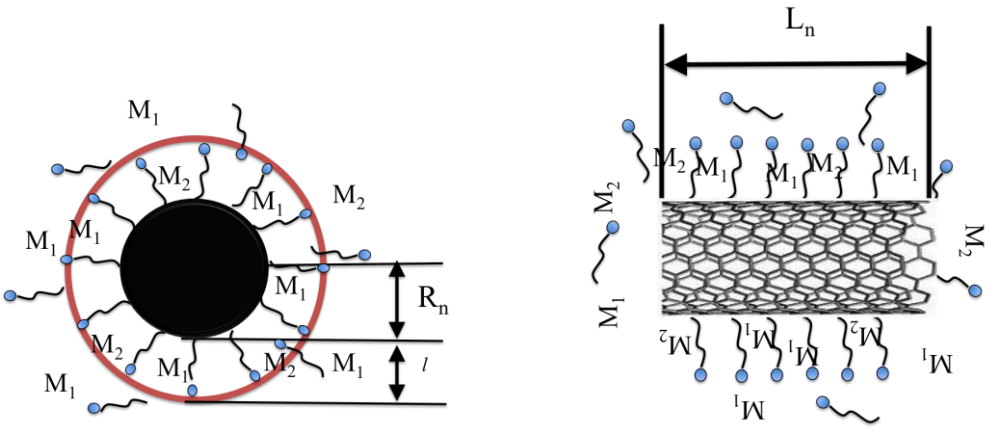
$$N_{avg} = \frac{2\pi(l^2+2lR_n)}{A_A}\left(\frac{\Gamma_a}{\Gamma_s} - \left(\frac{K_b C_a}{1-(K_b C_a)}\right)\right)^{-1} \quad (7)$$

Table C.1: Numerical values used for calculating aggregation numbers in modified two-site adsolubilization model

Category	SDS	BA	MMA
l^a (nm) **[66]**	1.6	-	-
$A_A{}^b$ (nm^2)**[66]**	-	0.263	0.263
$K_b{}^c$(M^{-1})	-	956.09	674.22
Molecular weight[d]	288.38	128.14	100.12

[a]Theoretical length of fully extended tail of surfactant, [b]Cross sectional area per monomer head group, [c]Estimated from an experimentally measured partition coefficient at full coverage of nanotube surface (This paper), [d]Molecular weight obtained from MSDS of respective chemicals.

Binary Adsolubilization model



(a) (b)

Figure C.2: Schematic representation of binary adsolubilization model (a) cross-sectional view (b) side view

The total number of moles in the hemimicelle N_{tot} is

$$N_{tot} = N_1 + N_2 + N_3 \tag{8}$$

Where N_1 and N_2 are the moles of adsolubilized monomers and N_3 is the number of moles of surfactant adsorbed and V is volume of aqueous phase

$$N_3 = \left((SDS)_0 - (SDS)_{eq}\right)V \tag{9}$$

If $C_{1,0}$ is the initial concentration of monomer 1 and M_{sol} is the molarity of water, then at equilibrium

$$X_1 = \frac{(VC_{1,0}) - N_1}{VM_{sol}} \tag{10}$$

$$Y_1 = \frac{(VC_{1,0}) - N_1}{VM_{sol}/K_1} \tag{11}$$

Noting that $Y_1 = N_1/N_{tot}$, once can show that

$$N_1 = \frac{VC_{1,0}N_{tot}K_1}{(K_1N_{tot}) + (VM_{sol})} \tag{12}$$

With a similar expression for N_2. Substitution in Eq. 9 yields

$$N_{tot} = \frac{VC_{1,0}N_{tot}K_1}{(K_1N_{tot}) + (VM_{sol})} + \frac{VC_{2,0}N_{tot}K_2}{(K_2N_{tot}) + (VM_{sol})} + \big((SDS)_0 - (SDS)_{eq}\big)V \tag{13}$$

Where N_{tot} is total number of moles in the admicelle, N_1 and N_2 are moles of adsolubilized monomers, $C_{1,0}$ and $C_{2,0}$ are initial concentration of monomers, M_{sol} is molarity of water and K_1, K_2 are partition coefficients of adsolubilized monomers and V is volume of aqueous phase.

Appendix –D Theory of Surfactant Science

Introduction:

Surfactants are vital components in biological systems, for key ingredients in consumer products and play an important role in many industrial processes. In addition to detergents and personal care products surfactants have found uses in almost every branch of chemical industry as well as in several other industries. The applications of surfactants in chemical industry are legion ranging from primary production processes to finished products. Figure D.1. demonstrates some important traditional and non-traditional application of surfactants in industry.

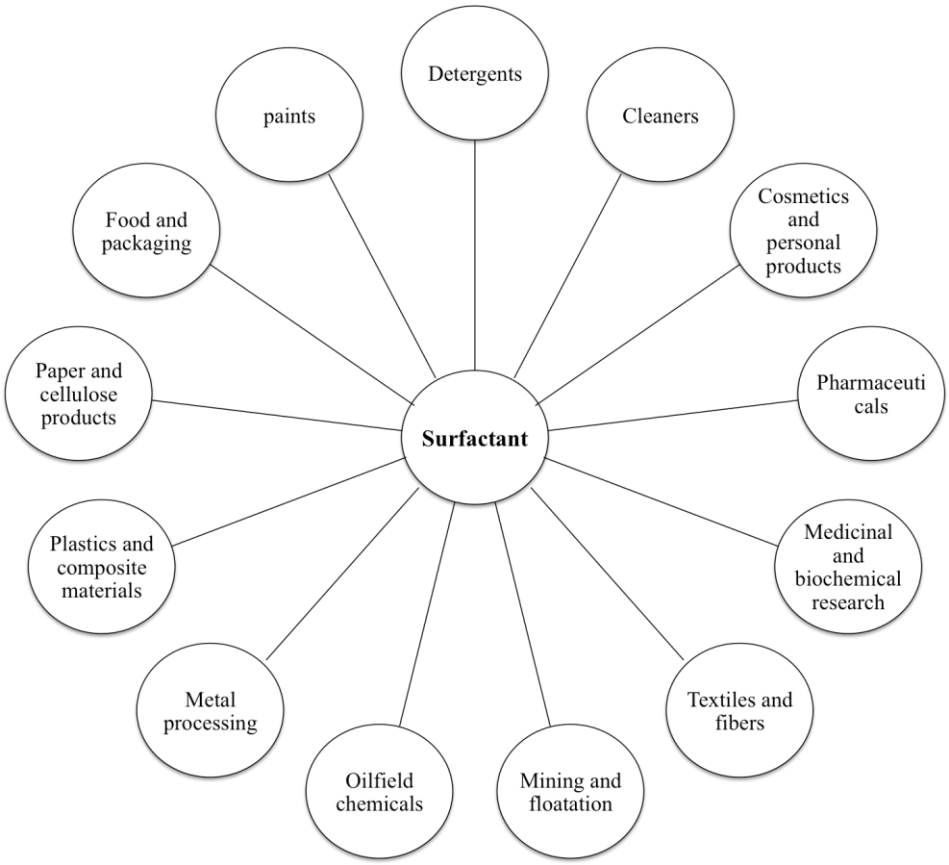


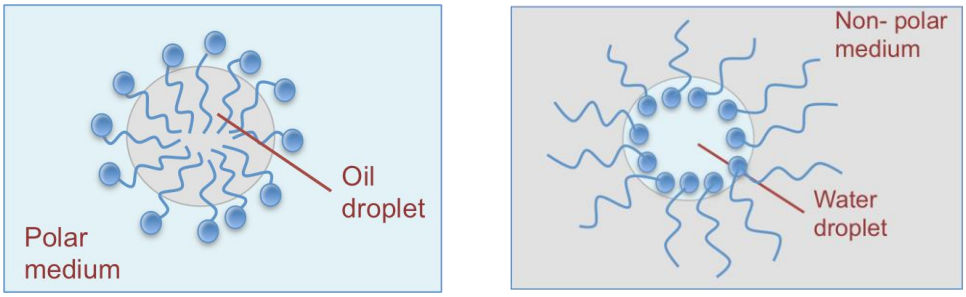
Figure D.1: Application of surfactants in different industries

Properties such as solubility, surface tension reduction capability, critical micelle concentration (cmc), detergency power, wetting control and foaming capacity help in increasing performance of surfactant in some applications as well as others. The Surfactant a contraction of the term surface-active agent, when present in the system has the property of lowering the surface or interfacial free energies of the surfaces. Surfactants are usually organic compounds, which are amphiphilic with a hydrophobic tail group and hydrophilic head group (Figure D.2). Thus a surfactant molecule contains both water-soluble and water insoluble component. The water insoluble hydrophobic head group may extend out of the bulk water phase, into the air or into the oil phase, while the water-soluble head group remains in the water phase. The properties and application of surfactants are determined by the balance between solvent-loving and solvent-hating properties of the molecules.



Figure D.2: Example of surfactant structure

When surfactants molecules are dissolved in aqueous media, they tend to form aggregates, which are called micelles where the hydrophobic tails form the core and the hydrophilic head groups are in contact with the surrounding liquid. Several types of aggregates are formed depending on the type liquid media and concentrations of surfactant. Figure D.3. shows an example of two different micelles with solubilizate in middle, the first micelle is an example of micelle formation in polar medium and second micelle is an example of reverse micelle in non-polar medium and can be classified as oil in water and water in oil solubilizate micelles.



(a) (b)

Figure D.3: Example of micelle formation with hydrophobic tail group and a hydrophilic head group (a) polar medium (b) non-polar medium

Micelle formation is an important phenomenon of surfactant not only because of interfacial phenomena such as detergency and solubilization but also because it affects the surface and interfacial tension reduction that do not directly involve micelles. Micelles have become a topic of great interest because of their unusual catalysis of organic reactions and similarity to biological membranes and globular protein.

Classification of surfactants

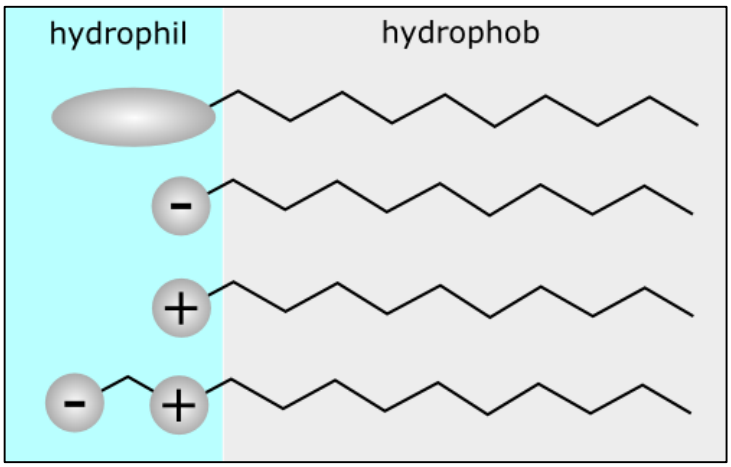


Figure D.4: Surfactant classification according to head group

(Obtained from

http://upload.wikimedia.org/wikipedia/commons/d/d1/TensideHyrophilHydrophob.png)

The hydrophobic group of surfactant is similar in most types of surfactants, consisting of a hydrocarbon chain, which can be linear, branch or aromatic. Some flurosurfactants have hydrophilic tails containing fluorocarbon chains and siloxane surfactants. Surfactants usually have one or two tails; those with two tails are called double chained surfactants. Mostly surfactants are classified based on polar head group. The head of ionic surfactant has a net charge. If the charge is negative the surfactant is called anionic and if the charge is positive the charge is called cationic. If the surfactant does not have charge is called non-ionic surfactant and surfactant with two oppositely charged head groups are called zwitterionic.

Anionic surfactant

Anionic surfactants usually consist of hydrophile as negatively charged group such as sulfate, sulfonate, phosphate and carboxylates. Examples of anionic surfactant are sodium dodecyl sulfate, ammonium lauryl sulfate, linear alkylbenzene sulfonates, and sodium lauroyl sarcosinate.

Cationic surfactant

The hydrophile bears a positive charge as quaternary ammonium cations, amines. Examples of surfactants are cetyl pyridinium chloride, cetyl trimethylammonium bromide, benzethonium chloride.

Non-ionic surfactant

The hydrophile that has no charge but derives it water solubility from highly polar groups such as polyoxyethylene or R-polyol groups including sugars. Examples of surfactant are polyoxyethylene glycol, glucoside alkyl ethers, glycerol alkyl esters, polyethoxylated tallow amine.

Zwitterionic (amphoteric) surfactant

The molecules that contains both positive and negative charge. Sulfo-betaines, phospholipids phosphatidylserine, phosphatidylcholine are some examples of zwitterionic surfactants.

In general hydrophobic groups may be significantly more varied than hydrophile. Variation of hydrophobic groups such as long straight chain alkyl groups, branched chain alkyl groups, unsaturated alkenyl chains, alkylbenzenes, alkylnaptththalenes, fluoroalkyl groups (partially or completely fluorinated), polydimethylsiloxanes, polyoxypropylene glycol derivatives, biosurfactants and derivatives of natural and synthetic polymers. With a wide variety of structures, possibility of searching a surfactant for an application would be a significant problem.

Surface tension/interfacial tension

A surface or interface can be described as the boundary between immiscible phases. Geometrically single surface exits between two surfaces. There are basically five types of surfaces (1) solid-vapor (S/V) (2) solid-liquid (S/l) (3) solid-solid (S/S) (4) liquid-vapor (L/V) (5) liquid-liquid (L/L). Traditionally interfaces involve one vapor and one condensed phase. When understanding the surface and interfacial phenomena, one needs to understand that atoms and molecules located at interface will experience different force field fields compared to the bulk materials. When involving water at interface there is an existence of electrical potential across the interface as the electrostatic effects are most important in aqueous suspensions, dispersions, emulsions, foams and aerosols often contributing to the overall stability of the system. The

interfacial energy and electrical statistics of a system are determined by quantities such as temperature, pressure and chemical composition of the phases.

The surface tension or surface energy of a material either liquid or solid can be significantly altered by small changes in its bulk composition. Addition of a surfactant to the system will change the surface tension, as the surfactant presence will change the net free energy for the system at the interface. The surface tension of the liquid is determined by the energy of the molecules in interfacial region and displacement of surface molecules at the interface. Various surfactant types are differentiated by the relationship between chemical structure of an adsorbing molecule and rate and extension of adsorption under different circumstances. The extent of reduction of surface tension depends on the substitution of surfactant molecules at the interface. The relative concentration of surfactant in bulk and interfacial phases should serve as an indicator of adsorption efficiency of surfactant and as a quantitative measure of the activity of the material at solution-vapor interface. The presence of surfactants will either raise or lower the surface tension, although very small amounts of surfactants reduce surface tension of water by 50% or more while a fully saturated electrolyte will increase by only few millinewtons per meter (mN/m). The changes in the surface tension of liquid by addition of surfactant can be a quantitative indicator of changes to be expected in interactions with other phases. The surfactants because of their hydrophilic-hydrophobic interactions drive them to reduce unfavorable energetic interactions by adsorption, aggregation, precipitation or phase separation. When low concentrations of surfactant are present in the system, the high-energy bulk phase molecules at interface are replaced by surfactants thus reduction of overall free energy

of the system. In a low concentration environment of surfactant, distortion caused by hydrophobic group increases the overall energy of the system thus the surfactant will preferentially adsorb at the surface/interface. As the concentration of surfactant increases, to reduce the overall energy of the system, surfactants tend to form aggregation or micellization (Figure D.5). The hydrophilic-hydrophobic structure of surfactant not only causes alteration of surface tension but also causes the orientation of adsorbed molecules such that the lyophobic groups are directed away from the bulk solvent phase. The hydrophilic group also serves the purpose of imparting sufficient water solubility to the molecule to provide a workable concentration to surfactant. The hydrophobic group plays two important roles in determining surfactant properties, favorably alter the energy of interaction between liquid interface and the contacting gas molecules and preferentially adsorb at the water/vapor interface.

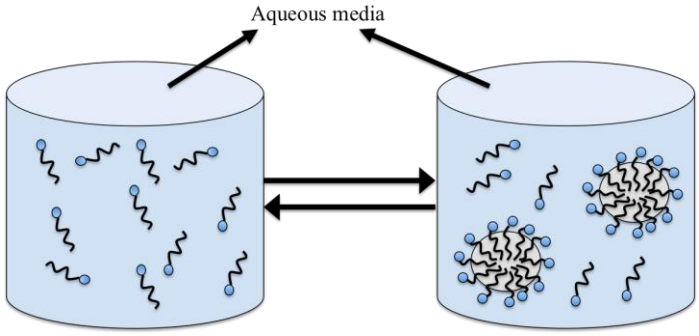


Figure D.5: Aggregation or micelle formation in surfactant

The efficiency and effectiveness of surfactant decreases when slightly polar groups like ether, ester, amide linkages or hydroxyl groups are introduced into system compared to system with no polar units. Because of polar units, change in orientation of adsorbed molecules at surface occurs due to interaction of polar groups and the water. If the polar group is situated close to primary hydrophilic group, very minimal effect was observed

but there might be a significant effect on the cmc of the material. Change in hydrophobic group where fluorine atoms are substituted, significant increase in the efficiency and effectiveness of surfactant is observed. Fluorinated organic materials have relatively low cohesive energy density and therefore have very favorable thermodynamic driving forces for adsorption leading to high efficiency as well as low surface energies.

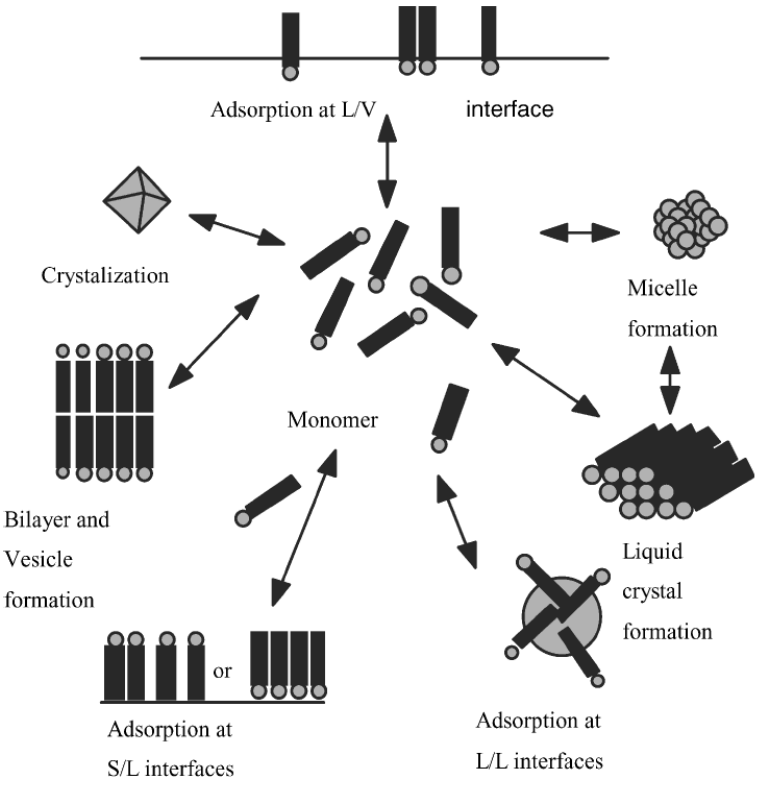


Figure D.6: Modes of surfactant action for the reduction of surface and interfacial energies (obtained from Chapter 4 in Surfactant Science and Technology 3rd edition, Drew Myers)

Surfactants in solution

As the special molecular structure of surfactants, possess a love-hate relationship in most solvents, resulting in among competing forces striving for a comfortable

accommodation in a given environment. The primary mechanism for energy reduction in liquids is adsorption at available interfaces, but when all interfaces are saturated the mechanism is the crystallization or precipitation of surfactant from solution. The alternative options include the formation of micelles, liquid crystals mesophases that remain in solution as thermodynamic stable, dispersed species with properties from those of monomeric solution (Figure D.6). Most common surfactants have a substantial solubility for water, but changes with significantly changes with length of hydrophobic tail, nature of head group, the electric charge of the counterion, temperature and solution environment. For example, many ionic surfactants have increased overall solubility when the temperature increases.

The solubility of the material depends not only on the solubility of monomeric material but also the solubility of the micelles or other aggregates structures. The important characteristic of a surfactant in solution relative to critical concentration at which thermodynamic concentrations results in onset of micelle formation or molecular aggregation. Since micelle formation is of critical importance for many applications of surfactant, over understanding of surfactant structure-property relationship is an important element. When one considers range of structures for surfactant molecules in presence of solvents, the nature of structure depends on the chemical structure of surfactant, the total bulk-phase composition, temperature, pH, cosolutes etc.,

Critical micelle concentration (cmc)

The micelle can be viewed as structurally resembling the solid crystal or a crystalline hydrate so that the energy change in going from crystal to the micelle is less than the crystal going to monomeric species in solution. The formation of micelles

thermodynamically favors the overall increase in solubility. At a fixed temperature, the concentration of surfactant may increases or decrease slightly at higher concentrations but the formations of micelles will be predominant above a critical surfactant concentration called critical micelle concentration (cmc). Several factors affect the cmc of surfactant in aqueous solution. The factors include structure of surfactant, presence of added electrolyte, presence of organic compounds in solution, presence of second liquid phase and temperature of solution. The cmc of surfactant decreases as the hydrophobic character of surfactant increases. In aqueous medium the cmc of surfactant decreases as the number of carbon atoms increase to about 16. If the hydrophilic group position is moved from terminal position to central position of hydrophobic group, there is an increase in cmc of surfactant. If the degree of binding of the counterion in aqueous solution increases there is a decrease in cmc of surfactant. The presence of electrolyte has a profound effect only in case of anionic and cationic surfactants compared to zwitterionic and non-ionic surfactants. The change in cmc of zwitterionic and non-ionic in presence of electrolyte is due to “salting out” or “salting in” of the hydrophobic groups in aqueous solvent. Small amounts of organic materials may change the cmc in aqueous media. As some of the materials may be present as impurities or by products by the manufacture of surfactants. Materials such as alcohols, amides does affect the cmc at lower liquid phase concentrations but materials like urea, formamide and guanidinium salts affect the bulk phase concentrations of the surfactant. The presence of secondary liquid phase has a very little effect on the cmc of surfactant. The effect of temperature on in aqueous medium on cmc of surfactant is complex. The values of cmc would decrease with increase in temperature and then to increase with further increase

in temperature. Temperature increase will cause decreased hydration of the hydrophilic group which favors micellization.

The phases occurring between micelles and crystals are natural consequences of removal of water from water from micellar system but do not constitute thermodynamically distinct states. The hydrophilic group may possess an electrostatic charge so that the process of adsorption or micellization can introduce electrostatic repulsions, which act to inhibit the removal of molecule from the system. Concentration of micelle formation and micellization of a given surfactant are determined by relative balance of forces favoring and retarding the molecular aggregation process. The shape of micelle produced in aqueous media is of importance in determining various properties of solution such as viscosity, capacity to solubilize water molecule. Major types of micelles appear in solution are (1) spherical structure (aggregation number < 100), (2) elongated cylindrical, rod-like micelles with hemispherical ends, (3) large, flat lamellar micelles, (4) vesicles – more or less spherical micelles arranged in one or more concentric spheres. In aqueous media the surfactant molecules are oriented, in all these structures with their polar heads towards aqueous phase and their hydrophobic groups away from it. In vesicles, there will also be an aqueous phase in the interior of the micelle. In non-polar media, the structure of micelle remains same but the hydrophilic head comprise the interior region and hydrophobic groups and non-polar solvent as outer region. Dipole-dipole interactions hold the hydrophilic groups together in the core. Structural changes occur when the temperature, concentration of surfactant and additives in liquid phase differ. Structural groups in surfactant may cause the change in

size, shape and aggregation number of micelle with the structure varying from spherical through rod or dislike to lamellar in shape.